PRESTRESSED CABLE DOMES:
STRUCTURAL BEHAVIOR AND DESIGN

BY

SUDARSHAN KRISHNAN

DISSERTATION

Submitted in partial fulfillment of the requirements
for the degree of Doctor of Philosophy in Civil Engineering
in the Graduate College of the
University of Illinois at Urbana-Champaign, 2015

Urbana, Illinois

Doctoral Committee:

Professor Daniel P. Abrams, Chair and Director of Research
Professor German R. Gurfinkel
Professor James M. LaFave
Professor David A. Pecknold

ABSTRACT

The introduction of tension as the predominant means of load transfer offers the potential for using less material to carry more loads. Cable domes are such unconventional structures based on the tensegrity principle. They rely on the assembly of prestressed cables in equilibrium with vertical struts. Members are stressed purely in axial tension or compression and as a consequence, the materials are used efficiently. Not much has been written about the structural design of cable domes. This study was based on an extensive review of technical literature and direct correspondence with the designers of cable domes. The contributions of this study will benefit both structural designers and academic researchers interested in the design of roofs for novel structures such as large arenas and stadia.

The primary objective of this dissertation was to provide both an intuitive and mathematical understanding of the structural behavior of radial-type cable domes subject to various loadings, and to determine their limit states. An accompanying objective was to find improved methods for their design and construction. To accomplish these goals, a series of twelve 400 ft. span domes with varying depth-to-span ratios, number of polygon sides and number of polygonal hoops were examined. Three limit states were evaluated, namely 1) buckling of struts, 2) serviceability, and 3) rupture of cables. The main cause of instability was established and a potential design solution in the form of enhanced struts has been recommended.

The study was made efficient by the use of a two-dimensional model. For dome designs governed by axisymmetric loads, the planar model was sufficient for member design. The analysis procedure was further streamlined using an influence surface analysis (based on the Müller-Breslau principle) that helped to identify governing load combinations for the design of members. Domes vulnerable to wind uplift were recognized and prestressing force levels were increased accordingly. As such, the findings from the influence surface analysis proved to be a good indicator of the adequacy of prestressing forces assigned to a dome. Further, the results revealed that additional prestressing forces were necessary to meet the serviceability criterion, beyond simply ensuring that cables remained in tension under all loading conditions.

The most important geometric parameters for structural design were identified as: the number of sectors, the number of polygonal hoops, hoop radii, rise-to-span ratio, and depth-to-span ratio. They greatly influenced the amount of prestressing forces required for the overall stability of a dome. The results showed that the radial stiffness of a hoop cable is inversely proportional to the hoop radii and the number of sectors. Domes with smaller depth-to-span ratios required higher prestressing forces for stability and to achieve a desired elevation (shape).

The critical loads for strut members were determined using the Stiffness-Probe Method. The method gave a physical understanding of the loss of capacity in struts due to applied axial loading. The use of prestressed stays increased a strut's buckling capacity to more than four times when compared with the critical loads of struts without stays. Consequently, stayed-struts are recommended as an alternative design solution for enhancing the load-carrying capacity of cable domes.

The erection procedure for cable domes typically constitutes 40% of the project cost. Noting that the strut forces were relatively small when compared with the diagonal cable forces, prestressing the struts as part of the erection process may prove to be an economical alternative for reducing the overall project cost. This approach has been proposed for future study.

For well-designed cable domes, i.e., domes that are adequately prestressed and whose cables remain in tension under all loading conditions, the study revealed that the cause for potential dome demise is usually due to buckling of struts or displacements exceeding the acceptable ranges for serviceability. As these limit states were found to occur well within the elastic range of the members, the findings justify the use of elastic design for cable domes.

Dedicated to

my parents and grandparents – at whose feet I sit,

and to

my sister – on whose shoulders I stand.

ACKNOWLEDGMENTS

I extend my heartfelt gratitude to my Advisor and Chair of the Doctoral Committee, Professor Daniel P. Abrams, for letting me pursue a topic of my interest and for his insightful contributions to the content and direction of this work. Professor Abrams provided practical advice and essential guidance throughout my Ph.D. years. Among many other things, I learned from him *that a goal is a dream with a timeline*. I truly appreciate the highest standards that he set, for the many prompt reviews despite his busy schedule and for the constructive comments that helped shape my ideas and technical writing. He has done a lot for me to remember and be thankful for.

While I was initially passionate about researching on tensegrity structures, it was Professor German Gurfinkel's emphasis on the practical significance and usefulness of tensegrity structures that led me to visit the Illinois State University's Redbird Arena. This set forth my research on cable domes. Professor Gurfinkel's contribution to the value of my research was immense. How to simplify a complex problem, how to develop analysis models, and how to obtain a physical understanding of intricate phenomena such as buckling, are some of the many things that I learned from him. I will be forever grateful for the many years of association with him, first as a student in CEE 469-Wood Structures, then as his teaching assistant for three summers and later for collaboration on different structural projects. He gave his time selflessly and I learned from him how to work devotedly to accomplish your goals. A true inspiration, he knew how to show the importance of an idea and raise my interest in a subject matter. Professor Gurfinkel has been more than just a great educator. He has been a caring mentor whose encouragement during difficult times meant very much. He always found a way to lighten situations and made sure that I stay focused on my goal. I sincerely thank him for helping me in many ways -- professionally and personally.

I value my association with Professor David Pecknold, first through my work with him as a teaching assistant for CEE 470-Structural Analysis, where I developed keen interest and comfort in advanced structural analysis. Professor Pecknold always had a unique and smart approach to structural analysis. And he showed me simple and efficient ways to derive expressions for the analysis model in this research. I also thank Professor James LaFave for his questions and comments that helped clarify and articulate my ideas and writing. Essentially, the knowledge I have gained from my Advisor and committee members has helped me develop a deeper understanding of the intricate structural principles and behavior of cable structures -- a subject that will sustain my interest for a long time as I pursue my career as an academic. Needless to say, the endeavor has prepared me for advanced research and technical work in structural engineering, and I cannot thank my committee enough for this.

Special thanks are due to Mr. Wesley Terry from Birdair Inc. for information about the industry practices for cable dome construction and for his succinct responses to my questions. I am also thankful to Messrs. Matthys Levy and Tian-Fang Jing from Weidlinger Engineers and Messrs. David Campbell and Paul Gossen from Geiger Engineers for insightful conversations about cable dome design. I value the exchange with Kenneth Snelson on the practical applications of tensegrity structures and for kindly lending me photographs of his built tensegrity sculptures for use in this dissertation. I would like to thank the Illinois State University (ISU) Campus Planning Office and Ms. Jenna Self of ISU Library Archives, who were generous in offering photographs of the

construction of the Redbird Arena Dome.

The various teaching appointments and opportunities given to me by the Department of Civil and Environmental Engineering and the Illinois School of Architecture at UIUC helped me develop as a teacher and educator. Through teaching, I enjoyed the association of students who always helped me keep my mind sharp and fresh with new ideas. For the many special moments, I thank the University of Illinois.

Today, I have achieved this significant milestone because of the constant prayers, unwavering support and many sacrifices of my grandparents, parents and sister. I am also thankful to my aunts and uncles of the R. Raghunath Patrachari family (paternal) and Thilasthanam Raman family (maternal) who have generously and lovingly supported my various needs during the formative years of my education and career. There is no way I could have gotten here without my parents. My father taught me art and gave me the intellectual stimulus to explore the professional path of my liking. My mother showed me how to live by faith, how to be patient and resilient, and how to stay poised regardless of the circumstances that life presents. My sister Mythili's 'never-say-no' attitude, her creative ideas, constructive criticisms and her continuous encouragement not just through this dissertation but for all aspects of life have kept me on-track. Most of all, she never let me paralyze during challenging times. I owe her eternal gratitude for who she is and for everything she has done. This doctoral degree is a small dedication for her many sacrifices.

I would like to thank the following people who have guided and helped me in different capacities through the journey of life: Navalpakkam Acharyaas, K.S. Raghavan, Bhooderi Swami, Govindachar, Srinivasan Gopalachari, and Drs. Andal, Gopalachari, Rodrigues, Varadachari, Varadarajan and Krishnamoorthy. I extend sincere thanks to my teachers, friends and well-wishers: Lalita Vaswani and other teachers from high-school and college, Professor Tarun Kant, Professors Helen and Edward Kuznetsov, Professor Robert Miller, Joyce Snider, Ana Gurfinkel, Shekar Swamy, Kashmira and Percy Fouzdar, Vimala and Raghavan, Janardan, R.S. Vasan, Nancy Diamond, Barbara Bolser, the late Professor Malcolm Quantrill, the late Professor Dale Perry, the late Professor Norris Stubbs, Professor Robert H. Dodds Jr., Professor Al Valocchi, Joan Christian, Mary Pearson, Professor Harshad Bhatia, Pradeep Khanna, Professor Raj Echambadi, Prof. Dr.-Ing. Rosemarie Wagner, Megan Mahoney, William Mischo, Carla Roberts, Anne Kopera, Ephraim Lasar, Arvind Hariharan, Pablo Caiza, Nishanth Lingala, Hari Gajendran and Nikoli Dryden. There are many more who helped in other ways and I thank them all.

This milestone would not have been possible without the grace of God and His wonderful operations of time. I am really glad to be able to experience this monumental moment.

TABLE OF CONTENTS

List of Symbols

The following symbols are used in this dissertation:

Symbol	Description
A	cross-sectional area of a member
C_e	exposure factor for snow loads
C_s	compression force in vertical strut or slope factor for snow load
C_n	concentrated load at the bottom of strut
C_p	external wind pressure coefficient
C_{pi}	internal wind pressure coefficient
C_t	Thermal factor for snow loads
D	dead load or dome diameter
d	depth of the lowermost hoop cable measured from the eave
E	modulus of elasticity or member elongation
e	member elongation
F	externally applied load
F_D	tension force in diagonal cable
F_f	force in cable stay at buckling (cable-stayed strut)
F_i	force in cable stay due to prestress only (cable-stayed strut)
f	rise of dome from the eave for wind pressure calculations or strand stress
f_y	yield stress of steel strands
f_{pu}	rupture stress of steel strands
G	gust factor
H	horizontal reaction at compression ring
h	height of vertical strut
h_D	height from ground to eave of the dome
I	importance factor for snow load calculations or moment of inertia
K	structure stiffness matrix
K_e	axial stiffness of the strut in a cable-stayed strut
K_d	wind directionality factor
K_{ca}	axial stiffness of the cross-arms in a cable-stayed strut
K_s	axial stiffness of the stays in a cable-stayed strut

K_z	velocity pressure coefficient
K_{zt}	topographic factor
k	member stiffness matrix or support factor for strut slenderness calculations
k_e	elastic stiffness matrix
k_g	geometric stiffness matrix
L	span of dome or length of member
ΔL	change in length of hoop cable
l	deformed length of a member
l_c	half-length of strut in a cable-stayed strut
l_{ca}	length of cross-arms in a cable-stayed strut
l_s	length of stays in a cable-stayed strut
m	direction cosine (cos θ)
N	number of interior polygonal hoops or internal member force
n	number of sectors (or sides) of polygon, direction cosine (sin θ), or internal member force
P	pretension force in diagonal or externally applied axial load
P_i	force in strut due to prestress only (cable-stayed strut)
P_{cr}	Euler (elastic) buckling load
p_f	flat roof snow load
p_g	ground snow load
Q	internal member force
q	design wind pressure
q_i	internal pressure due to wind
R	radius of hoop or residual force
ΔR	change in length of radial cable
r	rise above the compression ring
S	snow load
S_s	symmetric snow load
S_{as}	asymmetric snow load
T_H	tension force in hoop cable
T_{CR}	radial tension force in compression ring
T_f	force in stays at buckling (cable-stayed strut)
T_i	force in stays due to prestress only (cable-stayed strut)

T_R	tension force in ridge cable
T_r	radial tension in hoop cable
T_V	tension force in valley cable
u	nodal displacement in the horizontal direction
U_i	displacement of node
v	nodal displacement in the vertical direction
V	vertical support reaction or basic wind speed
V_H	volume of hoop cables
V_R	volume of equivalent radial cables in an "all-radial" dome
W	vertical concentrated load or self-weight of member(s)
W_s	symmetric wind suction
W_{as}	asymmetric wind suction
x, y	nodal coordinates in the deformed configuration
X, Y	nodal coordinates in the undeformed configuration
Z	global vertical axis in SAP2000
β	angular distortion between the ridge cables due to torsional movements
ε_p	prestrain in diagonal
ε_u	ultimate strain of strands
ε_y	yield strain of strands
Δ	unit deformation given to a member or change in length of a member
δ	vertical nodal displacement caused by the unit deformation of a member or influence coefficient.
γ	ratio of hoop cable and equivalent radial cable volumes
γ_t	density of HSS steel material in a stayed column
γ_{ca}	density of cross-arm material in a stayed column
γ_{sc}	density of stay cable in a stayed column
υ	Poisson's ratio
σ	axial stress

Subscripts	**Description**
as	asymmetric
ca	cross-arm
cm	critical member
D1-D4	diagonal cable (to outer)
e	elastic
ext	external
H1-H3	hoop cable (inner to outer)
h	horizontal component

int	internal
p	prestress
R	radial cable or radial direction
R1-R4	ridge cable (inner to outer)
S1-S3	vertical strut (inner to outer)
s	symmetric
sc	stay cable
T	hoop cable or hoop direction
V	valley

CHAPTER 1 OVERVIEW

Tensegrity structures are prestressed, pin-jointed systems of continuous cables and discontinuous struts. Prestress assigned to the cables gives structural integrity to the system (Figure 1.1). Hence, the term 'tensegrity' was coined by R. Buckminster Fuller (Fuller 1962), combining the words 'tension' and 'integrity.' However, the construction of the first true tensegrity structure is attributed to Kenneth Snelson in 1948. His patent (Snelson 1965) described tensegrity as "…. a class of structure possessing, what may be termed discontinuous compression, continuous tension characteristics." Tensegrity structures have *infinitesimal* mobility and obtain their structural stiffness by means of prestress, at the expense of material strength of a member rather than increased member sizes (Kuznetsov 1991).

In tensegrity structures, the predominant means of load transfer is via tension. As a consequence, tensegrity structures are light and flexible. Their flexibility renders applications in adaptive, outer-space and deployable structures.

Figure 1.1 *Kenneth Snelson Expo '70 Osaka,* stainless steel 33 x 16 x 16 ft. Collection: Japan Iron and Steel Federation, Kobe, Japan (Permission to use granted on 02/07/2014 by Mr. Kenneth Snelson)

Among terrestrial structures, the tensegrity principle has found its most successful application in cable domes. Cable domes are tensegrity-like structures, in the sense that they are a network of cables and struts. Conventional domes made of reinforced concrete are heavy and resist forces mainly through compression, while cable domes are light and transfer loads predominantly through tension. The latter are stabilized by prestressing diagonal cables to support external loads while limiting deflections. Carrying loads in tension is advantageous as the permissible stress in cables is governed by strength and not by stiffness considerations. Moreover, as opposed to conventional domes, cable domes are made from translucent fabric, which allows for naturally bright interiors.

1.1 Evolution of Cable Domes

Air-supported domes and cable domes are the two types of tensile domes, which have been used as roofs for sports arenas and stadia. Air-supported domes were Geiger's first lightweight solution for roof stadia. Access to the roof and rigging for stage events was limited. A significant drawback was the roof's ability to support heavy snow loads with internal pressure. They demanded complicated and costly snow-melting systems. Such problems were witnessed at the Hubert H. Humphrey Metrodome in Minneapolis, MN and the Silverdome in Pontiac, MI. Another problem was that the internal air-pressure had to be maintained for the working of the special revolving doors and vehicular airlock doors (Gardner 1987). Geiger was familiar with Buckminster Fuller's tensegrity structures. He simplified Fuller's cable-net and made the dome shallower and more aerodynamic with the roof weighing only slightly more than his pneumatic roofs. The drawbacks in air-supported domes were eliminated with the advent of cable domes where catwalks were used to provide access to the roof and rigging capabilities were improved. Since the cable dome roof does not require air pressure for stability, there is no need for special doors and control systems (Gardner 1987).

1.2 Characteristics of Cable Domes

Before introducing cable domes, it is important to recognize the fundamental difference in the structural characteristics of a prestressed cable-truss and a cable dome. Cable trusses are double-cable systems developed to control wind-induced flutter that make simple suspended cables problematic (Schodek 2014). In the double-convex cable trusses of Lev Zetlin's Utica Auditorium completed in 1959 (Figure 1.2a, Bethlehem Steel Company, 1968), the lower cables consist of 72

zinc-coated, prestretched, 2-in. strand assemblies that were prestressed to 175 kips; they serve as the primary load-resisting members transferring loads via a catenary-like action. The upper cables consist of 72 zinc-coated, prestretched 1-5/8-in. strand assemblies and are prestressed to 135 kips (Bethlehem Steel Company, 1968). The upper cables are ancillary members for gravity load resistance but essential to resist uplift forces. The vertical members between the top and bottom chords resist forces through compression. Cable trusses may also be double-concave, where the top chord has a catenary-profile while the bottom chord has an arch-profile. Here, the role of the top and bottom chord members are the reverse of that shown in the double-convex cable-truss. The vertical members resist in this case forces through tension. Irvine (1981) extensively discussed the static and dynamic response of cable trusses, as well as their lateral stability.

In cable domes, on the other hand, the bottom chords are substituted by radially placed diagonal cables and circumferentially placed polygonal hoop cables (Figure 1.2b). Structurally, this makes the cable-strut system three-dimensional with the hoop cables providing the required torsional stiffness. The main members of a cable dome are the diagonal cables, hoop cables, ridge cables, vertical struts and the central hub with horizontal tension rings. The radial thrusts from the cable-trusses are equilibrated by the compression ring in lieu of heavy anchorage mechanisms. As a result, the walls or columns only need to be designed for vertical loads. Because prestressed cables are *ten* times stronger in tension compared to mild steel in compression the cable dome roof weight is likely to be *one-tenth* the weight of a compression dome for the same span (Gardner 1987).

With reference to stiffness, Hanaor (1988) classified structures as *geometrically rigid* and *geometrically flexible.* Geometrically rigid structures are capable of supporting loads in their unloaded geometry; their deflections under load are elastic and therefore relatively small. Conventional bar structures are considered to be geometrically rigid. Geometrically flexible structures possess *infinitesimal mechanisms*[1]*;* they change their geometry to fit the load (think of a stretched cable loaded transversely). Cable and membrane structures are typically geometrically flexible and are subject to larger deflections under loads when compared to geometrically rigid structures. As such, geometrically rigid structures are typically surfaced with a stiff roof covering such as metal sheeting, while geometrically flexible structures are usually covered by flexible

[1] An infinitesimal mechanism is a mechanism having only infinitesimal (i.e. not finite) motion.

membrane (which may or may not be part of the main load bearing structure). Cable domes are geometrically flexible and prestressable structures that possess *infinitesimal mechanisms* (Hanaor 1988, Kuznetsov 1991). Adequate prestressing forces are assigned to eliminate the mechanisms.

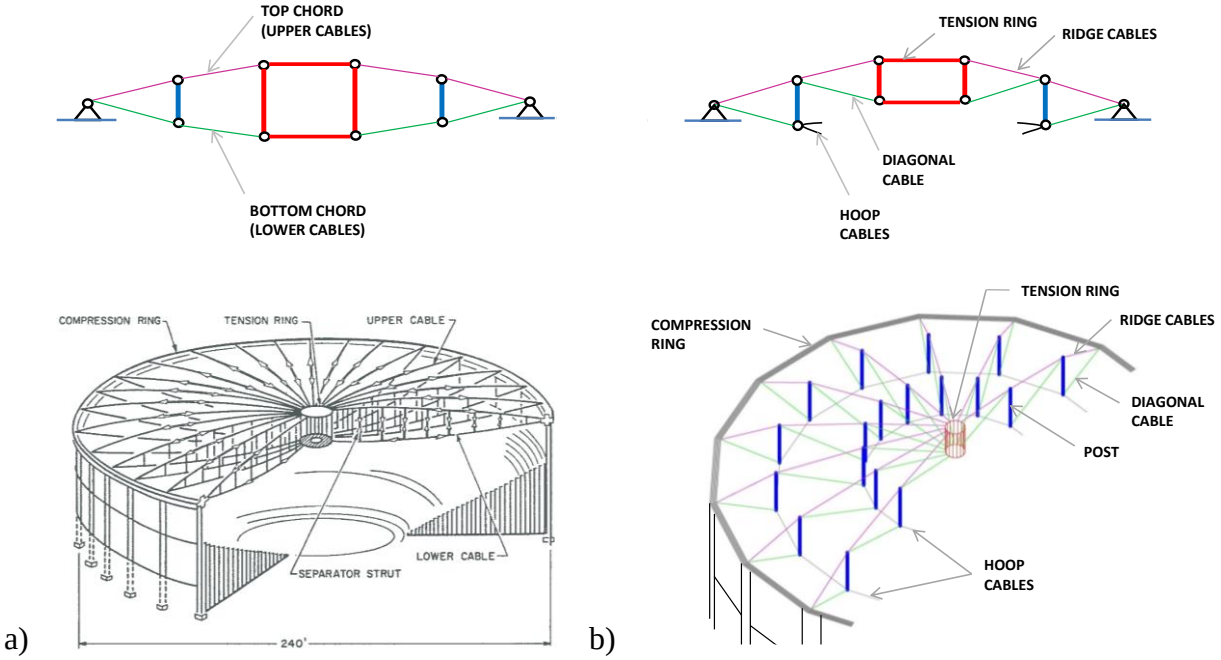

Figure 1.2 (a) Typical cable truss (Utica Auditorium); and (b) Typical cable dome system

1.2.1 Types of Cable Domes

Cable domes were first popularized first by David Geiger, and later by Matthys Levy. The main difference between the Geiger dome (radial) and the Levy dome (triangulated) is in the arrangement of the diagonal cables which affects the torsional stability of the roof system.

Radial-type (Geiger Dome)

The first radial-type cable domes was built in Korea with two hoops (N = 2), 16 polygon sides (n = 16), span L = 394 ft., rise r = 32 ft. and depth d = 40 ft. Such a dome is designated as $N2{:}n16{:}L400{:}r/L0.08{:}d/L0.10$. In radial-type cable domes, the vertical struts and diagonal cables lie in the same vertical plane (Figure 1.3b). The diagonal cables provide radial and axial stiffness while the hoop cables provide the necessary transverse stiffness. Inward radial forces are transmitted to the perimeter and subsequently brought to equilibrium by a compression ring. The

ridge cables provide stability to the vertical *struts* and support the fabric membrane roof. Geiger's rationale for not transversely bracing the tops of the struts was to take advantage of the flexibility (due to large deformations) that could be accommodated by the roof membrane (Campbell et al., 1994). Also, the lower rise was cost-efficient. When compared to conventional compression domes, Geiger's low aspect ratio tension system benefitted from considerably less surface area and, therefore, required far less roofing material. For this reason, the radial cable dome is deemed a minimalist cable dome.

a)

b)

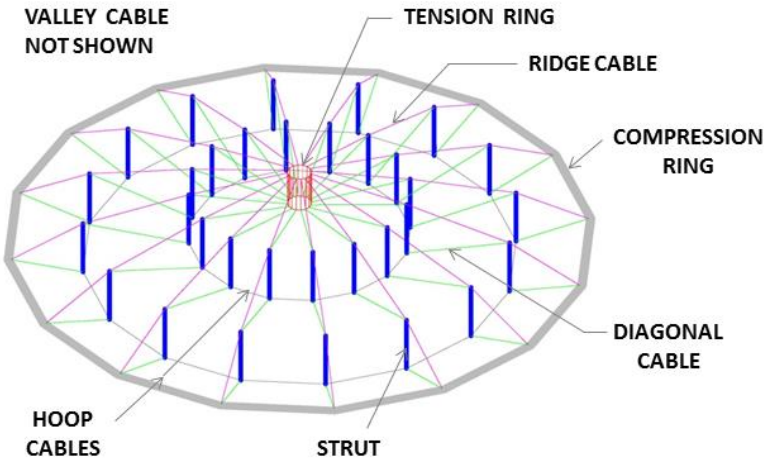

Figure 1.3 (a) Fencing Arena Dome, Seoul (Rastorfer 1988); and (b) Structural components of the *N*2:*n*16 configuration

There are only six radial-type domes (Table 1-1) with flexible roof membranes. The first such dome in the US, the Redbird Arena at the Illinois State University was constructed in 1989. The dome has an elliptical plan with one hoop and 32 radiating trusses, i.e., *N*1:*n*32. The ridge profile visually emphasize the peaks created by their top ends and therefore does not have a smooth dome-like appearance.

Figure 1.4 Tropicana Dome in St. Petersburg, Florida (Fleiger 2012)

The Tropicana Dome in St. Petersburg, FL (Figure 1.4) built in 1990, has the longest span to date with three hoops each forming a 24-sided polygon, i.e., *N*3:*n*24. The dome is unique because it was tilted 6 degrees to provide more seating behind home plate and the infield area of the baseball stadium (Shaeffer 1996). The outer hoops of this dome required 135 strands compared to 40 strands in the outer hoop of the Fencing Arena dome.

Triangular-type (Levy Dome)

In triangulated domes, the vertical struts and diagonal cables are not in the same vertical plane. The positions of the struts in the neighboring rings are offset from one-another by $180^{\circ}/n$ in the transverse direction (Figure 1.5). Note also that the top end of the vertical strut in the outer ring is connected to the neighboring inner ring with *two* adjacent diagonal cables, thus providing radial, axial and transverse stiffness to the cable–strut system. The struts in a triangulated dome have adequate restraint and stability. The most recent triangulated dome was designed for the city of La Plata, Argentina (Table 1-1). The project was completed in 2012 after almost a decade of interruption in its construction.

For domes having the same rise, span, number of sectors and number of hoops, the radial dome will obviously be lighter than the triangulated dome. Moreover, the radial dome is easier to construct because there are fewer connections. For the aforementioned reasons, this research focuses on radial-type domes (referred to as 'cable domes' hereafter).

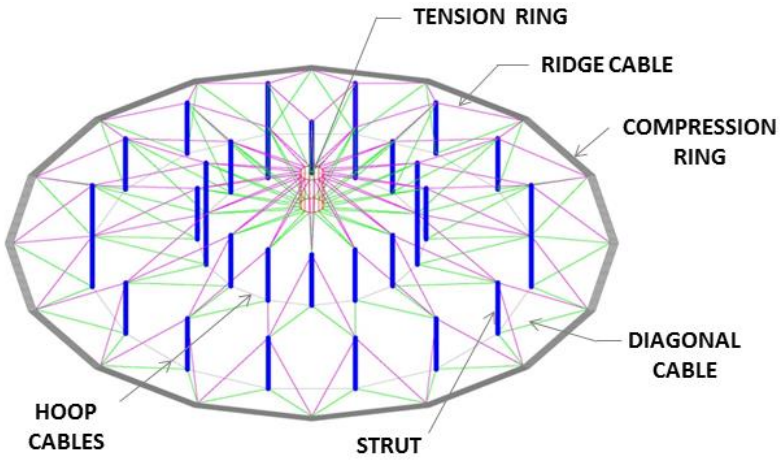

Figure 1.5 Triangulated *N*2:*n*16 dome

Table 1-1 Complete list of built cable domes with flexible membrane

Cable Domes (built)	Year	Location	Type	Span, ft. (m)
Gymnastics Arena	1986	Korea	Radial	305 (93)
Fencing Arena	1986	Korea	Radial	394 (120)
Redbird Arena	1988	United States	Radial	299 x 253 (91 x 77)
St. Petersburg Dome	1989	United States	Radial	689 (210)
Georgia Dome	1992	United States	Triangulated	787 x 305 (240 x 93)
Taoyuan Arena	1993	Taiwan	Radial	394 (120)
Bifid Dome	2004	Spain	Radial	65.6 (20)
Twinstar Dome	2012	Argentina	Triangulated	656 x 550 (200 x 170)

To date, there are eight built cable domes, of which six are radial-type (Table 1-1). Much of the construction happened in the late 1980s and early 1990s. There have been no large span radial domes constructed since the Taoyuan Arena in 1993.

1.3 Erection Procedure

The erection of cable domes is an expensive operation and constitutes approximately 40% of the total cost of a project. When first laid out at the construction site, cable domes lack initial stiffness. Prestressing the diagonal cables facilitates the erection by stabilizing the dome and thereby defining its geometry. After the erection, additional prestress may be assigned to support external loads. The erection procedure was developed keeping in mind how the structure will be dismantled in case of such an event (Geiger, Stefaniuk, & Chen 1986).

The erection sequence for an *N*2 cable dome is illustrated in Figure 1.6. Construction begins by laying the inner tension ring, ridge cables and struts on the ground and connecting their bottom ends together by affixing them with bolts to the castings. The assembly is then hoisted and secured to the perimeter compression ring (Stage 1). The outermost hoop and outermost diagonals are then joined together at the castings of the already erected ridge cables. The outermost diagonals, which run from the top of the compression ring to the bottom of the struts are then prestressed thereby pulling the corresponding hoop cables into its final position (Stage 2). The process of adding hoops and diagonals and then prestressing the diagonals is repeated for the inner rings until the entire network is in place (Stages 3, 4, and 5). After the main structure has been erected, the fabric is unfurled from the inner tension ring to the perimeter compression ring (Figure 1.7a). The fabric membrane is installed by bolting it to aluminum castings that cover the ridge cables. Valley cables are then installed over the membrane and prestressed to stretch the fabric membrane (Figure 1.7b). This completes the erection process. Prestressing forces may be adjusted, if needed.

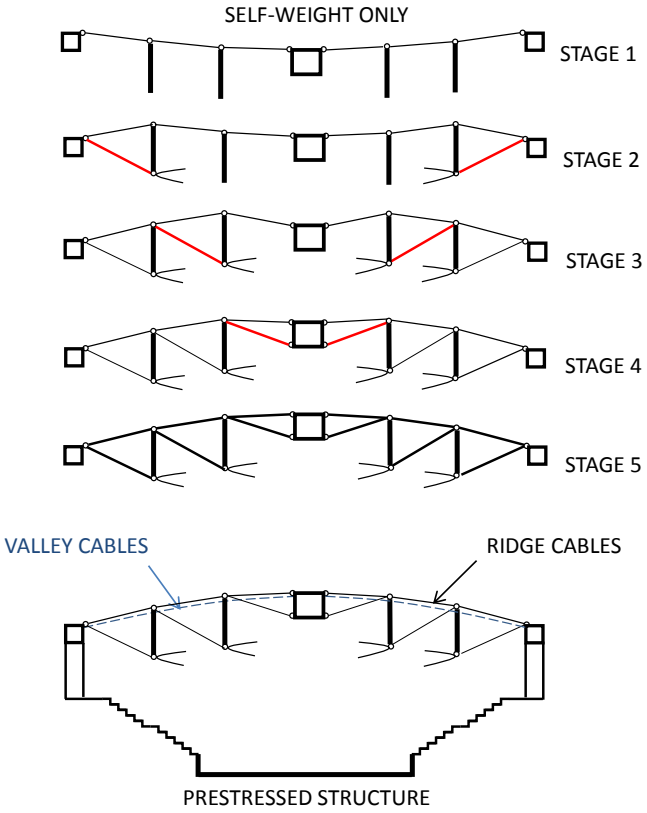

Figure 1.6 Erection sequence of roof structure; prestressed diagonals shown in red

a)  b) 

Figure 1.7 (a) Unfurling of fabric membrane; and (b) Installation of valley cable (Permission to use granted on 05/17/2013 by Dr. Joann Rayfield Archives, Illinois State University)

1.4 Geometric and Structural Parameters

Although a cable dome is a complex network of members, its behavior and design can be described in terms of *five* fundamental geometrical parameters, namely:

N	Number of interior polygonal hoops
n	Number of sectors (or sides) of polygon
L	Span of dome or length of cable, depending on context
r	Rise above the perimeter compression ring
d	Structural depth below the perimeter compression ring

In addition, the level of prestressing force (p) applied to the diagonals determines the initial stiffness of a cable dome.

i. Number of concentric polygonal hoop rings (N)

The number of hoop rings N determines both the overall shape of a dome as well as the force distribution. More hoops lead to a smother ridge profile. More hoops also means more struts and therefore more connections required to form the cable-strut system. Consequently, cable

and strut lengths are reduced which increase the member stiffnesses. The number of hoop rings *N* were varied in this study from 1 to 3 to determine their effect on structural behavior.

ii. Number of sectors or polygon sides (*n*)

The number of sectors has a direct impact on the member forces and fabric stress. This is because a smaller *n* would mean fewer cable-trusses and therefore higher applied loads in each truss. The number of sectors *n* in practice are chosen based on the dome span and external loads experienced. The stiffness of hoop cables is inversely proportional to *n* (Eq. 5.12). Therefore, in order to have stiff hoops and reduced applied loading, the designer is expected to make a sound judgment considering all factors. Domes with *n* =16 and 24 are examined as part of this study.

iii. Rise-to-span ratio (*r/L*)

Radial cable domes built to date have used a rise-to-span ratio of less than 1:12. In this study, a 1:12 ratio has been used for all domes.

iv. Depth-to-span ratio (*d/L*)

The depth-to-span ratio is important because the location of hoops, especially the outermost hoop determines the sightlines from the upper-level seats. Moreover the structural depth significantly affects the dome's stability; an increased depth reduces the required diagonal prestress and increases the moment resistance of the dome (Section 8.3). Three different depth-to-span ratios *d/L* are examined herein, i.e., three different inclinations of the diagonal cables (Figure 1.8).

v. Level of Prestressing Force (*p*)

The level of prestress is fundamental to the successful design of cable domes. The magnitudes of the prestressing forces must ensure that all cables remain in tension and the maximum deflections are within the acceptable limits for serviceability. If the prestressing force is too high, the member capacities may be reduced significantly. In this study, an initial prestress equal to 50% of the yield stress of the cables is assigned to the diagonals.

1.5 Literature Survey

The literature survey on cable structures begins with a review of methods that have been used for solving the geometric nonlinear analysis problem. This is followed by a description of experimental work on cable-strut structures and cable domes. All the literature reviewed is relevant to the development of this thesis.

1.5.1 Numerical Methods

Design of cable and membrane structures has relied on several nonlinear finite element analysis techniques. The various nonlinear theories and solution methods developed in the late 1960s and early 1970s for the analysis of cable structures proved pivotal in the design of cable-strut structures. Several nonlinear theories were developed for analyzing cable problems. However, no analytical method was available for solving the resulting nonlinear equations of equilibrium and compatibility. Consequently, iterative methods were developed to solve the governing equations. For an iterative procedure to be viable, the method must ensure convergence, and for it to be efficient, convergence should be rapid to minimize computational time and costs. First-order methods like the secant-stiffness method show moderate convergence rates. For this reason, second-order iterative methods with their high convergence rates are more popular. The Newton-Raphson procedure (Weisstein 2014) or modified Newton methods are the most popular of these second-order methods; they used tangent stiffness. Essentially, these techniques strive to achieve rapid convergence, resulting in minimal computational time (Tezcan & Özdemir 2000).

Baron and Venkatesan (1971) presented a secant stiffness matrix scheme, a modification of it, and a combined technique using tangent and secant stiffness matrices. They concluded that the use of tangent stiffness matrix instead of secant stiffness leads to rapid convergence. For improving the convergence in highly nonlinear cable-net problems, Siev (1963) and Thornton and Birnstiel (1967) suggested incrementally applying loads. To enhance convergence, Haug and Powell (1971) limited the norm of response increments between iterations. Argyris and Scharpf (1972) performed large displacement analysis of complex prestressed structures subject to the usual external loading. In fact, their method was used to design the 1972 Olympic Stadium in Munich; the model contained over 10,000 degrees of freedom.

1.5.2 Cable Domes

Researchers and practitioners have studied cable domes from different points-of-view. Earlier works included experimental studies aimed at understanding their structural behavior. Later studies were more analytical, dealing with static and dynamic analyses. Numerical modeling gained popularity because of the cost and time savings they offered when compared to developing and testing numerous prototypes. More recent research has predominantly focused on structural behavior at ultimate and construction methods.

Yamaguchi et al. (1987) tested *N*2:*n*8 domes with 9 m. and 30 m. spans. They studied dome behavior via experiments and numerical modeling and concluded that cable domes are quite stiff and stable even when some of the ridge and valley cables go slack. Taniguchi et al. (1987) tested an *N*1:*n24* dome with an 8 m. span and found that geometric nonlinearity is more pronounced when the prestressing force levels are small. They later extended their study to larger structures. Gasparini et al. (1989) studied the static and dynamic response of an *N*3:*n*8 dome of 2.5 m. span using a linear-elastic two-dimensional axisymmetric model. One of their conclusions was that cable domes behave like a compression membrane under gravity loads when the ridge cables are sufficiently prestressed to avoid slackening. However, if the inner ridge cables go slack, the dome behaves like a tension membrane. Kawaguchi et al. (1999) optimized cable dome shapes in order to maximize their stiffness. Their results showed that optimum shape depends greatly on the lengths of the outermost vertical struts. Campbell et al. (1994) compared triangulated and radial cable domes and concluded that triangulation is not required for structural stability. Using the LARSA software program, Levy (1992) provided insights about the need for nonlinear finite element analysis to account for large deformations in cable domes. This software was also used to design the Georgia Dome in Atlanta, GA (USA). The program MCM/BLD3D was used for the Tenstar Dome in La Plata, Argentina (Levy 2013).

Hanaor (1988) developed a unified algorithm based on the flexibility method for analysis of optimum prestressing force levels for pin-jointed cable domes. Hanaor (2002) later concluded that the main load-bearing components of a cable dome are the outermost hoop and the perimeter compression ring. Yuan and Dong (2003) developed the concept of feasible integral prestress which uses the number of independent self-stress states for a given dome configuration to determine uniform prestressing force for members in groups, e.g. for all members along a radial

truss. This was later used for geometric stability analysis of various cable domes.

Pellegrino (1992) studied the behavior of an *N*2:*n*24 radial-type dome. Among other characteristics, the inextensional loads which induce large rigid-body-like displacements, were identified and contrasted to extensional loads which induce linear-elastic displacements. Wagner (2002) also studied such rigid-body-like deformations. Using graphical analysis, the effect of ridge cable geometry on member forces was studied and comparisons were made between radial and triangulated dome behavior.

Recent research on cable domes has focused on inelastic behavior (Li 2012; Ye 2012; Zhu 2013), manufacturing errors and construction analysis (Liu, 2012; Jin, 2012).

1.5.3 Cable-stayed columns

Based on the findings of this study, the use of prestressed cable-stayed struts has been recommended as a design solution for increasing the buckling capacity of the struts. As a consequence, the load carrying capacity of cable domes is expected to improve. Smith et al. (1975) and Hafez et al. (1979) developed analytical methods to predict the critical load of a simply connected single cross-arm prestressed stay column and compared their results with experimental results. Expressions were derived for the buckling load in terms of the final tension in the stays due to initial prestressing force. Smith et al. (1975) claimed that a cable-stayed column buckles when the tension in the stays become zero. They also found that the use of cable stays with single cross-arms can increase the buckling strength of the column by as much as 8.18 times the elastic buckling load of a simple pin-ended column. The maximum buckling load corresponded to the load when the tension in the stays was reduced to zero. Temple (1979), on the contrary, said that there will be some residual tension in the stays at buckling. Hafez et al. (1979) built on the study done by Smith et al. (1975) and clarified the effect of initial prestress on the buckling load of a single cross-arm stayed column. Whether the tension force in the stay-cables reduces to zero depends on the initial prestressing force. Essentially, if the prestressing force is smaller than a certain value T_{p_min}, then the tension in the stays on the concave side goes to zero under an increasing load. If the prestressing force is above the minimum but less than a certain optimal value T_{p_opt}, there will be residual tension in all cables even when the strut system has buckled (Hafez, Temple and Ellis, 1979).

Most of the studies on structural behavior of cable domes are based on the assumption of elastic material behavior, which may be fair from a design point-of-view. There has been no work done to determine the collapse load of cable domes. This dissertation studies the inelastic behavior of cable domes by assuming a bilinear stress-strain curve for the cable material. The nonlinear structural analysis program SAP2000 is used for large-displacement analysis. A displacement-controlled procedure is used to determine the ultimate capacity of a dome as the load at which a cable member ruptures or a strut buckles. For domes that failed by strut-buckling, a design solution using prestressed stays is suggested to increase the capacity of the struts. A perturbation analysis with the aid of the stiffness probe method (Gurfinkel et al. 2009) was used to determine the buckling load of struts in an efficient way. This method provides a physical understanding of the loss of capacity of struts.

1.6 Research Problem: Importance, Motivation, and Contributions

Members in a cable dome are stressed purely in tension or compression. Prestress forces applied to select members transform compression stresses into more favorable tension stresses. The result is a lightweight long span dome significantly lighter than conventional reinforced concrete domes. Not part of main-stream building structures, cable domes remain relatively unknown to most structural designers. Only six radial-type cable domes have been built over the past 25 years (Table 1-1). Because of their unique structural characteristics and erection process, design of cable domes demands specialized engineering knowledge. The ASCE/SEI 19-10 *Standard for Design of Cables in Buildings* (ASCE 2010a) and the ASCE/SEI 55-10 *Provisions for Design of Tensile and Membrane Structures* (ASCE 2010b) provide general guidelines regarding design of tensile and membrane structures. Because of the many planning and engineering design decisions involved in cable dome construction, an ASCE/SEI Standard specifically devoted to prestressed domes will increase interest and visibility of cable domes. Moreover, no research has been done on estimating the load carrying capacities of cable domes or to provide alternative design solutions to enhance their capacities.

This research investigates radial-type cable domes under various loading conditions for their elastic and inelastic behavior to formulate design guidelines for an ASCE Standard on prestressed domes. A series of 12 cable domes, each with 400 ft. span were examined as part of this study. Layouts for two groups of domes are studied – one with 16 polygon sides and the other with 24

polygon sides (n = 16 and 24) with polygonal hoops N varied from *one* to *three* (Figure 1.8a). A rise-to-span ratio (r/L) of 0.083 was used for all domes so as to keep the applied loading identical. The hoop rings were radially equidistant from each other. The depth-to-span ratio (d/L) was varied and this determined the hoop elevations (Figure 1.8b) and diagonal inclinations.

First, an axisymmetric two-dimensional model (i.e., a structure in which the cables were replaced by two-force members) subject to full snow load was analyzed to establish the initial prestressing force levels and member areas. The design procedure was further streamlined using influence surface analysis to determine the controlling load combination for member designs. For dome designs governed by symmetric loading conditions, an equivalent two-dimensional model was sufficient for member designs.

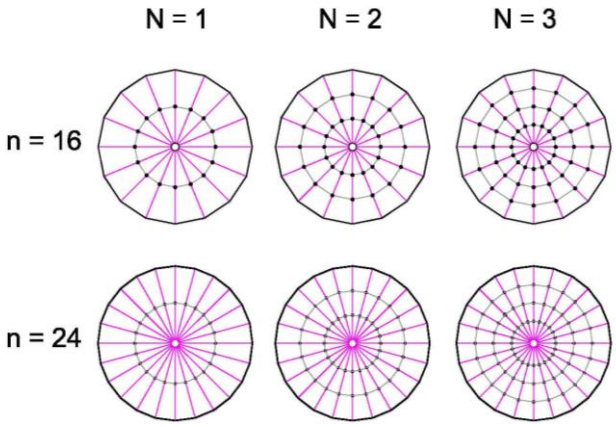

(a)

n	r/L	d/L	N=1
16 or 24	0.083	0.14	
		0.10	

n	r/L	d/L	N=2
16 or 24	0.083	0.09	
		0.07	

n	r/L	d/L	N=3
16 or 24	0.083	0.07	
		0.05	

(b)

Figure 1.8 (a) Plan configurations with varying polygon sides (n) and hoop rings (N); and (b) Elevation configurations with varying depth-to-span ratios (d/L)

The elastic behavior was studied to understand the general trend in member behavior under various loading conditions. Thereafter, the inelastic behavior was examined using a bi-linear material model for the steel strands. The analysis was done to get insights into the progressive yielding of

the cables. Based on the findings, prestressed cable-stayed struts have been recommended to prevent premature buckling and thereby increase the capacity of cable domes.

The following represent the contributions of this research:

i. Development of two-dimensional model parameters for simplified analysis and design.
ii. Use of influence surface analysis to identify critical load combinations for member design.
iii. Identification of limit states and validation of elastic design for cables.
iv. Alternative design solution for struts to improve their buckling strength.
v. Insights from parametric studies and structural design guidelines.

1.7 Organization of Dissertation

In this chapter, an overview of cable dome configurations and their characteristics was presented. The important geometric parameters in structural design and the erection process were discussed. The motivations to undertake this study and the importance of the topic were discussed along with main contribution of this dissertation. As a summary of what is to follow, materials, members and connection details are the subjects of Chapter 2. Emphasis is given to the properties of cable members and their unique arrangement in a dome. The various loads to be resisted by cable domes are discussed in Chapter 3. The rationale for using the ASD load combinations from the ASCE19-10 *Standard for Design of Cables in Buildings* (ASCE 2010a) are discussed and the critical load combinations for member design are found from influence surface analysis. In Chapter 4, the geometrical nonlinear analysis procedure is formulated, taking into account large displacements and geometrical effects. The Newton Raphson Method, owing to its quadratic convergence, is used to solve the set of nonlinear equilibrium equations. In Chapter 5, the two-dimensional model parameters for a cable dome are derived. The planar model simplifies the analysis of domes governed by axisymmetric loading and facilitates quick parametric studies. Chapter 6 deals with the conceptual behavior of cable-strut structures. One and two-post structures are analyzed to understand the trend in member behavior. Much of the observations from these simple structures are later noted in cable domes as well. In Chapter 7, the structural behavior of *twelve* 400 ft. cable domes is discussed extensively. Stability (buckling of struts), serviceability and strength (rupture of cables) limit states are evaluated. In Chapter 8, the influence of the critical design parameters on structural design are explained. Prestressing force is recognized as the essential force parameter and dome span, number of polygon sides, radii of hoop cables, depth and rise of the roof are

identified as critical geometric parameters. The effect of these parameters on the stability of cable domes is evaluated. In Chapter 9, an alternative design for vertical struts is recommended using prestressed cable-stays attached to the struts in order to increase their load carrying capacity. The summary and conclusions of this study are presented in Chapter 10. To an aspiring cable dome researcher, some interesting problems are presented for future research. Finally, design guidelines along with supplementary results from this study are presented in the appendices.

CHAPTER 2 MATERIALS, MEMBERS AND DESIGN DETAILS

From the main structural system of the roof, including cable material and their composition to the arrangement of members and special connection details, this chapter gives an overview of the cable dome's major components including the supporting perimeter beam and roof membrane materials. The construction materials used for the main structural system are described in Section 2.1. As the materials used are not as conventional as reinforced concrete or rolled steel, the cable material in particular is extensively discussed in Section 2.2. Easy dismantling was the original intent for the unique arrangement of cable members; as such, the placement of the members is described in Section 2.3 along with the heavy connections required to transfer forces between strut members and cables. This is followed by a brief description of the supporting perimeter beam and the roof membrane materials in Sections 2.4 and 2.5, respectively.

2.1 Materials

Knowledge of material properties is as important as knowledge about loads and analysis procedures for cable domes. Steel for the cables and struts, reinforced concrete for the perimeter beam and polytetrafluoroethylene (PTFE) for the roof membrane are the basic materials used for the construction of cable domes. Their mechanical properties are listed in Table 2-1.

Table 2-1 Material properties used for structural analysis (* Source: Birdair)

Member Type	Modulus of Elasticity (ksi)	Ultimate Tensile Strength (ksi)	Area (in^2)	Number/Description
Bridge and Hoop Ropes	20,000	254	0.596	1 for bridge and 1 for every hoop
Strands for ridge, diagonal, and hoop cables	24,000	270	0.215	Varies
Pipe (for vertical strut)	29,000	58	Varies	Varies by polygon dimension and number of hoop rings
Fabric Membrane (PTFE)	10,500*	500*	N/A	Usually 4 layers
Reinforced Concrete Polygonal/ Ring Beam		Assumed rigid		

The performance of the fabric membrane contributes greatly to the overall success of a cable dome system. The fabric not only provides an envelope for protection against the environment, but also provides a means to transfer the external loads such as snow and wind to the main structural system (Valerio 1985).

2.2 Cable Members

There are several different steels used for the diagonal, hoop and ridge cable members. The term *cable* will be generally used to refer to them. To understand the specific composition of the diagonal, hoop and ridge cables, it is essential to know their make-up (Figure 2.1).

A strand is usually an assembly of six *wires* twisted about a seventh core *wire* and a rope is an assembly of one or more strands. The diagonal cables are comprised of several independent *strands*, whereas the ridge and hoop cables have a continuous rope in addition to multiple independent strands.

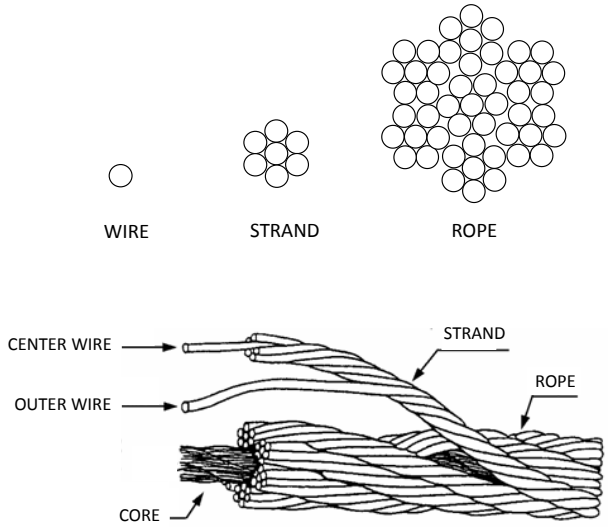

Figure 2.1 Wire, strand, and rope

Wire is covered by ASTM A421 "Standard Specification for Uncoated Stress-Relieved Steel Wire for Prestressed Concrete" and *strand* is covered by ASTM A416 "Steel Strand, Uncoated Seven-Wire for Prestressed Concrete." The available grades for strand are Grade 250 (f_{pu} = 250 ksi) and Grade 270 (f_{pu} = 270 ksi). The Grade 270, 0.6 in. diameter low-relaxation strand is most commonly used in cable domes (Table 2-2). The Young's Modulus for design is 24,000 ksi.

Table 2-2 Properties of prestressing steel

ASTM A 416, Seven-Wire Strand, Grade 270				
Diam.	**Weight**	**Area**	**Tensioning Load**	**Strength**
in.	lb./1000ft	in^2	lb., at 202.5 ksi	lb., at 270 ksi
3/8	290	0.085	17,200	23,000
7/16	390	0.115	23,300	31,000
1/2	520	0.153	31,000	41,300
0.6	740	0.217	43,900	58,600

The low-relaxation strands are pre-stretched by repeated loading and unloading cycles with traction values equal to approximately 50 percent of their fracture load. This operation produces some important changes in the crystalline structure of the metal. The stress-relieving operation alone reduces the amount of relaxation, which would occur in an as-drawn wire, and it also eliminates the tendency for the 7 wires in a strand to come unraveled (Gamble, 2003). An engineer is then able to predict the elastic behavior of the strand or rope after erection because of the elimination of construction stretch in the cables (Scalzi, Podolny, & Teng 1969). The strands are protected with anticorrosive material. This protection is provided by galvanizing the wire by the electrolytic zinc or the hot-dip process (Krishna 1978).

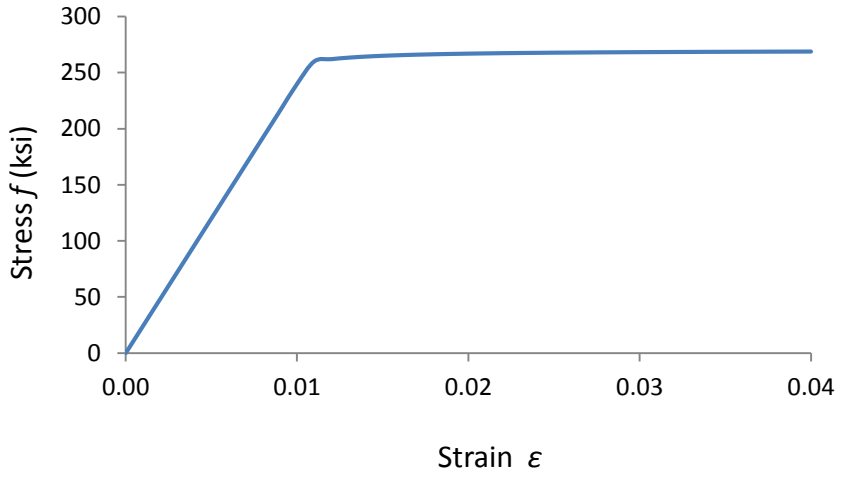

Figure 2.2 Stress-strain curve for Grade 270 low-relaxation steel

The stress-strain curve for strands does not exhibit a pronounced yield point, but instead gradually departs from the initial straight line, with a very high proportional limit (Figure 2.2). The yield stress for low-relaxation strand is taken as 90% of the breaking stress, i.e., 243 ksi, with a corresponding yield strain equal to 0.011. The equation for the curve in Figure 2.2 is a fitted curve using the Ramberg-Osgood functions and is a very good representation of a measured curve just meeting the A416 stress-strain requirements (Gamble, 2003).

While the modulus of elasticity recommended for strands is 24,000 ksi, a reduced value is used for strands protected with coatings. These values are less than that of a solid steel bar, because the strand has a tendency to twist and unwind as it is pulled. An engineer must therefore be cautious with cross-sectional areas of strands, which are considerably smaller than a solid bar of the same diameter. Ropes, because of more construction looseness, have a modulus of elasticity of approximately 20,000 ksi (Morris and Fenves, 1970).

2.3 Member Arrangement

In a cable dome, verticals struts appear to be floating in an articulated cable network. The cable members, i.e., diagonal, hoop and ridge cables, each have a different composition of strands and ropes.

The schematic arrangement of members used in the Seoul Fencing Arena dome is shown in Figure 2.3. Cable A is one continuous strand which forms the ridge between joints 1a and 3 and the diagonal from joint 3 to joint 7. Cable B is made of four continuous strands, which forms the ridge between joints 1a and 2 and the diagonal from joint 2 to joint 6. Cable C forms the outermost diagonal member, comprised of 10 independent strands, connecting joints 1 and 5. The ten strands are separated in two layers to facilitate the connection of the hoop cables at joint 5. Cable D is made of 20 independent and continuous strands to form the circumferential outer hoop member (see joint 5 detail in Figure 2.3). Cable E is made of 10 independent and continuous strands to form the circumferential outer hoop member (see joint 6 detail in Figure 2.3). Cables X, Y and Z are fixed length ropes connecting joints 1a to 2, 2 to 3, and 3 to 4, respectively. Similarly cables V and W (see joints 5 and 6 detail in Figure 2.3) are fixed length ropes in the circumferential direction.

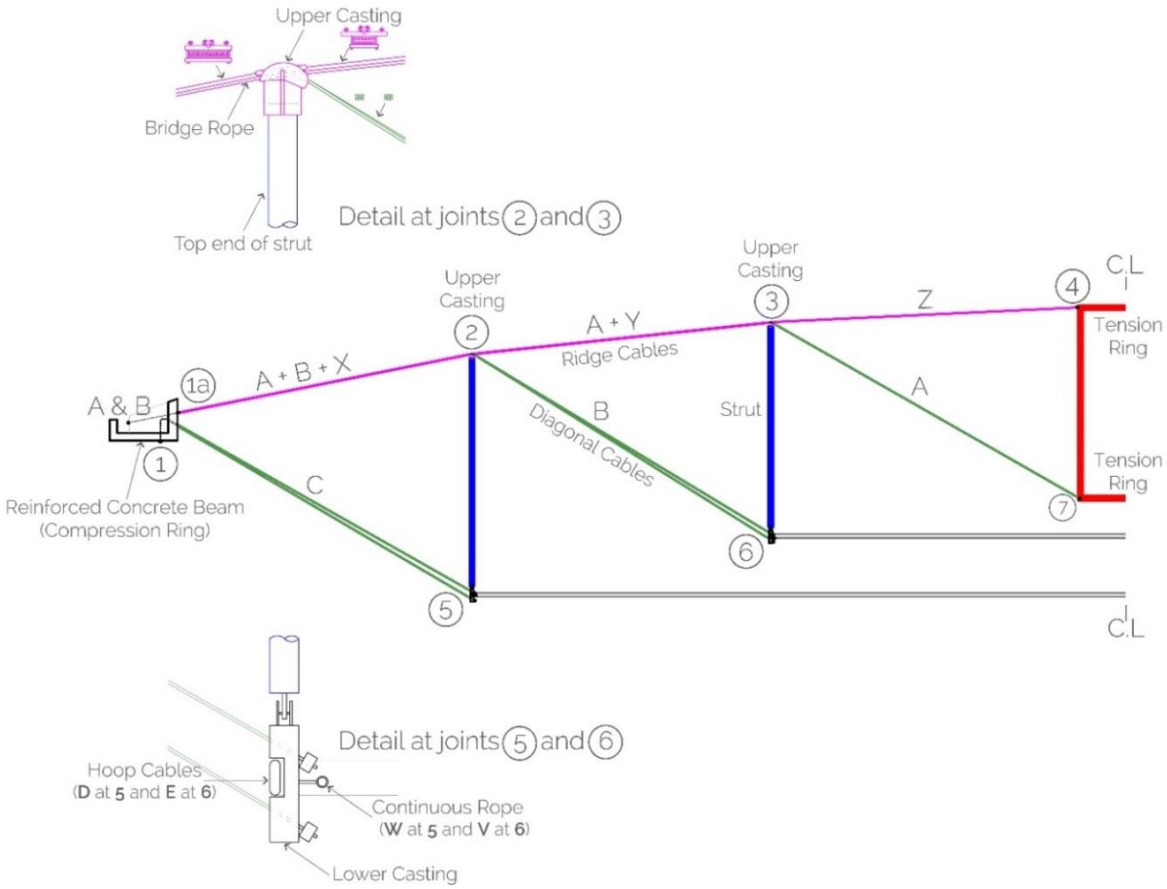

Figure 2.3 Cable composition and casting details

Table 2-3 Cable composition and arrangement for a sample *N*2 dome

Cable Label	Number	Cable	Type	Connectivity
A	1	Strand	Continuous	Diagonal from Joint 7 to Joint 3 and ridge from Joint 3 to Joint 1
B	4	Strand	Continuous	Diagonal from Joint 6 to Joint 2 and ridge from Joint 2 to Joint 1
C	10	Strand	Continuous	Diagonal from Joint 5 to Joint 1
D	20	Strand	Continuous	Around circumference
E	10	Strand	Continuous	Around circumference
V	1	Bridge Rope	Fixed length	From lower casting to lower casting
W	1	Bridge Rope	Fixed length	From lower casting to lower casting
X	2	Bridge Rope	Fixed length	From Joint 1A to Joint 2
Y	2	Bridge Rope	Fixed length	From Joint 2 to Joint 3
Z	2	Bridge Rope	Fixed length	From Joint 3 to Joint 4

The bridge ropes are additional members, which run continuously across the meridional and circumferential directions respectively. Their purpose is to maintain the geometry of the structure during construction and they are retained as part of the structure post-construction. A summary of the cable arrangement is provided in Table 2-3.

Castings (upper and lower in Figure 2.3) are large metal connections used to connect the struts and the cable members. Every strut has an upper and lower casting. The upper castings connect the ridge cables to the top of the strut. The continuous bridge rope from the perimeter compression ring to the inner tension ring has swage stops to grip the rope along the length. These swage stops are pinned to the upper casting. The upper castings prevent the bridge ropes from moving laterally. The cap on the castings restrains any vertical movement of the bridge ropes at the casting. The lower casting connects the bottom of a strut, the hoop and diagonal cables. Stefaniuk (1986) emphasized the importance of the role of the castings to assure the continuity of the varying length strands that start at the perimeter beam. For cable domes with the same number of sectors, equal hoop spacing, equal loading on tributary areas, rise-to-depth and span-to-depth ratios, the corresponding members of the domes of different diameters carry the same load as one moves from the center of the dome outward. This leads to repetition of details and castings (Geiger, Stefaniuk, & Chen 1986).

2.4 Perimeter Beam

The polygonal/ring beam is usually made of reinforced concrete. Alternatively, the compression ring may be made of a three-dimensional triangular steel truss, the members of which are made of hollow steel sections. The Twinstar dome in LaPlata (Levy 1998) used a steel space truss for the perimeter beam. Being quite massive, the ring beam is assumed as rigid as part of the structural analysis of cable domes in this study.

2.5 Fabric Membrane

The most common material used for fabric membrane is polytetrafluoroethylene or PTFE, “a strong, tough, waxy, nonflammable synthetic resin produced by the polymerization of tetrafluoroethylene” (Encyclopedia Britannica 2013) commonly known as Teflon-coated fiberglass. PTFE is inexpensive, strong, translucent, easy to fabricate and is widely used in

permanent structures. It has a life span of approximately 30 years. Teflon provides self-cleansing attributes, and fiberglass provides the necessary strength.

The development in membrane properties has led to newer materials with increased strength and transparency. Ethylene tetra fluoro ethylene or ETFE is a relatively new material gaining popularity as membrane cladding. It is lightweight, flexible, and transparent and, therefore, attractive for roofing spaces where natural light is desired (Birdair 2013). However, being a film, its strength is comparatively less than that of PTFE, making PTFE a more popular choice for cable dome roofs. More recently, the Twinstar Dome in La Plata employed a new fabric, UltraLUX, with a more open weave resulting in a translucency of over 24%, which benefits turf growth. This fabric however has a reduced tensile strength, i.e., 5% less than PTFE (Brzozowski 2011).

This chapter provided an overview of the materials used in cable dome construction emphasizing the properties of steel strands in cable members. The unique arrangement of cable members in the dome was illustrated along with the castings (connections). Finally, the salient characteristics of fabric membranes were briefly described including the use of newer materials with superior performance.

CHAPTER 3 LOADS AND CRITICAL LOAD COMBINATIONS

One of the most provocative characteristics of cable domes is the way it defies an engineer's expectation of a structure achieving stability, i.e. through a strategic assembly of prestressed cables and struts. The unconventional structure support the loads that are expected on any roof structure. In Section 3.1, the various loads to be resisted by the structure are discussed. This is followed by a description of the various load combinations for which the members must be designed, in Section 3.2. The rationale for use of the Allowable Stress Design (ASD) as the structural design philosophy for cable domes is explained. Finally, the influence surface analysis is discussed in Section 3.3, an approach that simplifies the design procedure and provides a cursory idea about the adequacy of the prestressing forces assigned.

3.1 Loads

Design loads and load combinations for cable domes are established using the ASCE/SEI 19-10 "Structural Application of Steel Cables for Buildings" (ASCE 2010a) and ASCE/SEI 7-10 "Minimum Design Loads in Buildings and Other Structures" (ASCE 2010c). Local codes must be considered based on site context and topography. This section describes the loads experienced by the roof structure and their estimation.

3.1.1 Prestress

Prestress is fundamental to the existence and stability of cable domes. Prestressing force levels depend on the structure's geometry, member sizes and deflections limits. By controlling the amount of prestressing force, a cable dome can be made flexible or stiff. Levy (1992) found that an average of 30% of the cable breaking strength was required for triangulated cable domes. Prestressing force levels are appropriately assigned to ensure that all cables remain in tension and the deflections are within acceptable limits, under all pertinent loading. For computational purposes, prestress is assigned by specifying axial prestrain to the diagonal members. An initial prestress equal to 50% of the cable yield stress is used in this study.

3.1.2 Dead and Live Loads

Gravity loads on a cable dome include dead, live, rain and snow loads. Of these, dead loads can be calculated with greater precision while other loads cannot be predicted with such certainty. Dead loads include the self-weight of the structural members as well as the fixtures attached permanently to the structure. Structural self-weight includes the weight of fabric, struts, strands, ropes, tension ring, and cast steel connections. This is calculated satisfactorily based on the dimensions and density of the materials. The permanent fixtures, which comprise mechanical/electrical/plumbing (M/E/P) and catwalks among other attachments, are assumed to weigh 8psf. In addition to the uniform loads, a minimum concentrated load of 100 kips is applied to one of the bottom nodes of the outermost hoop to accommodate any future attachment (Campbell 1994). As such, it is justified to design the fabric membrane for the usual live load, while a reduced live load can be used for designing the main cable trusses of the dome. Meanwhile, code requirements still call for a minimum roof live load of 12 psf (Campbell 1994).

3.1.3 Rain Loads

Rain loads may be relevant in certain configurations where the dome is relatively flat at the crown. This usually happens in *N*1 domes (Figure 3.1a and 3.1b). Water may collect as ponds, and with additional accumulation, the roof will deflect further allowing for a deeper pond formation. If the membrane does not possess enough stiffness to resist this progression, tearing or failure of the membrane will result due to localized overloading.

a)  b) 

Figure 3.1 Redbird Arena cable dome, Illinois State University (ISU)
(a) View of roof; and (b) Flatness at crown prone to ponding
(Permission to use granted on 05/17/2013 by Dr. Joann Rayfield Archives, ISU)

Water may also collect when the main drains get blocked. The potential standing water may lead to ponding instability. Such issues must be resolved in the original design by providing appropriate positive drainage. Needless to say, the truss geometry must be determined based practical considerations such as drainage and sight-lines, beyond structural efficiency.

3.1.4 Snow Loads

Designers of cable domes in colder regions must consider the effect of snow loads. Such loadings are complicated since snow accompanied by wind gusts can cause non-uniform loading. Alternate freezing and thawing may also lead to non-uniform snow accumulation. Ponding from melting snow may add to the asymmetric snow thereby magnifying the vertical deflections.

The fabric membrane resists snow loads before transferring them to the main cable-trusses. The slope of the roof may help to shed some of the snow load. Cable domes have a low-rise, with the slope at the eaves usually less than 30°. Considering this, Case-1 in Figure 7-3 of ASCE/SEI 7-10 (ASCE 2010c, p.37) is appropriate to determine the distribution of snow loads. However, depending on the ridge profile, the snow may or may not slide towards the compression ring. As such, snow loads are calculated in accordance with Sec. 7.6.3 of ASCE/SEI 7-10 (ASCE 2010c).

The calculation of symmetric snow loads is not straightforward, due to the complex tributary areas of the corrugated roof. As usual, first the flat roof snow load is calculated as

$$p_f = 0.7 C_e C_t I \, p_g \tag{3.1}$$

where:

p_f	=	Flat Roof Snow Load (for roofs with a slope less than or equal to 5°)
0.7	=	Basic Exposure Factor
C_e	=	Exposure Factor of 0.9 (Table 7-2, ASCE 2010c)
C_t	=	Thermal Factor of 1.0 (Table 7-3, ASCE 2010c)
I	=	Importance Factor of 1.10 (Table 1.5-2, ASCE 2010c)
p_g	=	Ground Snow Load of 35 psf (Fig. 7-1, ASCE 2010c)

Also, as there is a likelihood for more than 300 people to congregate in this facility during any event, the structure will fall under Category III as listed in ASCE/SEI 7-10 (ASCE 2010c).

The uniform load extends over the low-sloped portion of the roof where slope factor is C_s = 1.0 as determined from Figure 7-2 of ASCE/SEI 7-10 (ASCE 2010c, p. 36). Because of the flatness of

cable domes, the sloped roof factor C_s is taken as 1.0 for the entire dome span. The symmetric load is uniform near the ridge (or crown) and trapezoidal adjacent to the eaves (Figure 3.2a and Figure 3.3a).

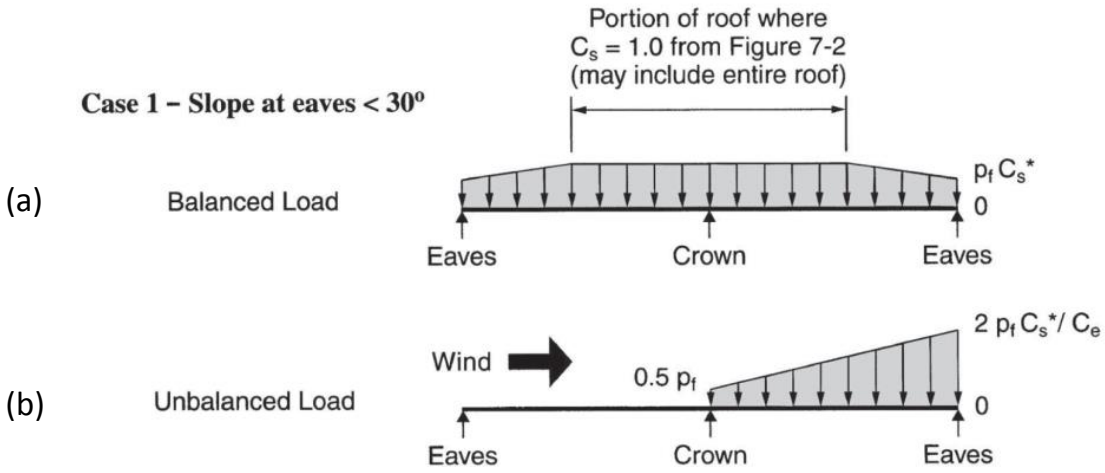

Figure 3.2 (a) Symmetric snow loads; and (b) asymmetric snow loads for eave slope < 30° (Permission granted by ASCE on 01/16/2014 to use Fig. 7.2 of ASCE/SEI 7-10, p.36)

Besides the geometry of the roof, there are other factors to be considered. Formation of ice dams may prohibit the sliding of snow depending on the surface roughness and roof insulation. These can occur at points of greater insulation in the valleys, down slope from a less insulated area. As such, the slickness of roof surface, insulation and cold bridges may have a significant influence. Some of the aforementioned factors for cold and warm roofs are addressed in Figure 7-2a and Section 7.9 of ASCE/SEI 7-10 (ASCE 2010c, p. 33 and p. 36 respectively).

Asymmetric load on a cable dome roof will occur mainly due to snow sliding from a high point (tension ring) to a low point (compression ring). This may also happen due to snow being blown from the windward to the leeward side. The provisions for asymmetric loads as applied to curved roofs are applicable to cable domes. Figure 7-3 of ASCE/SEI 7-10 (ASCE 2010c, p.37) illustrates the variation of asymmetric loads.

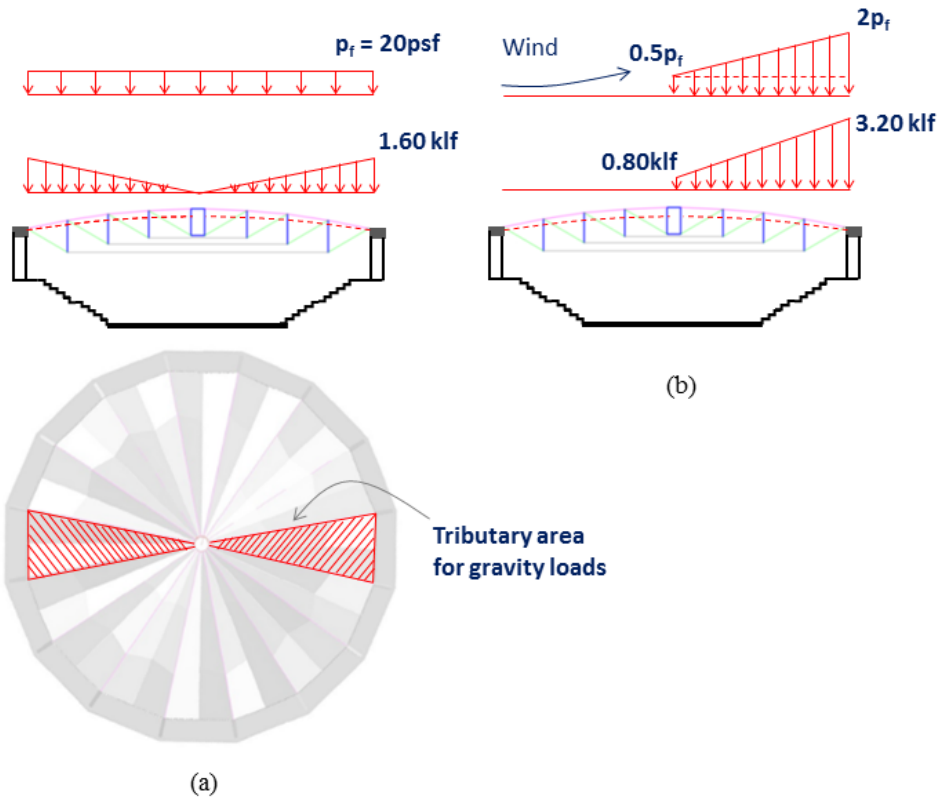

Figure 3.3 Snow load distribution per ASCE 2010c
(a) Symmetric Snow Load; and (b) Asymmetric Snow Load

Consequently, the load on the windward side is taken as zero and trapezoidal on the leeward side. The trapezoidal load is composed of a uniform load of $0.5p_f$ plus a triangular surcharge, which is maximum at the eaves. The asymmetric load therefore varies from $0.5p_f$ at the crown to a value of $2p_f\ C_s/C_e$ at the eave (Figure 3.2b and Figure 3.3b). This properly accounts for the effects of wind (O'Rourke, 2010). In a sense, the load at the eave is a multiple of the sloped roof snow load (p_s) divided by the exposure factor (C_e), where $p_s = 2\ p_f\ C_s$.

3.1.5 Wind Loads

Although relatively flat compared to conventional reinforced concrete domes, roof membranes of cable domes cover relatively large surface areas and, as a result, wind will have a significant effect. Therefore, careful attention must be given to the effect of winds to ensure that there is no loss of prestress in the membrane and cables. Wind tunnel tests as well as other experimental methods have successfully

been used to establish roof wind pressures for complex geometries (ASCE 2010b). Notably, these studies have shown that the relative flatness and folded form have very little impact on the main wind force resisting system (MWFRS[2]). As such, Figure 27.4-2 of ASCE/SEI 7-10 (ASCE 2010c, p.265) which pertains to spherical domes is applicable to cable domes.

Wind loads are dynamic loads, but they can be conveniently expressed as equivalent static loads proportional to the exposed area of the roof surface. The *directional procedure* for design of the MWFRS as described in Chapter 27 of ASCE/SEI 7-10 (ASCE 2010c) is followed. Only the main wind force resisting system (MWFRS) is considered in the analysis and the components and cladding (C&C) are neglected. The Allowable Stress Design (ASD) load factor of 0.6 for wind loads reduces the peak wind loads obtained from the *directional procedure* to service load values.

Table 3-1 Parameters for estimating wind pressure

Location	Midwest region, US (for example)
Topography	Homogeneous
Terrain	Open
Dimensions	400 ft. diameter in plan, eave height = 60 ft., dome rise = 33.2 ft.
Roof Framing	Cable-truss
Cladding	PTFE membrane
Exposure	Exposure Category = C
Building Classification	Category III (Table 1.5-1, ASCE7-10), sports arena
Enclosure	The roof structure is enclosed with PTFE membrane.
Basic Wind Speed, V	120 mph
Wind Directionality Factor, K_d	0.95, Section 26.6 and Table 26.6-1
Velocity Pressure Coefficient, K_z	Obtained from Section 27.3.1 and Table 27.3-1 for Exposure C
Topographic Factor, K_{zt}	1.0 for homogeneous topography, Section 26.8.2

The main parameters for estimating the design wind pressures are listed in Table 3-1.

The velocity pressure q_z can be now computed as:

$$q_z = 0.00256\, K_z K_{zt} K_d V^2 \ psf \qquad (3.2)$$
$$= 0.00256\, K_z (1.0)(0.95)(120)^2\, psf \quad = 35\, K_z \ psf$$

Values of K_z and the resulting velocity pressures are given in Table 27.3-1 of ASCE/SEI 7-10 (ASCE 2010c, p.261).

[2] MWFRS includes the radial cable trusses, valley cables and the perimeter compression ring.

Studies have shown very little windward pressure on the roofs because of their low rise. The external wind pressure coefficients C_p [3] are therefore taken as negative or as suctions throughout the roof; its value depends on the shape of the structure, wind direction and position of contact of wind with the roof (Figure 3.4).

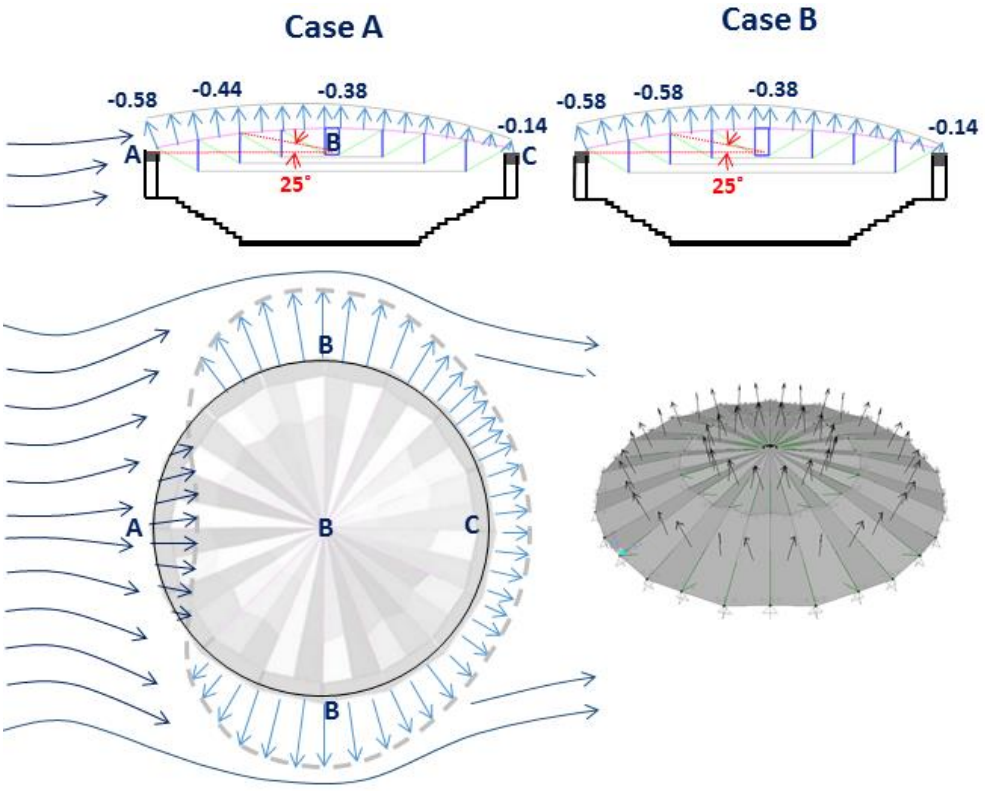

Figure 3.4 Pressure coefficients C_p for Case A and Case B

Two load cases are required for the MWFRS loads on domes (Figure 3.4). Case A is based on linear interpolation of C_p values from point A to B and from point B to C. Case B uses the pressure coefficient at A for the entire front area of the dome up to an angle $\theta = 25°$, then interpolates the values for the rest of the dome as shown in Case A. The coefficients found for Case A govern (Figure 3.5) and are, therefore, used for calculating the design wind pressure from:

$$p = qGC_p - q_i(GC_{pi}) \tag{3.3}$$

Details of the calculation procedure are provided in Appendix E.

[3] C_p is the external wind pressure coefficient, a measure of the variation of external wind pressure on the dome surface depending on the structural configuration and direction of the wind.

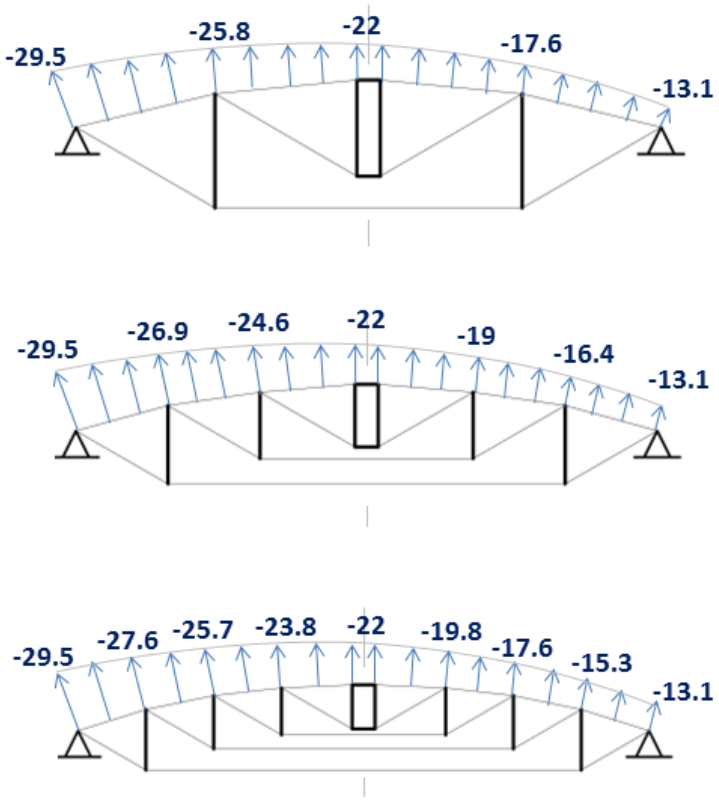

Figure 3.5 Design wind pressures (psf) using Case A for domes *N*1 through *N*3

In practice, more accurate estimates of wind pressure coefficients are obtained from wind-tunnel tests, particularly when local effects of wind on particular components is a concern.

3.1.6 Other Loads

In addition to the aforementioned loads, other environmental and construction loads must be considered in cable dome design. The effects of cable relaxation, temperature differentials and erection loads can adversely affect structural behavior if not accounted for appropriately.

i. Relaxation Loads

Cable relaxation may lead to slackening of cables, which will reduce the overall stiffness of a system and result in greater deformations. However, as mentioned in Section 2.2, the steel ropes and strands are pre-stretched to elevate their elastic modulus and eliminate cable relaxation. Cable members may, therefore, be assumed to be unaffected by effects of relaxation.

ii. Temperature Loads

The main structure, i.e., cable-trusses and valley cables, is sheltered and hence its temperature is controlled. Thermal effects, therefore, may not be a concern. However, extreme temperature differentials due to fire or power loss will significantly affect the structural integrity and thereby reduce the structure's stiffness (Cuoco 1997). This may happen due to thermal deformation, thermal stresses, thermal buckling and vibrations; hence, temperature effects must be considered as part of the design. Temperature effects are out of the scope of this dissertation.

iii. Erection Loads

The loads to which a cable dome structure may be subjected to during erection although temporary, can be significant. In this study, it is assumed that adequate care will be taken to ensure that no members are overstressed during the erection process. Although erection loads are out of the scope of this dissertation, they are a good subject for further research.

iv. Earthquake Loads

Earthquake (or seismic) loads are usually not a factor in design due to the low mass of the membrane and lightweight structural system (Campbell, 2009). Seismic performance of domes is therefore out of the scope of this research. That said, earthquake loads must be considered in the design of the compression ring and supporting columns.

3.2 Load Combinations

Cable domes are simultaneously subjected to the action of several loads. As such, the design of members should be based on the worst-case load combination. The more popular and current design procedure in structural engineering is the Load and Resisting Factor Design (LRFD), also called *strength design,* in which the service load is projected to an ultimate load level at which failure occurs. Load factors are applied to service loads, and members are selected or designed such that they have enough strength to resist the factored loads. In addition, a capacity-reduction factor is multiplied by the theoretical member strength. The member force based on the combination of factored loads must be less than the reduced member strength. Cable and membrane structures, because of geometric and material nonlinearities, present a challenge to the structural engineer not only in the determination of the applied loads but also in the understanding

of material behavior as per ASCE/SEI 55-10 (ASCE 2010b). Superposition of load effects with varying amplification factors is not applicable to nonlinear structures, and thus the strict application of LRFD will give erroneous results. Furthermore, the ultimate load approach may result in individual cables being stressed beyond their accepted level under service loads, while still satisfying the ultimate load design requirements (Gossen, 2004). The presence of prestress (an internal force) which is part of resistance, further complicates the use of LRFD. As a consequence of these peculiarities, there is currently no LRFD standard methodology for tensioned fabric structures (Campbell 2009).

Current industry practice uses the Allowable Stress Design (ASD) load combinations from ASCE/SEI 19-10 (ASCE 2010a) which follow the ASCE/SEI 7-10 Standard (ASCE 2010c). The design specifications define maximum allowable stresses that may not be exceeded under any load combination. This allowable maximum stress is obtained by dividing the yield stress or ultimate tensile strength by a factor of safety (usually taken as 2.2 for cables).

That said, different design standards have been used for the same structure, e.g., to design foundations using ASD and superstructure using LRFD. Similarly, designers of cold-formed steel and open-web steel joists often design using ASD, while designers of structural steel use LRFD (ASCE 2010c). In the same way, while the roof structure of cable domes is designed per ASD, the supporting compression ring and perimeter walls typically made of reinforced concrete are designed using LRFD.

The ASD load combinations from ASCE/SEI 19-10 are presented in Table 3-2. The notations used for dead load, snow load, wind load, prestress and concentrated load are D, S, W, P and C_n, respectively. The subscripts "*s*" and "*as*" refer to symmetric and asymmetric loads respectively.

Load Case 1 (or LC-1 in Table 3-2) comprises the structure self-weight and superimposed dead loads on the structure during the erection of a cable dome. The prestressed geometry is the outcome of LC-1. The prestressed structure will then be under the action of external loads. LC-2a and LC-2b referring to gravity-only combinations that include the effect of symmetric and asymmetric snow loads, respectively (Figure 3.3). LC-3a and LC-3b address the situation in which the effects of uplift forces counteract the effect of gravity loads.

Table 3-2 Allowable Stress Design (ASD) Load Cases and Load Combinations

Load Case	Load Combinations
LC-1	D + P (for prestressed configuration)
LC-2a	D + P + S_s (symmetric snow on full-span)
LC-2b	D + P + S_{as} (snow on half-span)
LC-3a	D + P + 0.6W_s (symmetric suction on full-span)
LC-3b	D + P + 0.6W_{as} (suction on half-span)
LC-4a	D+ P + 0.75(0.6W_s) + 0.75 S_s
LC-4b	D+ P + 0.75(0.6W_{as}) + 0.75 S_s
LC-4c	D+ P + 0.75(0.6W_s) + 0.75 S_{as}
LC-4d	D+ P + 0.75(0.6W_{as}) + 0.75 S_{as}
LC-5a	0.6D + 0.6P +0.6W_s
LC-5b	0.6D + 0.6P +0.6W_{as}
LC-6	D + P + C_n

Earthquake and wind loads need not be assumed to act simultaneously. As wind will produce the most unfavorable effects for the specified dome size and location, earthquake loads are neglected from LC-3a and LC-3b (and other later cases). LC-4a through 4d comprise combinations that include loads that vary with time in addition to dead loads. The possibility that all the variable loads will attain their maximum value at the same time is highly unlikely. As such, a reduction in the combined effect of variable loads is accomplished through the 0.75 factor as per the ASCE/SEI 7-10 (ASCE 2010c). LC-5a and 5b, like LC-3a and 3b, address the combined effects of uplift forces and gravity loads. This eliminates an inconsistency in the treatment of counteracting loads in allowable stress design and strength design, emphasizing the importance of checking variability in the destabilizing load. The factor 0.6 on dead loads is necessary for maintaining comparable reliability between strength design and allowable stress design and the factor 0.6 on prestress is for additional safety. LC-6 is a combination that accounts for a single concentrated load (C_n) of 100 kips attached to the bottom of one of the outermost struts. This load may be from a heavy lighting fixture, catwalk or a combination of such permanent attachments.

3.2.1 Influence Surface Analysis and Critical Load Combinations

A three-dimensional analysis would be cumbersome considering that a design must be checked for 12 different load combinations (Table 3-2). To simplify the procedure and to identify the critical load combinations, influence surface analysis is used. Constructing an influence surface for the design of critical members may eliminate several of these load combinations.

The influence surface analysis uses the *Müller-Breslau Principle* as a clever technique for the application of either the *Maxwell-Betti Reciprocal Work Theorem* or the *Principle of Virtual Work*. Although the Müller-Breslau Principle is limited to structures that exhibit linear-elastic behavior, it may be applied to cable domes whose members are adequately prestressed and for small loads and deformations to help identify the governing load combinations for design.

To illustrate the procedure using the Virtual Work approach, consider the two-dimensional model of the *N*1:*n*16 dome (Figures 3.6a and 3.6b). First take Figure 3.6b as the "actual" loading case with a load *W* applied at node C and consider Figure 3.6a as the virtual displacements. Imagine a turnbuckle inserted in cable AD were turned so that cable AD was shortened by a unit amount, the structure would take the shape indicated by the dashed configuration (Figure 3.6a). Let F_{AD} be the tension in diagonal AD due to load *W* (Figure 3.6b).

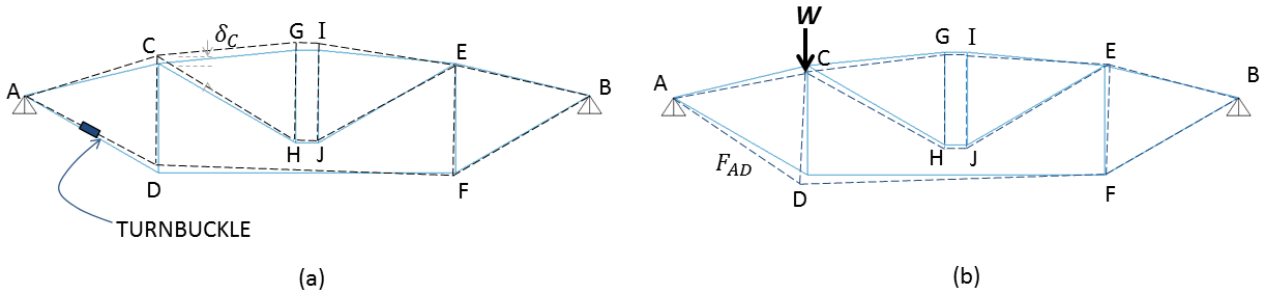

Figure 3.6 (a) Deformed configuration due to unit shortening of diagonal AD; and
(b) Deformed configuration due to application of load *W* at node C

The external virtual work is written as

$$W_{ext} = -W \cdot \delta_C + F_{AD} \cdot 1 \tag{3.4}$$

where δ_C is the vertical displacement caused by the unit displacement of member AD, and the negative sign is because the displacement δ_C is in the direction opposite to load *W*.

And the internal virtual work is given as

$$W_{int} = -\sum N_i e_i \tag{3.5}$$

where N_i are the member forces in Figure 3.6b and e_i are the member elongations in Figure 3.6a.

According to the *Principle of Virtual Work*, for a structure in equilibrium the algebraic sum of the virtual work done by all forces acting on the structure is zero for any virtual displacement of the structure. Thus,

$$-W\delta_C + F_{AD}1 - \sum N_i e_i = 0 \tag{3.6}$$

Now consider Figure 3.6a as the "actual" loading case and Figure 3.6b as the virtual displacements. As there is no "cut" in Figure 3.6b, the external virtual work is zero.

$$W_{ext} = F_{AD} \cdot 0 = 0 \tag{3.7}$$

And the internal virtual work is given as

$$W_{int} = -\sum n_i E_i \tag{3.8}$$

where n_i are the member forces in Figure 3.6a and E_i are the member elongations in Figure 3.6b. Thus,

$$\sum n_i E_i = 0 \tag{3.9}$$

But,

$$\sum N_i e_i = \sum n_i E_i = 0 \tag{3.10}$$

Equation 3.6 therefore becomes

$$-W \cdot \delta_C + F_{AD} \cdot 1 = 0 \tag{3.11}$$

which gives

$$+F_{AD} = W \cdot \delta_C \tag{3.12}$$

For loads applied at several or all top nodes of the struts, Eq. 3.12 can be generalized as

$$F_{cm} = \sum_{i=1}^{n} (W_i)(\delta_i) \tag{3.13}$$

where W_i = dead, snow, or wind load at node i
cm = critical member
and δ_i = influence coefficients, for unit deformation assigned to a critical member

To summarize the procedure, a unit axial distortion is first imposed on a single critical member of the prestressed dome. As a result, the vertical displacements of each roof joint will be the influence coefficients for the axial force in that member for gravity loads as well as for the vertical component of wind suction loads. Only the vertical components of wind suction forces (in terms of influence coefficients) need to be considered in the calculation as the horizontal components will cancel each other out for symmetric loading. For asymmetric loading, the vertical components will be dominant considering the low rise of the domes. The governing load combination for an individual member can be determined by multiplying vertical deflections of roof nodes resulting from a unit distortion in that member times the nodal loads across the roof resulting from the load combinations given in Table 3-2. The application of influence surface analysis on representative cable domes will be discussed next.

3.2.2 Numerical Results

To illustrate the influence surface analysis procedure, consider the *N*1:*n*16:*r/L*0.083:*d/L*0.14 dome with the node and member labels as shown in Figure 3.7. The dome is assumed to be located in an area prone to high snow loads and reasonable wind loads. Assuming the presence of full axisymmetric snow loads, a two-dimensional all-truss model is used for the estimation of prestressing force levels and preliminary member sizing. Preliminary member areas are selected based on a cable arrangement adapted from Section 2.4. The ridge cable cross-sectional areas (inner and outer) are 3.3 in^2 and 5.5 in^2, respectively; the diagonal cable areas are 2.17 in^2 and 4.34 in^2, respectively, and the hoop cable area is 9.51 in^2. The struts areas (inner and outer) are 14.9 in^2 and 18.1 in^2 with flexural stiffness EI = 49 x 10^6 k.in^2 and 86.77 x 10^6 k.in^2, respectively.

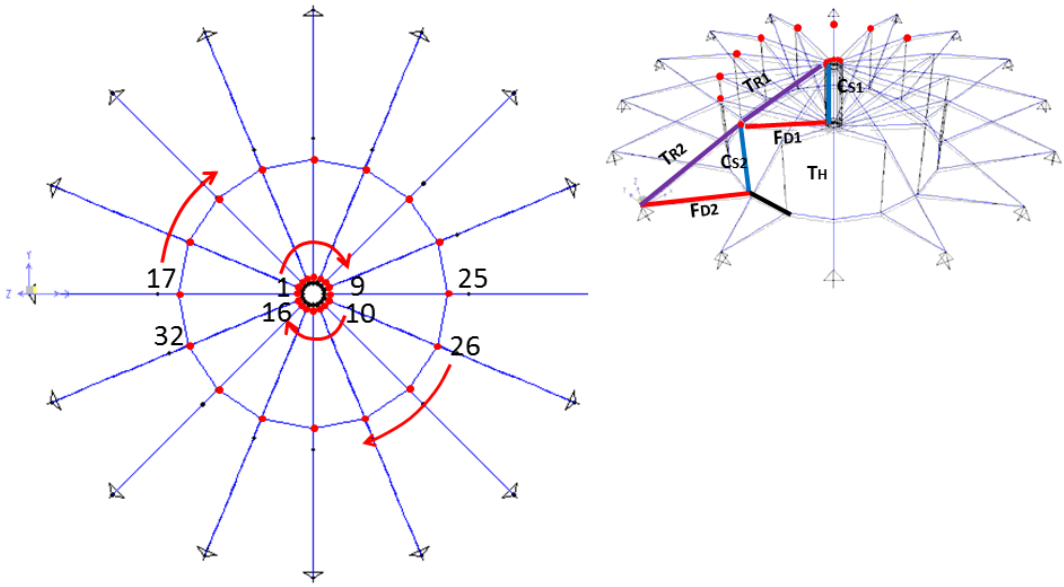

Figure 3.7 Node and member labels for influence surface analysis

The highlighted members (Figure 3.7) were given a unit deformation, each done as an individual case. The vertical deflections of the roof nodes caused by the unit member deformation were determined (Table 3-3) and then multiplied with the applied loads at the respective nodes (Eq. 3.13). The result is the magnitude of the internal member force in the selected members (Table 3-4).

The influence coefficients are better understood from the illustrations of influence surfaces in Figure 3.8. From Table 3-3, clearly, the design of outer members (T_H, F_{D2} and C_{S2}) is governed by axisymmetric loadings (LC-2a: symmetric snow load case). Noting that the inner ridge cable (T_{R1}) attached to the tension ring, experiences a reduction in tension under axisymmetric gravity loading, LC-2a will still govern the stability of the vertical strut due to the loss in ridge tension. However, asymmetric loadings (LC-4d) will govern the design of the inner cables. The analysis results confirmed the general intuitive understanding while providing fresh insights into the governing load combinations for the different cable members. Any negative values for cable forces in Table 3-3 would have indicated cables that went slack. For such cases, prestressing force levels must be increased to further stiffen the structure.

Table 3-3 Nodal Displacements or Influence Coefficients

Node #	F_{D2} shortened by 1 in.	F_{D1} shortened by 1 in.	T_H shortened by 1 in.	C_{S2} elongated by 1 in.	C_{S1} elongated by 1 in.	T_{R2} shortened by 1 in.	T_{R1} shortened by 1 in.
1-16	0.1023	0.0937	0.2266	0.0515	0.0465	-0.0257	-0.1069
17	0.1689	-0.9982	0.2306	0.2239	-0.1381	-1.0709	-0.1759
18	0.0889	0.1626	0.2310	0.0475	-0.0107	-0.0979	-0.2399
19	0.1078	0.1908	0.2240	0.0830	0.0445	-0.0223	-0.1903
20	0.1027	0.1394	0.2147	0.0681	0.0339	0.0011	-0.1216
21	0.0947	0.0748	0.2049	0.0470	0.0140	0.0212	-0.0446
22	0.0866	0.0098	0.1961	0.0257	-0.0032	0.0404	0.0319
23	0.0797	-0.0454	0.1893	0.0074	-0.0171	0.0568	0.0969
24	0.0751	-0.0825	0.1857	-0.0047	-0.0264	0.0679	0.1408
25	0.0735	-0.0956	0.1857	-0.0090	-0.0297	0.0722	0.1566
26	0.0751	-0.0828	0.1893	-0.0048	-0.0264	0.0689	0.1419
27	0.0797	-0.0460	0.1961	0.0074	-0.0171	0.0584	0.0991
28	0.0866	0.0091	0.2049	0.0256	-0.0032	0.0425	0.0346
29	0.0948	0.0741	0.2148	0.0470	0.0140	0.0235	-0.0417
30	0.1030	0.1388	0.2244	0.0681	0.0340	0.0036	-0.1187
31	0.1068	0.1893	0.2287	0.0824	0.0443	-0.0213	-0.1880
32	0.0891	0.1625	0.2310	0.0476	-0.0107	-0.0965	-0.2385

Table 3-4 Internal Member Forces (kips) in a N1:n16:r/L0.083:d/L0.14 located in a high-snow region

LC - #	ASD Load Combinations	F_{D2}	F_{D1}	T_H	C_{S2}	C_{S1}	T_{R2}	T_{R1}
LC - 1	D + P	71.2	50.3	380	83	24	124	76.9
LC – 2a.	D + P + S_b	307	54	682	152	25.9	53.4	5.0
LC – 2b.	D + P + S_{ub}	223	32.2	503	90.9	15.8	153	122
LC – 3a.	D + P + 0.6 W_b	67.8	49	151	30.9	23.3	178	131
LC – 3b.	D + P + 0.6 W_{ub}	107	34.4	244	36.6	16.9	200	166
LC – 4a.	D + P + 0.75 (0.6 W_b) + 0.75 S_b	196	52.1	434	95.4	24.9	111	63.3
LC – 4b.	D + P + 0.75 (0.6 W_{ub}) + 0.75 S_{ub}	225	41.2	504	99.7	20.1	129	90.1
LC – 4c.	D + P + 0.75 (0.6 W_{ub}) + 0.75 S_b	132	35.7	300	49.8	17.3	186	151
LC – 4d.	D + P + 0.75 (0.6 W_b) + 0.75 S_{ub}	161	24.8	370	54.1	12.5	203	178
LC – 5a.	0.6D + 0.6P + 0.6W_b	37	26	83	15.5	11.5	107	81.7
LC – 5b.	0.6D + 0.6P + 0.6W_{ub}	60.4	17.3	139	19	7.6	121	103

Further, the *N*1:*n*16:*L*400:*r/L*0.083:*d/L*0.14 dome was considered to be situated in a coastal area known for its occasional extreme wind speed. For Risk Category-II, the wind speed is assumed to be 168 psf. The wind pressure calculations are done as described in Appendix E. The governing load combinations are determined from a separate influence surface analysis. The final member forces, as obtained from the analysis are presented in Table 3-5.

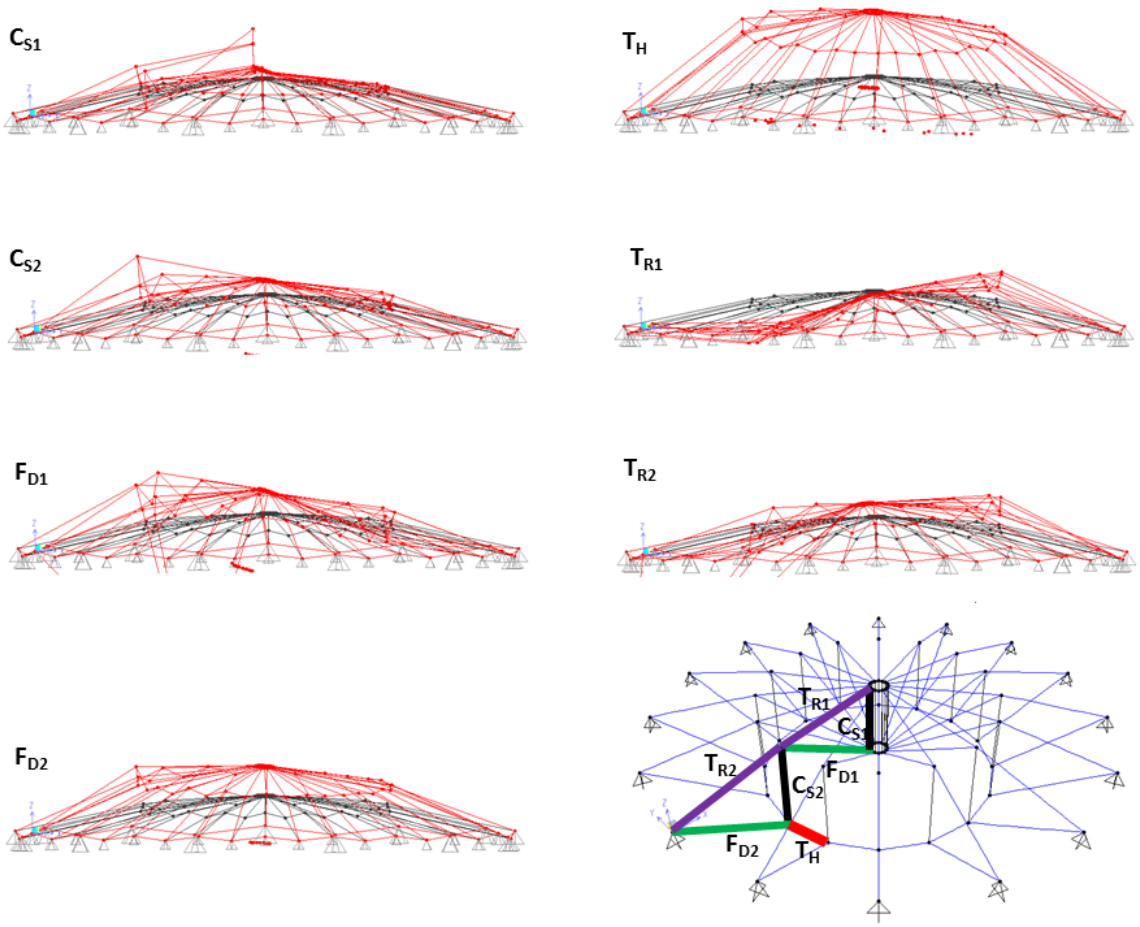

Figure 3.8 Influence Surface (in red) for *N*1:*n*16:*L*400:*r/L*0.083:*d/L*0.14; Scale = 2000

The results show that several cable members went into compression (in red) for multiple load cases (LC-3a, 4c, 5a and 5b). As such, the assigned prestressing forces are unacceptable and must be increased to overcome the significantly high negative forces in the hoop and outer diagonal cables. It should be kept in mind that these results are specific for the geometry and prestressing force levels for an *N*1:*n*16. Increasing the number of polygon sides (*n*), i.e., increasing the number of trusses will lead to a more reasonable load distribution. But doing so may result in a more flexible dome (hoop stiffness reduces with increase in *n*) and serviceability will have to be monitored.

Table 3-5 Internal member forces (kips) in a *N*1:*n*16:*r/L*0.083:*d/L*0.14 dome located in a high-wind region

LC - #	ASD Load Combinations	F_{D2}	F_{D1}	T_H	C_{S2}	C_{S1}	T_{R2}	T_{R1}
LC - 1	D + P	171	50.3	380	83	24	124	76.9
LC – 2a.	D + P + S_b	253	52.5	561	124	25.2	81.5	33.8
LC – 2b.	D + P + S_{ub}	202	39.4	454	87.7	19.1	141	104
LC – 3a.	D + P + 0.6 W_b	-90.5	48.7	-75.8	-20.6	23.1	231	183
LC – 3b.	D + P + 0.6 W_{ub}	3.4	19.1	109	-9.4	10.2	277	255
LC – 4a.	D + P + 0.75 (0.6 W_b) + 0.75 S_b	36.2	50.8	174	36.2	24.2	173	124
LC – 4b.	D + P + 0.75 (0.6 W_{ub}) + 0.75 S_{ub}	107	28.6	313	44.6	14.5	207	178
LC – 4c.	D + P + 0.75 (0.6 W_{ub}) + 0.75 S_b	-2.0	40.9	93.3	8.8	19.7	218	177
LC – 4d.	D + P + 0.75 (0.6 W_b) + 0.75 S_{ub}	68.5	18.8	232	17.2	10.0	252	231
LC – 5a.	0.6D + 0.6P + 0.6W_b	-57.9	25.9	-52.9	-15.4	11.4	139.1	113.2
LC – 5b.	0.6D + 0.6P + 0.6W_{ub}	-1.6	8.1	58.2	-8.6	3.6	167	156

The influence surface analysis procedure was applied to *N*2 and *N*3 domes, specifically to *N*2:*n*16:*L*400:*r/L*0.083:*d/L*0.09 and *N*3:*n*16:*L*400:*r/L*0.083:*d/L*0.07 domes to determine their performance (Appendix B). For the *N*2 dome, the full symmetric snow load combination LC-2a clearly governed the design of the hoop cables, diagonal cables and struts, and LC-5 governed the design of ridge cables. Smaller exposure areas to wind loads and more members to resist the applied loads led to a more reasonable load distribution. No cables went slack. Similarly, the results for the *N*3 dome indicate that LC-2a governed the design of the hoops, diagonals and struts. Again, the results were reasonable and no cables went slack. It can be concluded that for *N*1 domes with the specified geometries presented herein, prestressing force levels and loadings are vulnerable to wind uplift forces. It can be deduced that for *N*1 domes, a higher n = 24 or 32 will lead to an efficient design.

3.3 Summary

Dead, live, snow and wind are the typical loads for which a cable dome must be designed. Besides these usual loads, prestress loads make a cable dome interesting and complex, both in terms of form-finding and structural behavior. The complexities presented by nonlinearities and inclusion

of prestress makes the ASD procedure the preferred design methodology for cable domes.

Since the Müller-Breslau principle may be applied to structures displaying linear behavior in all members, it cannot be applied to cable domes that have cables going into compression. Therefore, it is essential to provide adequate prestressing force levels that satisfy all load combinations, in order to benefit from the Müller-Breslau principle-based influence surface analysis.

The following observations were made from the influence surface analysis of the sample dome:

1. For the prescribed geometry, member areas and prestressing forces, the *N*1:*n*16 dome was vulnerable to wind suction loads (Table 3-5) when compared to *N*2:*n*16 and *N*3:*n*16 domes (Appendix B). Several cables went slack for various load combinations that included symmetric and asymmetric wind uplift forces.
2. When adequately prestressed, LC-2a (full symmetric snow load) governed the design of the main load carrying members, i.e., the outermost hoop and diagonal cables.
3. Even for domes governed by gravity loading, the prestressing forces may need to be increased to stiffen the structure sufficiently against wind suction forces (Table 3-4).
4. Influence surface analysis provides guidance to a designer about the loading combinations that give the largest downward nodal forces and the largest net uplift forces. For example, the following symmetric load combinations (LC-2a, LC-3a, LC-4a, and LC-5a) could be considered. By observation, LC-2a (full symmetric snow load) should give the largest downward nodal loads since the wind forces are suctions and LC-5a (reduced dead loads plus wind uplift) would give the largest net upward nodal force, which actually could be a small downward force and therefore not control. A simple check can inform about any net uplift.

The Müller-Breslau principle can be extended to examine the influence surface for nodal displacements. This way, the critical loading combination that would result in the maximum vertical deflection at a particular roof joint can be found.

CHAPTER 4 GEOMETRIC NONLINEAR MODEL

In order to compare and verify the analysis results from SAP2000, the geometric nonlinear analysis procedure for analyzing cable domes was formulated and programmed using MATLAB. Large displacements are accounted for and relevant assumptions about material properties, member behavior and support idealization are included in the program. In Section 4.1, concepts of nonlinearity and geometric stiffness are discussed. The stiffness of a member is shown to be directly proportional to the amount of tension force in the member and inversely proportional to its length. The geometric nonlinear analysis procedure is developed in Section 4.2. The nonlinear equilibrium equations are then solved for the structural response using the Newton-Raphson iteration technique which shows superior convergence. The results from SAP2000 and MATLAB are verified in Section 4.3.

4.1 Nonlinearity and Geometric Stiffness

Two types of nonlinearities, namely material and geometric nonlinearities may exist in cable domes. Material nonlinearity, associated with the inelastic behavior of a member, is characterized by a force-deformation relationship that measures strength against translational or rotational deformation. Material nonlinearity is invoked in order to understand the behavior beyond yielding and at ultimate.

Geometric nonlinearity is the result of large displacements that cause significant geometrical changes to the structure. Cable trusses and cable domes experience large displacements, which cause significant changes in geometry of the system; as such, the linear theory is not applicable. A cable changes its geometric configuration as well as load distribution to accommodate applied displacements or loads. Equations of equilibrium are, therefore, written for the deformed configuration, unlike in a conventional truss structure where equilibrium equations are established for the undeformed configuration (Urelius, 1972, Kuznetsov, 1991). Although displacements may be large, the associated strains will be small; a linear-elastic constitutive relationship can therefore be assumed.

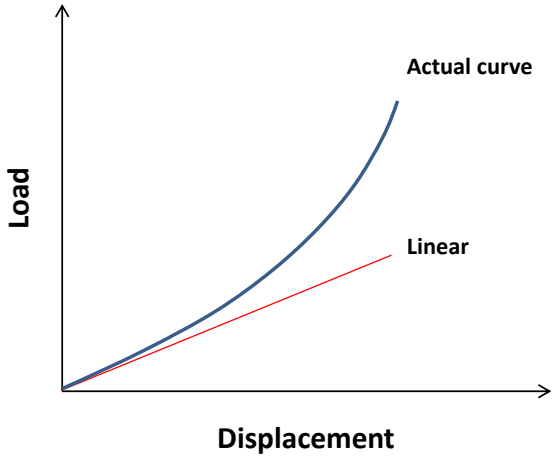

Figure 4.1 Nonlinear response of cable-strut structures

When cable structures undergo deformations due to loads, their resistance to further deflection increases, i.e., they become stiffer (Figure 4.1). This stiffness, which is in addition to the inherent *elastic stiffness*, is called the *geometric stiffness*. To understand the effects of geometric changes, consider an axial member of length L, cross-sectional area A, modulus of elasticity E and with an axial tensile load of F. The *change in length* Δ_a is found as:

$$\Delta_a = \frac{FL}{AE} \tag{4.1}$$

Define the *elastic stiffness* k_e as $\frac{F}{\Delta_a}$. Therefore,

$$k_e = \frac{AE}{L} \tag{4.2}$$

Now consider the two bar structures shown in Figure 4.2 (Levy and Spillers 1995). In its original horizontal configuration (Figure 4.2a), the structure will not be in equilibrium for any vertical loading.

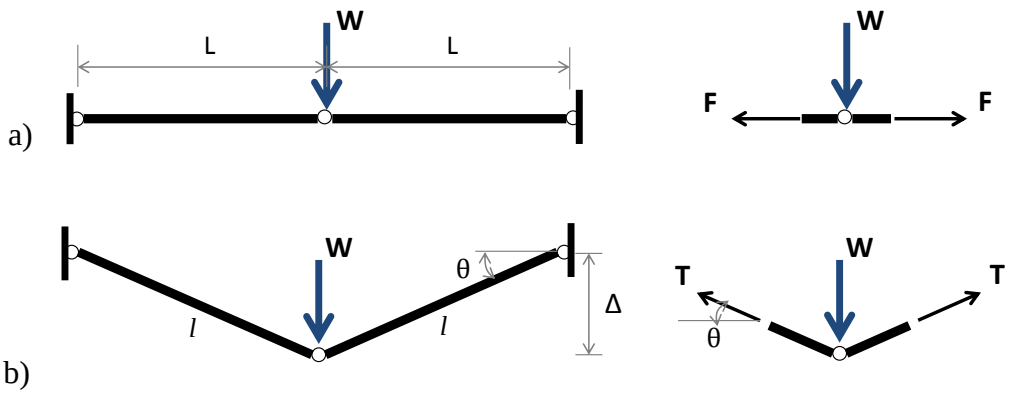

Figure 4.2 Joint equilibrium in (a) undeformed geometry; and (b) deformed geometry

The structure will achieve an equilibrium configuration only after undergoing a vertical deflection (Figure 4.2b). For small angles θ, assume that the horizontal prestress force equals the tension in the members. Equilibrium of the vertical forces gives,

$$W = 2T \sin\theta \tag{4.3}$$

For small angles,

$$\sin\theta = \theta = \frac{\Delta}{L} \tag{4.4}$$

Substituting Eq. 4.4 in Eq. 4.3 gives

$$W = \frac{2T}{L}\Delta \tag{4.5}$$

The geometric joint stiffness k_g is defined as $\frac{W}{\Delta}$ and therefore written as:

$$k_g = \frac{2T}{L} \tag{4.6}$$

Clearly, the geometric stiffness is a function of the tension T in the bar, and increases with T. In the case of a structure with axial members, the single elastic stiffness term becomes its elastic stiffness matrix. The total stiffness matrix for a cable dome can be deduced as the sum of the geometric stiffness and elastic stiffness. The derivation of the total stiffness matrix is explained next.

4.2 Nonlinear Analysis Formulation

A cable dome's desired shape is usually established by architectural and aesthetic considerations. The form-finding procedure is fundamental to cable dome design. This form-finding problem is to determine the prestressed configuration of a cable dome structure under self-weight and member prestressing forces, i.e., LC-1 (Section 3.2).

After the desired dome configuration is determined from LC-1, the prestressed structure is analyzed for the remaining load combinations. Should some cables go slack or should the vertical deflections exceed the serviceability criterion under any of these load combinations, the prestressing forces are increased. After the prestressing force levels are determined to be adequate, the dome is again analyzed for different design variants whereupon the process is repeated.

Certain assumptions are made to simplify the analysis; these considerations, which take into account material properties, support conditions and the nature of the forces that can be resisted by the members are: The commercial program SAP2000 is used for the nonlinear (geometric and material) analysis of the cable domes studied. Some assumptions are made to simplify the analysis. These considerations, which take into account material properties, support conditions and the nature of forces that can be resisted by the members are:

1. *Large displacement and small strain*. As previously mentioned, cable domes are stiffened and stabilized by prestressing the diagonal cables. Although the displacement may be large due to the flexibility of the cables, the associated strain will be small for member stresses within the elastic range.
2. *Material and Geometric Nonlinearity.* A bi-linear variation of stress-strain is assumed for the strand between the unloaded state and the ultimate state. As such, the first linear variation is from the origin and a yield strain of 1.1% (corresponding to the stress of 243 ksi) with an initial Young's Modulus of 24,000 ksi. Between the yield point and the ultimate state, the stress-strain variation is approximated as a linear variation. At ultimate, the strand strain is 4% with the ultimate stress as 270 ksi (Figure 2.2). The flexibility of the cable-strut structure may result in large deformations which increase as the external loads are applied. This type of deformation-dependent response requires a geometric nonlinear analysis.
3. *Cables are tension-only members*. The cables have negligible buckling, twisting and bending strength and transfer loads by developing direct tension only (Krishna, 1978).

4. *Cables are straight-line members.* While a cable under its own weight cannot be straight, this is a reasonable assumption considering that the cables are prestressed and may overcome the effects of self-weight.
5. *Cables have constant cross-sectional areas.* Any change in cable cross-sectional areas due to stressing is neglected.
6. *Roof membrane has negligible bending stiffness*. The fabric membrane is very light (1 psf) and flexible. The membrane has negligible bending stiffness and resists only tangential membrane forces–normal and shearing. Negligible bending stiffness implies no resistance to compression stresses as well (Kuznetsov, 1991).
7. *Snow loads are applied as point loads at the top nodes of the struts*. This assumption is necessary because the fabric membrane is supported by the ridge cables which behave as axial members.
8. *Rigid perimeter beam.* The perimeter reinforced concrete beam and the supporting columns are massive members, hence they are assumed to be rigid. The supports are idealized as pins in the computer model.
9. *Cable slackening and rupture.* For computational purposes, cable slackening is taken into account by ascribing a very small value of axial stiffness $EA = 1 \times 10^{-10}$. Cable rupture is taken into account in the same way as the slackening of cables, i.e., by reducing the stiffness of cables to approximately zero whenever the tensile stress in a cable is equal to or exceeds the breaking strength.

With the preceding assumptions established, a stiffness-based finite element analysis procedure (Tezcan and Özdemir, 2000) can be formulated. Consider a planar truss (axial) member connecting nodes 1 and 2 in the *XY*-plane, where (X_1, Y_1) and (X_2, Y_2) are the nodal coordinates in the initial configuration. Under load, the member deforms and the nodes move to new locations with coordinates (x_1, y_1) and (x_2, y_2) as illustrated in Figure 4.3.

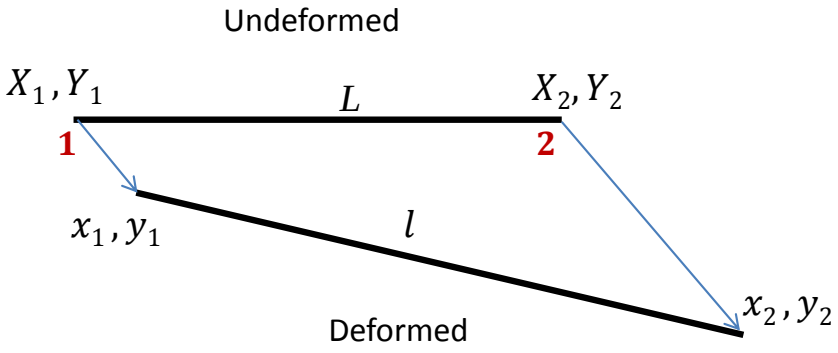

Figure 4.3 Undeformed and deformed geometry

Let u_1 and u_2 be the displacements of node-1 along the x and y axis, and u_3 and u_4 be the displacements of node-2 along the x and y axis respectively (Figure 4.4).

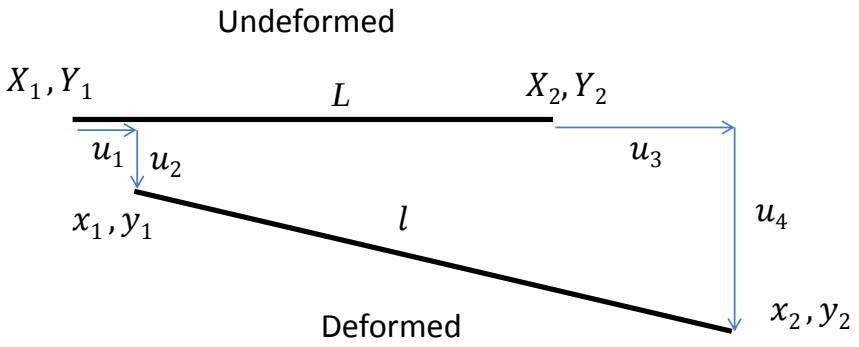

Figure 4.4 Nodal Displacements

Therefore, the net displacement along the global x-axis is:

$$u = (X_2 + u_3) - (X_1 + u_1) \tag{4.7}$$

And the net displacement along the global y-axis is:

$$v = (Y_2 + u_4) - (Y_1 + u_2) \tag{4.8}$$

The deformed length of the member is found as:

$$l = \sqrt{u^2 + v^2} = \sqrt{\left[\left(X_2 + u_3\right) - \left(X_1 + u_1\right)\right]^2 + \left[\left(Y_2 + u_4\right) - \left(Y_1 + u_2\right)\right]^2} \tag{4.9}$$

The direction cosines can be expressed as:

$$m = \cos\theta = \frac{\left[\left(X_2 + u_3\right) - \left(X_1 + u_1\right)\right]}{l} = \frac{u}{l} \tag{4.10}$$

and

$$n = \sin\theta = \frac{\left[\left(Y_2 + u_4\right) - \left(Y_1 + u_2\right)\right]}{l} = \frac{u}{l} \tag{4.11}$$

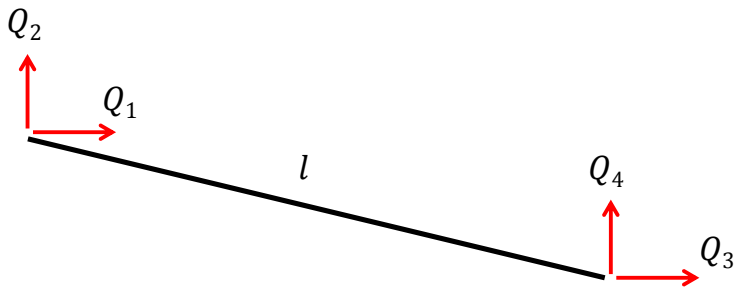

Figure 4.5 Member force components in global axes

The internal member force Q can be written in terms of the strains as

$$Q = A\sigma = AE(\varepsilon - \varepsilon_p) \tag{4.12}$$

where A is the member cross-sectional area, E is the member modulus of elasticity and ε_p is the prestrain assigned to the diagonal members.

And the member axial strain ε is defined as:

$$\varepsilon = \frac{l - L}{L} = \frac{l}{L} - 1 \tag{4.13}$$

The member force can therefore be expressed in terms of the strains as:

$$Q = \frac{AE}{L}(l - L) - AE\varepsilon_p \tag{4.14}$$

Therefore,

$$Q_1 = Q \cdot m = \left[\frac{AE}{L}(l - L) - AE\varepsilon_p \right] \frac{u}{l} \tag{4.15}$$

$$= \left[\frac{AE}{L}(l - L) - AE\varepsilon_p \right] \frac{1}{l}\left(X_2 + u_3 \right) - \left(X_1 + u_1 \right) \tag{4.16}$$

Similarly, expressions for Q_2, Q_3 *and* Q_4 can be written and expressed in vector form as:

$$\boldsymbol{Q} = \begin{Bmatrix} Q_1 \\ Q_2 \\ Q_3 \\ Q_4 \end{Bmatrix} = \begin{Bmatrix} Qm \\ Qn \\ -Qm \\ -Qn \end{Bmatrix} \tag{4.17}$$

Stiffness is defined as the change in the i^{th} force due to a unit change in the j^{th} displacement. As such, the stiffness terms of the member stiffness matrix are derived by taking partial derivatives of the end forces with respect to each of the end displacements, as:

$$k_{ij} = \frac{\partial Q_i}{\partial u_j} \quad \text{(j =1 to 4)} \tag{4.18}$$

Therefore,

$$\boldsymbol{k} = \begin{bmatrix} k_{11} & k_{12} & k_{13} & k_{14} \\ k_{21} & k_{22} & k_{23} & k_{24} \\ k_{31} & k_{32} & k_{33} & k_{34} \\ k_{41} & k_{42} & k_{43} & k_{44} \end{bmatrix} = \begin{bmatrix} \frac{\partial Q_1}{\partial u_1} & \frac{\partial Q_1}{\partial u_2} & \frac{\partial Q_1}{\partial u_3} & \frac{\partial Q_1}{\partial u_4} \\ \frac{\partial Q_2}{\partial u_1} & \frac{\partial Q_2}{\partial u_2} & \frac{\partial Q_2}{\partial u_3} & \frac{\partial Q_2}{\partial u_4} \\ \frac{\partial Q_3}{\partial u_1} & \frac{\partial Q_3}{\partial u_2} & \frac{\partial Q_3}{\partial u_3} & \frac{\partial Q_3}{\partial u_4} \\ \frac{\partial Q_4}{\partial u_1} & \frac{\partial Q_4}{\partial u_2} & \frac{\partial Q_4}{\partial u_3} & \frac{\partial Q_4}{\partial u_4} \end{bmatrix} \tag{4.19}$$

$$\boldsymbol{k} = \frac{AE}{L}\begin{bmatrix} m^2 & mn & -m^2 & -mn \\ mn & n^2 & -mn & -n^2 \\ -m^2 & -mn & m^2 & mn \\ -mn & -n^2 & mn & n^2 \end{bmatrix} - \frac{Q}{l}\begin{bmatrix} 1-m^2 & -mn & -(1-m^2) & mn \\ -mn & 1-n^2 & mn & -n^2 \\ -(1-m^2) & mn & 1-m^2 & mn \\ mn & -(1-n^2) & mn & 1-n^2 \end{bmatrix} \tag{4.20}$$

In three-dimensional problems, $\boldsymbol{k}$ will be a 6 x 6 matrix and $\boldsymbol{Q}$ will be a 6 x 1 vector. The structure stiffness matrix $\boldsymbol{K}$ is then assembled using the member stiffness matrices and destination vectors. $\boldsymbol{K}$ is the sum of elastic and geometric stiffnesses and because the geometric stiffness is dependent on the change in geometry of the structure under load, $\boldsymbol{K}$ is a function of $\boldsymbol{U}$.

Let the sum of internal forces $\boldsymbol{Q}$ and external loads $\boldsymbol{F}$ at each node *i* of the dome be represented as $\boldsymbol{R}$, the residual force vector.

Therefore,

$$\sum \boldsymbol{Q} + \boldsymbol{F} = \boldsymbol{R}(\boldsymbol{U}) \tag{4.21}$$

where $\boldsymbol{Q}$, $\boldsymbol{F}$ and $\boldsymbol{R}$ are the global internal force, external force and residual vectors, respectively.

Note that $\boldsymbol{Q}$ and $\boldsymbol{R}$ are functions of $\boldsymbol{U}$.

The response of the cable dome structure is obtained from solving the equilibrium equations:

$$\boldsymbol{K}\,\Delta\boldsymbol{U} = \boldsymbol{R} \tag{4.22}$$

Equation 4.22 is a set of nonlinear equilibrium equations. Since $\boldsymbol{R}$ is a function of the unknown displacements, there is no direct solution for the equation. Iterative numerical schemes such as the *Modified Newton-Raphson Method*, *Newton-Raphson Method* or *Incremental Loading Method* have to be used (Krishna 1978). The *Newton-Raphson Method* exhibits the much desired terminal quadratic convergence, making it an attractive iterative method and is adopted as the solution method for Eq. 4.22. The computations in this method are based on the instantaneous stiffness of the structure derived anew at each iterative cycle. The method demands significant computational effort because the stiffness matrix has to be computed at every iteration. The structure is, therefore, loaded incrementally and the equations are solved iteratively in a piecewise linear manner until the values of $\Delta\boldsymbol{U}$ or $\boldsymbol{R}$ converges to be within an acceptable tolerance.

The following steps illustrate the procedure (Figure 4.6):

1. Assume $\boldsymbol{U}^{(0)} = \boldsymbol{R}^{(0)} = \boldsymbol{0}$
2. Solve $\boldsymbol{K}^{(0)}\boldsymbol{U}^{(1)} = \boldsymbol{Q}$ to evaluate $\boldsymbol{U}^{(1)}$
3. Compute $\boldsymbol{R}^{(0)}$ using $\boldsymbol{U}^{(1)}$
4. Solve $\boldsymbol{K}^{(1)}\Delta\boldsymbol{U}^{(1)} = \boldsymbol{R}^{(1)}$ to obtain $\Delta\boldsymbol{U}^{(1)}$ which is the correction to $\boldsymbol{U}^{(1)}$

5. Determine $\boldsymbol{U}^{(2)} = \boldsymbol{U}^{(1)} + \Delta\boldsymbol{U}^{(1)}$ and $\boldsymbol{R}^{(2)}$
6. Solve $\boldsymbol{K}^{(2)}\Delta\boldsymbol{U}^{(2)} = \boldsymbol{R}^{(2)}$ and continue until $\Delta\boldsymbol{U}$ or $\boldsymbol{R(U)}$ converges to the specified limit.

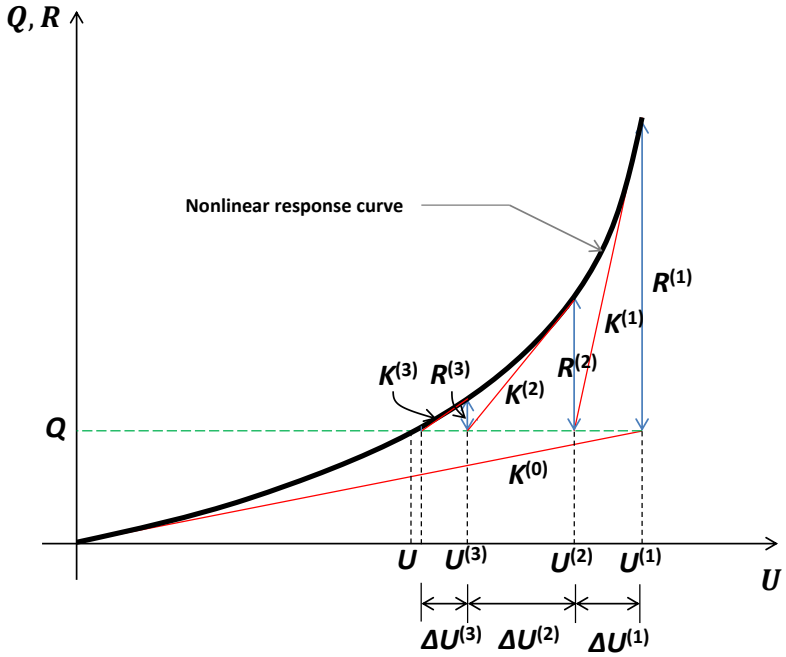

Figure 4.6 Newton-Raphson Method on a stiffening response (adapted from Krishna 1978)

The *Newton-Raphson Method* will work efficiently for adequately prestressed domes and for domes with a satisfactory rise-to-span ratio. For *N3* domes with small depth-to-span ratios, there may be convergence problems. For such cases, the *Incremental Loading Method* may provide the necessary enhancement with the application of the load in several steps. In fact, incorporating the *Newton-Raphson Method* within the *Incremental Loading Method* will form a powerful solution scheme that may handle any degree of nonlinearity.

As a summary, a flow-chart showing the fundamental steps involved in the nonlinear analysis procedure is presented in Figure 4.7.

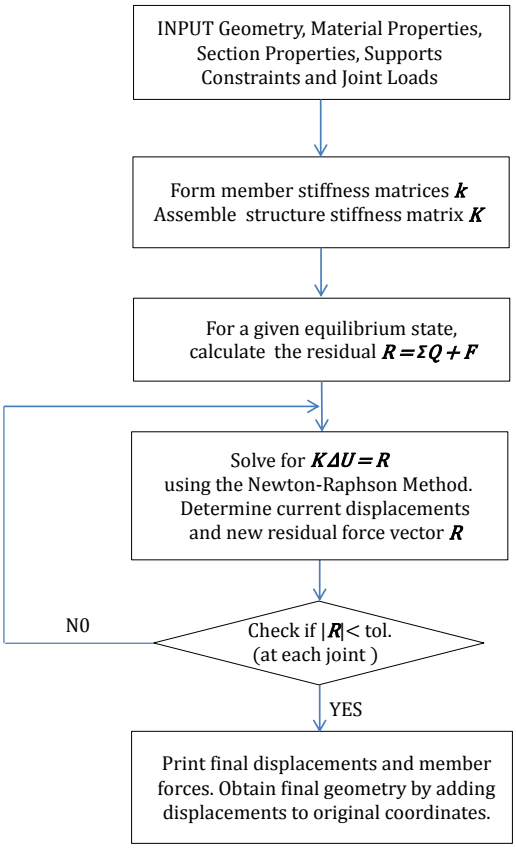

Figure 4.7 Nonlinear analysis procedure

4.3 Comparison of SAP2000 and MATLAB results

A numerical example to compare the results of the aforementioned procedure and SAP2000 is presented here. Consider the two-dimensional model of *N*1:*n*16:*L*400:*r/L*0.083:*d/L*0.14 dome (Figure 4.8). This is the planar model of the same dome in Figure 3.7.

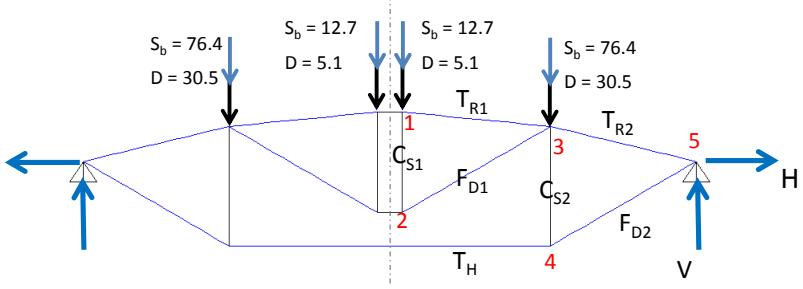

Figure 4.8 Two-dimensional model of *N*1:*n*16:*L*400:*r/L*0.083:*d/L*0.14 dome with node labels, member labels and gravity loads in kips

The results are generated using the MATLAB code supplemented in Appendix F. The results show good agreement for both LC-1 (shape-finding case) and LC-2a (uniform snow load case). The error is almost negligible for the latter case, both for member forces and joint displacements (Tables 4-1 and 4-2).

Table 4-1 Comparison of MATLAB and SAP2000 results: Member Forces (kips) for *N*1:*n*16:*L*400:*r/L*0.083:*d/L*0.14 dome

		MATLAB	SAP2000	MATLAB	SAP2000
Member Type	**Member Force (kips)**	**LC-1 D + P**	**LC-1 D + P**	Prestressed Structure **LC-2a D + P + S_b**	Prestressed Structure **LC-2a D + P + S_b**
Diagonal	**F_1**	36.27	35.84	47.76	47.54
Cable	**F_2**	147.3	146.2	297.3	296.7
Hoop Cable	**T_1**	328.2	325.6	661.5	660.3
Ridge Cable	**T_{R1}**	121	119	56.44	55.4
	T_{R2}	156.4	154	100.7	99.5
Vertical Strut	**C_1**	-17.87	-17.66	-23.6	-23.5
	C_2	-73.01	-72.42	-148.3	-148

Note: Negative sign indicates either downward reaction force or compressive member force
Numbers in parenthesis are equivalent hoop force values in a three-dimensional dome

Table 4-2 Comparison of MATLAB and SAP2000 results: Displacements (inches) for *N*1:*n*16:*L*400:*r/L*0.083:*d/L*0.14 dome

	MATLAB	SAP2000	MATLAB	SAP2000
Node Number	**LC-1 D + P**	**LC-1 D + P**	Prestressed Structure **LC-2a D + P + S_b**	Prestressed Structure **LC-2a D + P + S_b**
1	20.674	20.762	13.518	13.537
2	20.707	20.794	13.561	13.579
3	8.121	8.162	2.920	2.941
4	8.251	8.290	3.185	3.205

Note: Negative indicates downward displacement with respect to the nodal elevation obtained from LC-1

4.4 Summary

In this chapter, a geometric nonlinear analysis model was developed using the stiffness method. The effects of large displacements were considered in the formulation. The nonlinear effects of cable slackening and member yielding were also included. The Newton-Raphson iteration method was performed at each load level to solve the system of nonlinear equilibrium equations. A

MATLAB code was written based on the procedure formulated in this chapter (Appendix F). The accuracy of the analytical procedure was verified for a sample dome and the MATLAB results showed good agreement with those from SAP2000.

The nonlinear model featured in this chapter offers the possibility of including more parameters depending on the engineer's needs. Material nonlinearity may be added and parametric analyses may be automated. A code for graphical interface can be included for visualizing and plotting the deformed shaped and member forces. The code can therefore be enhanced to make a powerful tool for a structural engineer.

CHAPTER 5 DERIVATION OF TWO-DIMENSIONAL MODEL

The analysis and design of cable domes were greatly simplified in this research, using a two-dimensional model for axisymmetric loadings, leading to computational efficiency. This chapter is devoted to developing the two-dimensional model parameters equivalent to that of a three-dimensional model. In Section 5.1, the geometrical and nodal force equilibrium relationships are derived. The two-dimensional hoop area, force and stiffness parameters are derived using the *Principle of Virtual Work* in Section 5.2. In Section 5.3, preliminary member areas and prestressing force levels are computed using a truss model under full snow load. In Section 5.4, the results from the two-dimensional analysis are compared and validated with the results from a three-dimensional analysis. In Section 5.5, an "all-radial dome" is analyzed and compared with a conventional cable dome. The "all-radial" dome has some unique characteristics with regard to its cable weight and construction ease. The challenge, like in conventional radial domes, is to find a solution to enhance the torsional stiffness of the overall system.

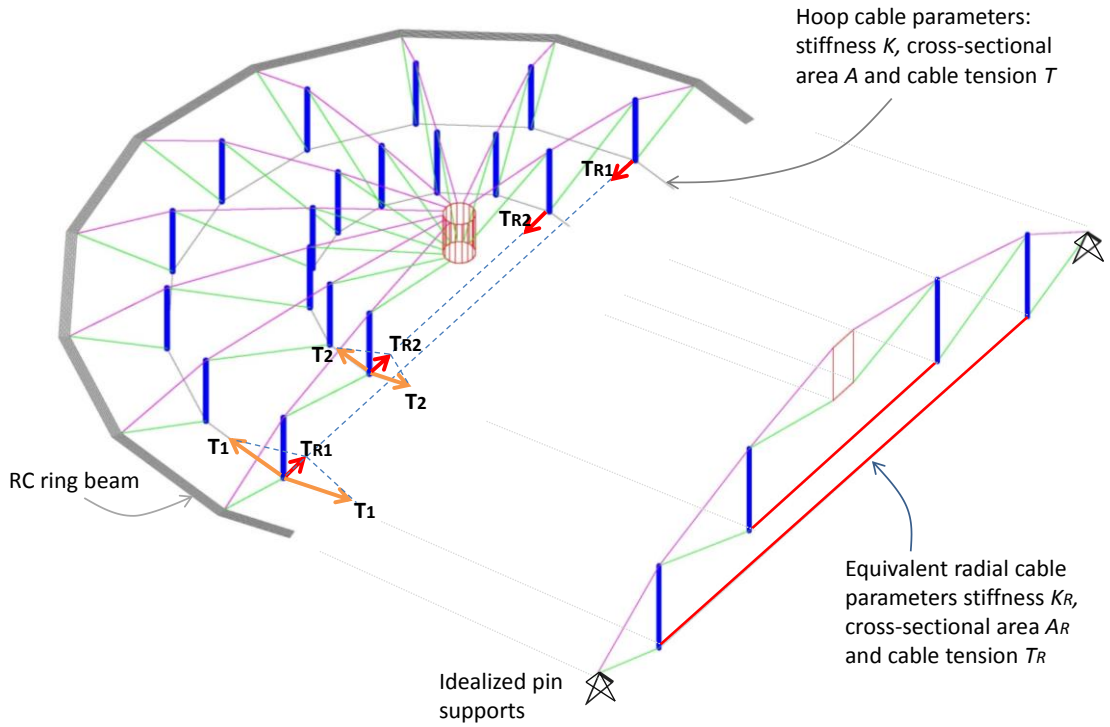

Figure 5.1 Three-dimensional hoop parameters and equivalent two-dimensional parameters for an *N*2:*n*16 dome

5.1 Geometry and Force Relationships

To understand static behavior, a cable dome was idealized as a set of two-dimensional radial trusses. To achieve this, hoop cables were replaced by radial cables to form an equivalent two-dimensional model (Figure 5.1). The notations used for the hoop cable stiffness, cross-sectional area and tension force are K_T, A_T and T, respectively. The corresponding parameters for a two-dimensional dome are K_R, A_R, and T_R. The principal geometric variables are recognized to be the radius of the circumscribing polygon (R), the number of sides of the polygon (n), along with the section and material properties (A and E, respectively) of the hoop cables.

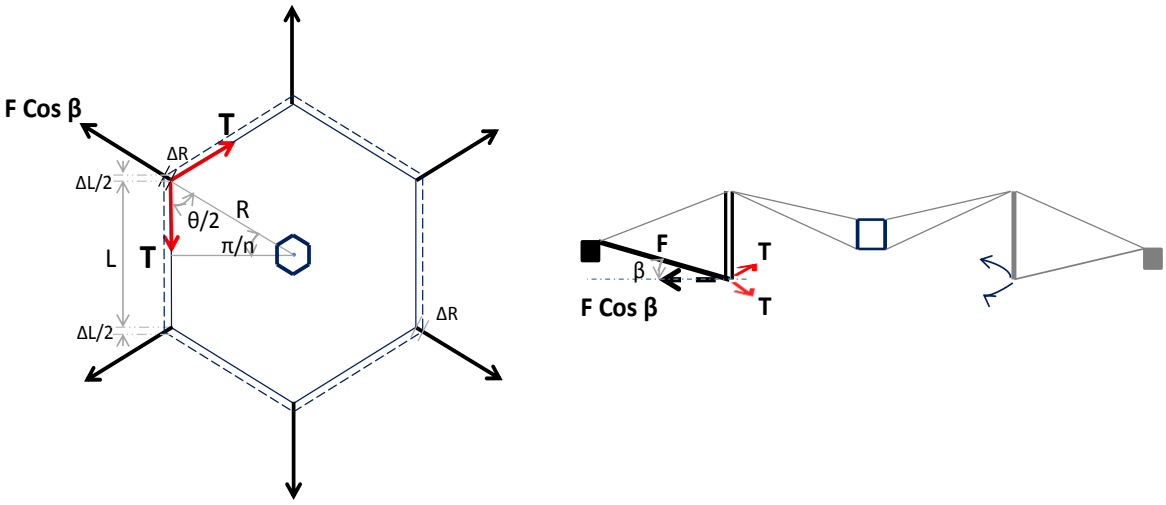

Figure 5.2 Geometric relationships and joint equilibrium

For simplicity, consider an $N1{:}n6$ dome (Figure 5.2), for which the geometric and force relationships are developed. To begin, the interior angle of a regular polygon is given as:

$$\theta = \pi\left(1-\frac{2}{n}\right) \tag{5.1}$$

where n is the number of sides of the polygonal hoop.

The radius of the polygon can be written in terms of L and n as:

$$R = \frac{L}{2\sin\left(\frac{\pi}{n}\right)} \tag{5.2}$$

For an infinitesimal length ΔL, Eq. 5.2 can be written as:

$$\Delta R = \frac{\Delta L}{2\sin\left(\frac{\pi}{n}\right)} \tag{5.3}$$

The horizontal force equilibrium of the bottom node gives:

$$F_h = 2T\cos\left(\frac{\theta}{2}\right) \tag{5.4}$$

where $F_h = F\cos\beta$ represents the horizontal component of the diagonal tension and T is the hoop tension.

From Figure 5.2, $\cos\left(\frac{\theta}{2}\right) = \sin\left(\frac{\pi}{n}\right)$ and therefore,

$$F_h = 2T\sin\left(\frac{\pi}{n}\right) \tag{5.5}$$

which gives

$$T = \frac{F_h}{2\sin\left(\frac{\pi}{n}\right)} \tag{5.6}$$

Strain in the hoop cable,

$$\varepsilon_R = \frac{\Delta R}{R} \tag{5.7}$$

Force in the hoop cable,

$$T = AE\varepsilon_R = AE\frac{\Delta R}{R} \tag{5.8}$$

$$F_h = 2\left(AE\frac{\Delta R}{R}\right)\sin\left(\frac{\pi}{n}\right) \tag{5.9}$$

Rearranging the terms,

$$F_h = 2\frac{AE}{R}\sin\left(\frac{\pi}{n}\right)\Delta R \tag{5.10}$$

Now, the equivalent radial stiffness of the hoop is defined as:

$$K_R = \frac{F}{\Delta R} \tag{5.11}$$

Therefore, the equivalent radial stiffness becomes:

$$K_R = \frac{F}{\Delta R} = 2\frac{AE}{R}\sin\left(\frac{\pi}{n}\right) \tag{5.12}$$

A dimensionless stiffness parameter can be established by bringing the stiffness terms to one side:

$$\frac{K_R}{\left(\frac{AE}{R}\right)} = 2\sin\left(\frac{\pi}{n}\right) \tag{5.13}$$

The variation of the dimensionless stiffness parameter $\frac{K_R}{\left(\frac{AE}{R}\right)}$ with the number of segments n is shown in Figure 5.3. The hoop cable stiffness reduces by half when the number of polygon sides is doubled and likewise when the hoop radius is doubled.

Table 5-1 Hoop Stiffness Coefficients

n	θ	$\sin\left(\frac{\pi}{n}\right)$	$\frac{K_R}{\left(\frac{AE}{R}\right)}$
6	120	0.5	1.000
8	135	0.3827	0.7654
12	150	0.2588	0.5176
16	158	0.1951	0.3902
24	165	0.1305	0.2611
32	169	0.098	0.1960

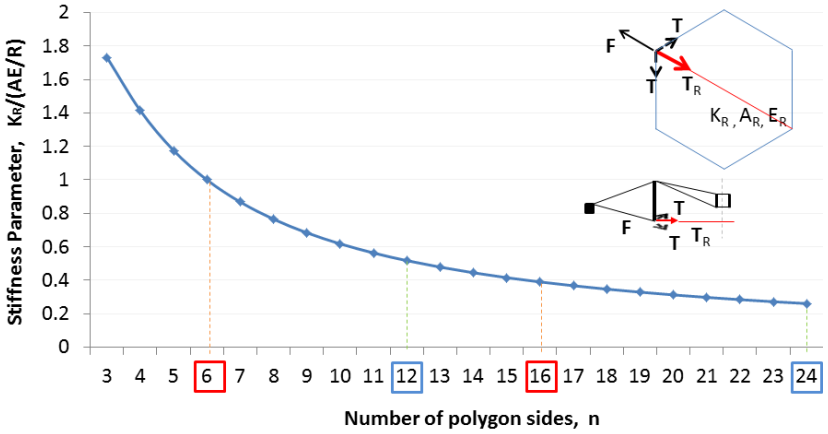

Figure 5.3 Hoop stiffness variation versus polygon sides

Rewriting K_R in terms of the hoop cable force T,

$$K_R = \frac{F_h}{\Delta R} = \frac{2T\sin\left(\frac{\pi}{n}\right)}{\left(\frac{\Delta L}{2\sin\left(\frac{\pi}{n}\right)}\right)} = 4\frac{T}{\Delta L}\sin^2\left(\frac{\pi}{n}\right) \tag{5.14}$$

The equivalent radial (two-dimensional) stiffness of the hoop cables can be expressed in terms of the stiffness of the three-dimensional hoop cables as:

$$K_R = 4K_T\sin^2\left(\frac{\pi}{n}\right) \tag{5.15}$$

Equation 5.15 can be expanded to develop a relationship between the radial cable areas A_R, and the three-dimensional hoop cable areas A_T *as*:

$$\frac{A_R E}{R} = 4\frac{A_T E}{L}\sin^2\left(\frac{\pi}{n}\right) \tag{5.16}$$

Therefore,

$$A_R = 2A_T\sin\left(\frac{\pi}{n}\right) \tag{5.17}$$

The actual hoop forces (in three-dimension) can be determined from the following relationship:

$$T_R = 2T\sin\left(\frac{\pi}{n}\right) \tag{5.18}$$

A summary of the equivalent parameters for a two-dimensional analysis model is provided in Table 5-2. The modeling parameter is the equivalent radial cross-sectional areas for the hoops. After analyzing the two-dimensional model to determine T_R, the actual force in the hoop cables T can be determined using the expression in Eq. 5.18.

Table 5-2 Equivalent Two-dimensional Model Parameters

Type	Three-dimensional Parameter	Equivalent Two-dimensional Parameter
Hoop Area	A_T	$A_R = 2\ A_T\ sin\left(\frac{\pi}{n}\right)$
Hoop Force	$T = \frac{T_R}{2\ sin\left(\frac{\pi}{n}\right)}$	T_R
Hoop Stiffness	K_T	$K_R = 4(K_T)\ sin^2\left(\frac{\pi}{n}\right)$

5.2 Estimation of Preliminary Member Sizes and Prestressing Force

Consider the three-dimensional model of *N*1:*n*16:*L*400:*r*/*L*0.083:*d*/*L*0.14 dome (Figure 5.4a). Assuming that full axisymmetric snow loads governs the member design, a two-dimensional all-truss model is used for the estimation of prestressing force levels and preliminary member sizing. Preliminary member areas were selected based on a cable arrangement adapted from Section 2.4. The ridge cable cross-sectional areas (inner to outer) are 3.3 in^2 and 5.5 in^2 respectively, the diagonal cable areas are 2.17 in^2 and 4.34 in^2 respectively, and the hoop cable area is 9.51 in^2. The struts areas (inner to outer) are 14.9 in^2 and 18.1 in^2 with flexural stiffness EI = 49 x 10^6 k.in^2 and 86.77 x 10^6 k.in^2 respectively.

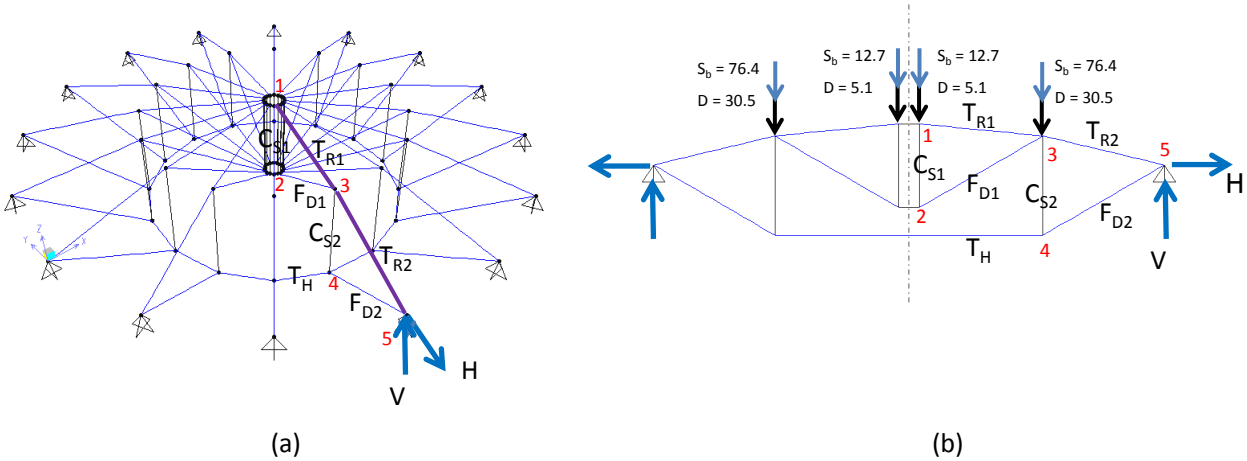

Figure 5.4 (a) Three-dimensional model of *N*1:*n*16:*L*400:*r*/*L*0.083:*d*/*L*0.14 dome with node labels, member labels and gravity loads in kips; and (b) Equivalent two-dimensional model

The equivalent two-dimensional cable-truss is shown in Figure 5.4b, however, the ridge cables are now replaced with two-force members. Under the action of the loads, the ridge members experience compression, and the diagonal and hoop members experience tension.

In the original cable dome, all cables including the ridge cables must be in tension to avoid any potential instability. As such, the compression in the top chord members of the cable-truss have to be overcome. This is done by applying an appropriate prestressing force to the diagonal cables until the ridge compression forces became tension forces. An initial prestress equal to 50% of the yield stress of the steel strands was given to the diagonal members. With the yield stress of strands f_y = 243 ksi and the Young's Modulus = 24,000 ksi, the assigned prestrain to the diagonals = 0.005. The prestrain values can be adjusted until all cables are in tension under the full snow load. Alternatively, the same prestress force can be obtained by increasing the member areas so as to keep the prestressing force levels small, as

$$P = EA\mathcal{E}_p \tag{5.19}$$

where P is the prestressing force, E is the modulus of elasticity, A is the cable area that is prestressed and $\mathcal{E}_p$ is the prestrain.

Usually, prestressing force levels must be such that the tension induced in the ridge cables is 5-10% of the cable breaking stress. This is done to ensure that the ridge cables don't go slack under the action of live load or snow load.

5.3 Validation of the Two-dimensional Model

To validate the two-dimensional cable-truss model, consider again the $N1{:}n16{:}L400{:}r/L0.083{:}d/L0.14$ dome shown in Figure 5.4b. Once the prestressed configuration was determined (LC-1: D + P), the dome was analyzed for the remaining loading conditions. Only the full symmetric snow load case (LC-2a) was used for the validation of the two-dimensional model. Valley cables were neglected in this comparative analysis, as they offer no resistance to gravity loads. The computer program uses the *Newton-Raphson Method* to solve the nonlinear problem, which provides the much desired terminal quadratic convergence, i.e., the solution converges at a faster rate.

The results from the two-dimensional analysis were compared with the three-dimensional SAP2000 analysis results. The results and differences are quantified in Tables 5-3 and 5-4.

Table 5-3 Summary of Member Forces (kips) for *N*1:*n*16:*L*400:*r/L*0.083:*d/L*0.14 dome

Member Type	Member Force (kips)	2D LC-1 D + P	3D LC-1 D + P	% difference	2D Prestressed Structure LC-2a D + P + S_b	3D Prestressed Structure LC-2a D + P + S_b	% difference
Diagonal Cable	F_1	39.9	39.3	1.50	49.9	49.2	1.40
	F_2	164.7	160.2	2.73	309.3	304.6	1.52
Hoop Cable	T_1	143 (366.5)	355.4	3.03	267.7 (686.1)	675.5	1.54
Ridge Cable	T_{R1}	90.4	91.5	1.22	17.4	18.7	7.47
	T_{R2}	128.2	128.9	0.55	62.8	63.5	1.11
Vertical Strut	C_1	-18.9	-18.7	1.06	-23.8	-23.7	0.42
	C_2	-77.7	-77.3	0.51	-150.8	-150.5	0.20
Horz. Reaction	H	267.5	263.6	1.46	328.1	324.6	1.07
Vert. Reaction	V	53.3	50.7	4.88	142.3	139.7	1.83

Note: Negative sign indicates either downward reaction force or compressive member force
Numbers in parenthesis are equivalent force values for the hoop in a three-dimensional dome

Table 5-4 Summary of Displacements (inches) for *N*1:*n*16:*L*400:*r/L*0.083:*d/L*0.14 dome

Node Number	2D LC-1 D + P	3D LC-1 D + P	% difference	2D Prestressed Structure LC-2a D + P + S_b	3D Prestressed Structure LC-2a D + P + S_b	% difference
1	17.34	17.43	0.519	-9.38	-9.20	1.92
2	17.37	17.46	0.518	-9.37	-9.19	1.92
3	5.59	5.61	0.358	-6.99	-6.85	2.00
4	5.72	5.75	0.524	-6.86	-6.73	1.90

Note: Negative indicates downward displacement with respect to the nodal elevation obtained from LC-1

Knowing the bottom radial cable force, the actual three-dimensional hoop force is calculated using Eq. 5.18, i.e., $T_R = 2T\sin\left(\frac{\pi}{n}\right)$, where T is the hoop force in the three-dimensional model and T_R is the radial cable force. As such, the actual hoop force for LC-1:

$$T_1 = \frac{T_R}{2\sin\left(\frac{\pi}{n}\right)} = \frac{143}{2(0.1951)} = 366.5\,\text{kips} \tag{5.20}$$

This gives a percentage difference of 0.44% when compared with 228.3 kips obtained from a three-dimensional analysis.

Similarly, the actual hoop force for LC-2a:

$$T_1 = \frac{T_R}{2\sin\left(\frac{\pi}{n}\right)} = \frac{267.7}{2(0.1951)} = 686.1 \text{kips} \tag{5.21}$$

This gives a percentage difference of 0.02% when compared with 624.2 kips obtained from a three-dimensional analysis. The percentage difference in member forces is slightly greater in the prestressing stage. The difference is almost insignificant for full snow load case (Table 5-3). The latter is reassuring for dome design governed by the full axisymmetric snow load case. Displacements values (Table 4-4) indicate a larger percentage difference for LC-2a (symmetric snow load case). However, the differences are very small for design purposes.

5.4 "All-radial" cable dome

Consider the *N*1:*n*16:*L*400:*r*/*L*0.083:*d*/*L*0.14 "all-radial" dome as shown in Figure 5.5a. The "all-radial" cable dome as an alternative is interesting to examine, where the polygonal hoops are replaced by radial cables in the plane of each truss. The dome is first modeled as a two-dimensional structure (Figure 5.5b) using the equivalent two-dimensional parameters from Table 5-2 and an analysis for axisymmetric gravity loads is performed. Valley cables are neglected for meaningful comparison of the "all-radial" dome and the conventional radial dome. The results are listed in Tables 5-5 and 5-6.

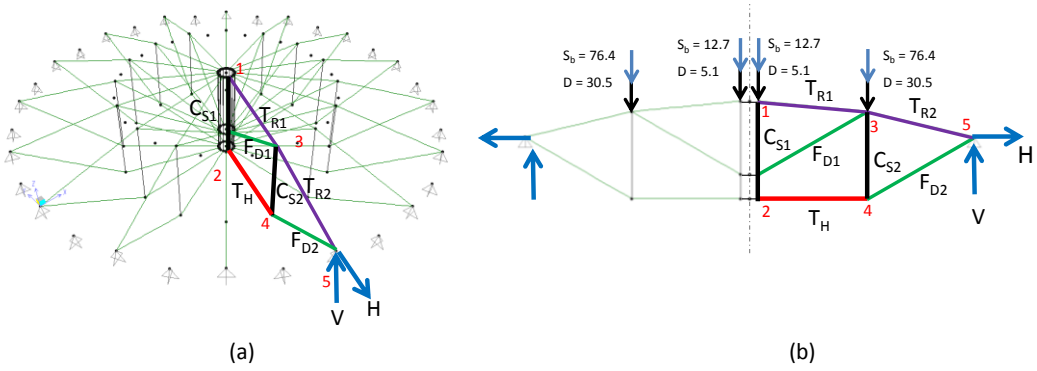

Figure 5.5 (a) Three-dimensional model of *N*1:*n*16:*L*400:*r*/*L*0.083:*d*/*L*0.14 "all-radial" dome; and (b) Equivalent two-dimensional model

The results from the analysis of the "all-radial" show that the member forces are slightly larger. This may be due to the added weight of the extended posts in the central cage. That said, an "all-radial" solution may require easier connections with all the cables attached to the central cage at parallel tension rings. This dome will also require less labor to erect as the cables may be prestressed individually, and not all at the same time as otherwise required. Radial cables along the same direction must be prestressed simultaneously to keep the compression ring in place.

Table 5-5 Summary of Member Forces (kips) for *N*1:*n*16:*L*400:*r/L*0.083:*d/L*0.14 dome

Member Type	Member Force (kips)	LC-1 D + P	LC-2a D + P + S_b
Diagonal Cable	F_1	39.7	54.5
	F_2	150.3	306.5
Hoop Cable	T_1	130.5	266
Ridge Cable	T_{R1}	59.8	8.1
	T_{R2}	97	58
Vertical Strut	C_1	-15.2	-22.5
	C_2	-73.6	-153.4
Horz. Reaction	H	224.5	321.7
Vert. Reaction	V	53.9	143

Note: Negative sign indicates either downward reaction force or compressive member force

Table 5-6 Summary of Displacements (inches) for *N*1:*n*16:*L*400:*r/L*0.083:*d/L*0.14 dome

Node Number	LC-1 D + P	LC-2a D + P + S_b
1	12.44	-10.54
2	12.46	-10.53
3	3.67	-7.35
4	3.79	-7.2

Note: Negative indicates downward displacement with respect to the nodal elevation obtained from LC-1

A comparison of weight between the "all-radial" cable dome and the conventional cable dome will be insightful. First, the volume of the hoop cables in a conventional cable dome is calculated as:

$$V_H = n\, L\, A_H \tag{5.22}$$

where n is the number of sides of the polygon, L is the length of the side of the polygonal hoop and A_H is the area of one hoop segment.

The volume of the radial cables in the "all radial" dome can be found as:

$$V_R = n\,R\,A_R \tag{5.23}$$

where A_R is the area of one radial segment measured from the bottom of a post to the central cage.

Let the ratio of the two volumes be given as γ. As such,

$$\frac{V_H}{V_R} = \gamma \tag{5.24}$$

The relationship between the polygonal dimensions R and L is given in Eq. 5.2. The relationship between the hoop tension T and the equivalent radial tension T_R was determined from nodal equilibrium in Eq. 5.18. Substituting Eqs. 5.22 and 5.23 in Eq. 5.24 and using the relationships given in Equations 5.2 and 5.18, Eq. 5.24 can be re-written as:

$$\gamma = \left(\frac{L}{R}\right)\left(\frac{T}{T_R}\right) = 2\sin\left(\frac{\pi}{n}\right)\left(2T\sin\left(\frac{\pi}{n}\right)\right) = 1 \tag{5.25}$$

Equation 5.25 shows that the total weight of cables in an "all-radial" cable dome is the same as that of a conventional radial cable dome. Therefore, the cost of cables for both domes will be the same. The fact that the theoretical weight of steel for the cables is the same for both domes is significant.

Given that such is the case then, why is it that the all-radial solution has not been used more frequently? The answer lies in the lack of torsional stiffness offered by this system when compared to the conventional radial cable dome, where the hoops provide the much-needed torsional resistance. If prestressing forces are less than the required minimum, the dome will be unstable for asymmetric loads, and the cost of reinforcing the vertical struts with cross-bracings may cancels any cost benefits the "all-radial" cable dome can gain.

5.5 Summary

In this chapter, a two-dimensional analysis model was derived in order to simplify the analysis and design procedures. Equivalent planar parameters were derived to replace the three-dimensional hoop and tension ring members. The two-dimensional model analysis results compared well with the three-dimensional model analysis results. Essentially, a two-dimensional model will suffice to design cable domes governed by axisymmetric loading. Moreover, such an analysis provides a

designer with a time-saving and efficient means for parametric studies.

A notable departure from the conventional radial dome is the new "all-radial" dome developed using the two-dimensional model; this dome has radial bottom chords connected to the central hub. The highlight of this dome lies in its constructional efficiency. The simpler connection details will result in less labor to erect as the cables will be prestressed individually and not all at the same time around the perimeter ring; i.e., the radial cables along the same direction must be prestressed simultaneously to keep the ring in the same place. A comparison of weight between the "all-radial" cable dome and the conventional cable dome showed that the total weight of cables used is the same for both. This proves that the cost of cables for both domes will be the same. However, the lack of torsional stiffness under asymmetric loading had to be remedied by using cross-bracing between vertical struts in alternate sectors.

CHAPTER 6 CONCEPTUAL BEHAVIOR OF CABLE-STRUT STRUCTURES

Before examining larger domes, a study of simple cable-strut structures is necessary to obtain insights about the fundamental structural behavior of all cable structures. This chapter presents three basic structures, namely, a one-strut cable truss (Figure 6.1), a two-strut cable truss (Figure 6.5) and a four-strut cable dome (Figure 6.8), analyzed for symmetric and asymmetric loads. Analyzing the one-strut structure discussed in Section 6.1 helped in understanding the conceptual structural behavior of strut, diagonal and ridge members. The two-strut structure discussed in Section 6.2 includes a radial bottom chord (comparable to a hoop cable in three-dimensional structure) and is closer to a two-dimensional model of a cable dome. The effects of asymmetrical gravity loading is studied using the two-strut cable truss model, otherwise not possible with the one-strut model. Lastly, in Section 6.3, a three-dimensional four-strut structure is studied for the effects of asymmetric loads. The depth-to-span ratios were varied for a comparative parametric study. The analysis of the aforementioned structures is nonlinear elastic ─ nonlinear because of geometric effects and elastic because the member stresses are kept within the elastic range of the materials.

6.1 One-strut Cable Truss

Consider the one-strut cable-truss illustrated in Figure 6.1. The rise-to-span ratio of the truss, is r/L=0.083, and the depth-to-span ratio d/L varies as 0.13, 0.29 and 0.50. The cross-sectional area of the strut is 4.0 in^2 and the cross-sectional area of all cables is 1.0 in^2. The modulus of elasticity of the struts and cables are 29,000 ksi and 24,000 ksi respectively.

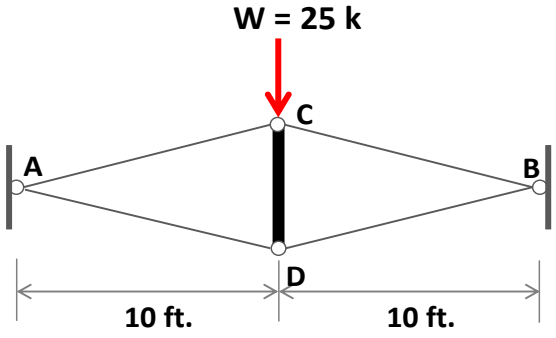

Figure 6.1 Prestressed geometry of one-strut structure under gravity load

A load W = 25 kips is applied at node C in the downward direction. For the same prestressing force in the diagonal members and for various d/L ratios, comparative results of member forces and thrust on the perimeter beam are presented. Several useful observations can be made from comparing three different one-strut cable trusses with varying d/L ratios. The stiffness of the three cable-trusses did not change much under increasing loads. This can be attributed to the effect of prestress. When the load is increased beyond a certain limit, the stiffness abruptly dropped to zero. This is the load at which the ridge cable goes slack and is the first indicator of ensuing strut instability. The deeper the truss, the greater its stiffness and, thus, higher loads are required to cause the ridge cable to go slack.

Of all the plots, the most important one is the ridge cable force versus the applied live load W (Figure 6.2a). The other insightful plot is the ridge cable force versus deflection at the ridge caused by W (Figure 6.2b). When the ridge cable force equals zero (goes slack), the structure becomes unstable. It can be seen that the ridge cable force equals zero at a deflection such that the latter overcomes the initial upward deflection of the ridge caused by prestressing of the bottom cable. This is seen better by plotting the elevation of the ridge (i.e., of node C) from the level of supports, against W (Figure 6.3a). Thus, at W=0, the elevation of the ridge will be that reached after initial prestressing. As W is applied and increased, the ridge elevation will begin to come down until it reaches the value of W where the ridge cable forces become zero.

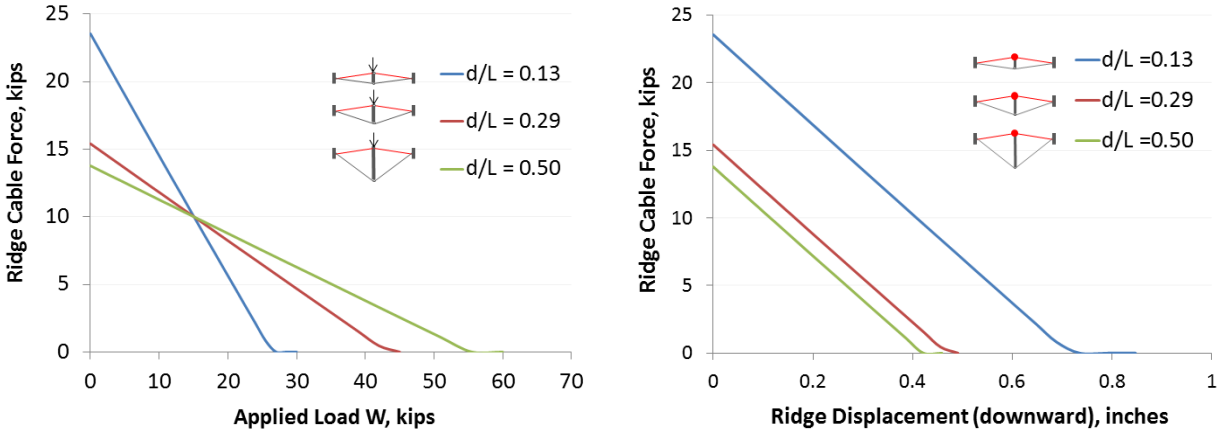

(a) (b)

Figure 6.2 (a) Ridge cable force variation with increase in load W; and
(b) Ridge cable force versus ridge displacement

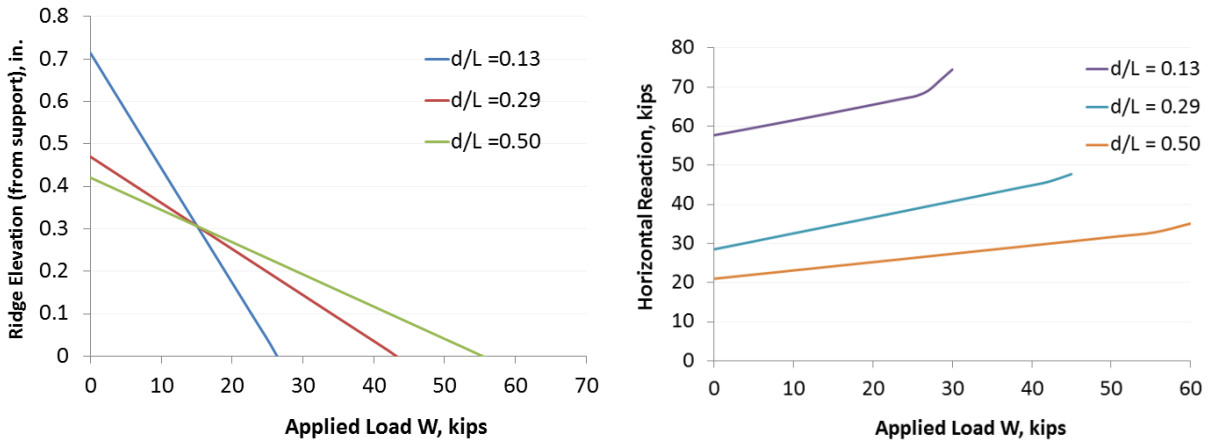

(a) (b)

Figure 6.3 (a) Ridge elevation versus applied load; and
(b) Variation in horizontal reaction with increase in applied load

Note also that the horizontal support reaction is significantly greater for the shallower trusses, particularly for the truss where d/L = 0.13 (Figure 6.3b). As a consequence, there will be a greater demand on the supporting walls or columns.

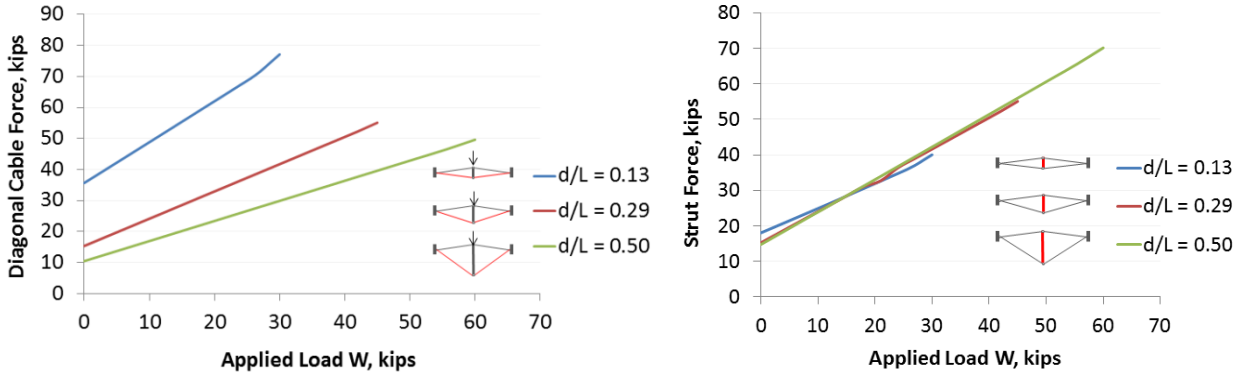

(a) (b)

Figure 6.4 (a) Diagonal cable force variation with increase in load W;
(b) Strut force variation with increase in applied load

The forces in the diagonal cables and vertical struts increase with an increase in W (Figure 6.4a and 6.4b, respectively). The rate of increase of diagonal forces is greater for a shallow truss whose d/L = 0.13 compared with the deeper trusses whose d/L = 0.29 and 0.50. This means that the possibility of diagonal cable failure by rupture is much greater in shallow trusses. The rate of

increase in internal forces of the struts is nearly identical. The plot in Figure 6.4b shows that the final compressions in the struts are not very different and, therefore, independent of the depth of the structure.

6.2 Two-strut Cable Truss

Consider the two-strut cable-truss shown in Figure 6.5. All members have an area of 1.0 in^2. The modulus of elasticity of the struts and cables are 29,000 ksi and 24,000 ksi, respectively. The same diagonal prestressing force levels were used for both cases. As a result, both cable-trusses have the same prestressed geometry with the same *r/L* and *d/L* ratios. The trusses are examined for symmetric and asymmetric loading conditions. The dead load is the same on both trusses while one of the trusses has axisymmetric live loads (Figure 6.5a) and the other has asymmetric live loads (Figure 6.5b).

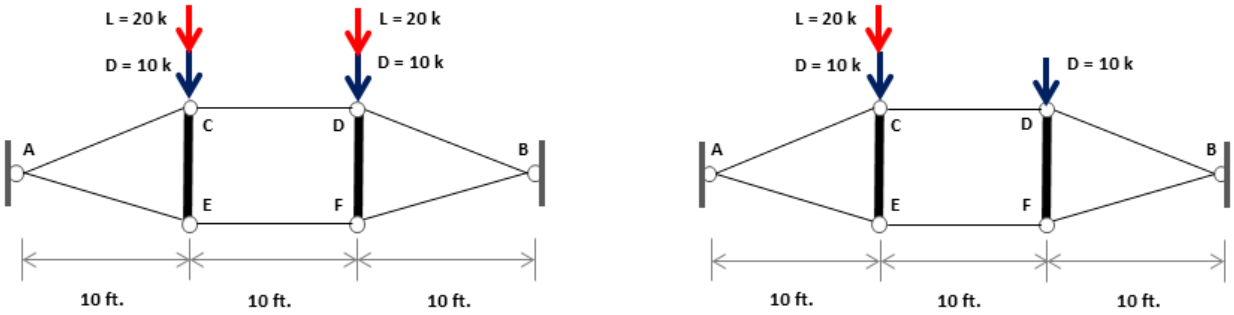

(a) (b)

Figure 6.5 (a) Two-strut cable truss with axisymmetric live loads; and
(b) Two-strut cable truss with asymmetric live loads

Many of the observations were similar to that seen in the one-strut cable truss. The system resists loads by losing tension in the ridge cables and absorbing tension in the diagonal and hoop cables. When the ridge cables go slack, the system resistance is from pure catenary action, i.e., like a cable system with two concentrated loads from the struts.

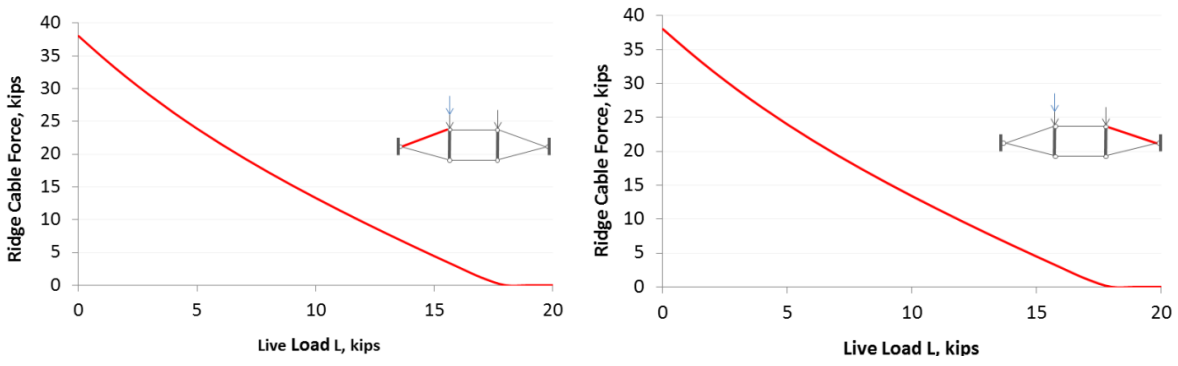

(a) (b)

Figure 6.6 Force variation in (a) ridge cables AC; and (b) BD with increase in live load

There was a noteworthy observation from the behavior of the truss under asymmetric loadings. The results in Figure 6.6 show the ridge cable force variation with increase in live load. Clearly, despite the asymmetric loading, there is very little variation in the ridge cable forces.

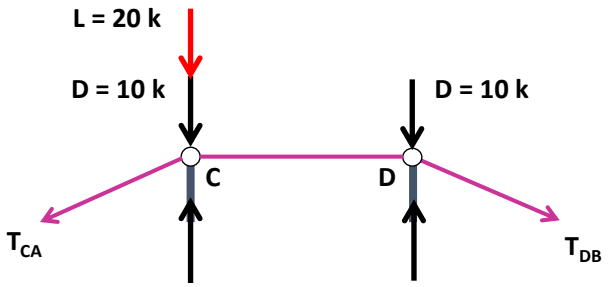

Figure 6.7 Two-dimensional free-body diagram showing equilibrium of forces

This is understood better from Figure 6.7 where the applied loads are directly absorbed by the vertical struts. The ridge cable forces have to equilibrate the force in member CD and as such the variation in the ridge forces will not be much if the in-plane strut displacements are within limits.

6.3 Three dimensional four-strut structure

Consider the *N*1:*n*4:*L*200:*r*/*L*0.083:*d*/*L*0.29 structure shown in Figure 6.8. Upon analyzing the three-dimensional model, its inefficiency was revealed from its lack of torsional stiffness. The reasons for this are quite obvious. Firstly, the very large tributary area supported by a four-sided dome makes the applied loads significantly high. When the transverse movements are motivated

at small asymmetric loads, P-Δ effects take over. Hoop cables are the only members to provide resistance to the lateral movements. The only way to contain the lateral movements was by increasing the prestressing force levels in the diagonals. As a consequence, very high levels of prestressing forces were required to stabilize the structure.

Calledine et al. (1986) derived a simple relation between the number of kinematic modes and self-stress states using only equilibrium and linear algebra principles. Pellegrino (1992) quantified the above type of mechanism for cable domes to be equal to N x n. As such, for the $N$1:n4 dome in reference, there will be 1 x 4 = 4 mechanisms of the aforementioned type. He identified and quantified three other mechanisms by examining the equilibrium (or coefficient) matrix that is formed from writing out the nodal equilibrium equations in matrix-vector form.

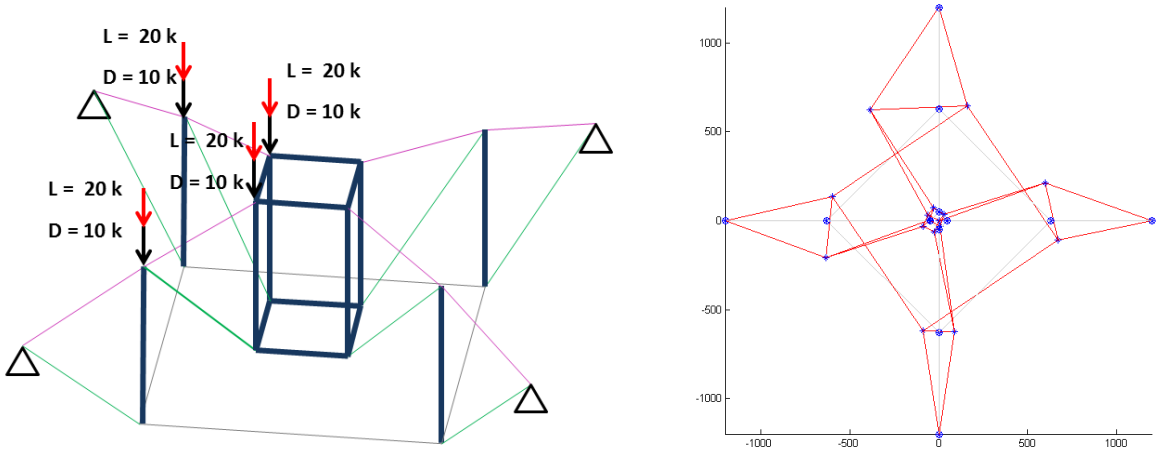

(a) (b)

Figure 6.8 (a) $N$1:n4 dome under asymmetric loading; and (b) torsional distortion in plan view

Taking note of the above mechanism, domes with n = 6, 8, 12, 16 and 24 were examined under asymmetric snow loading. The torsional distortions attenuate (Figure 6.9) with an increase in the number of polygon sides, n. This is because the tributary areas on each truss (and therefore the loads) are smaller for higher n. However, to restrain the torsional movements, the additional prestressing forces required were quite high.

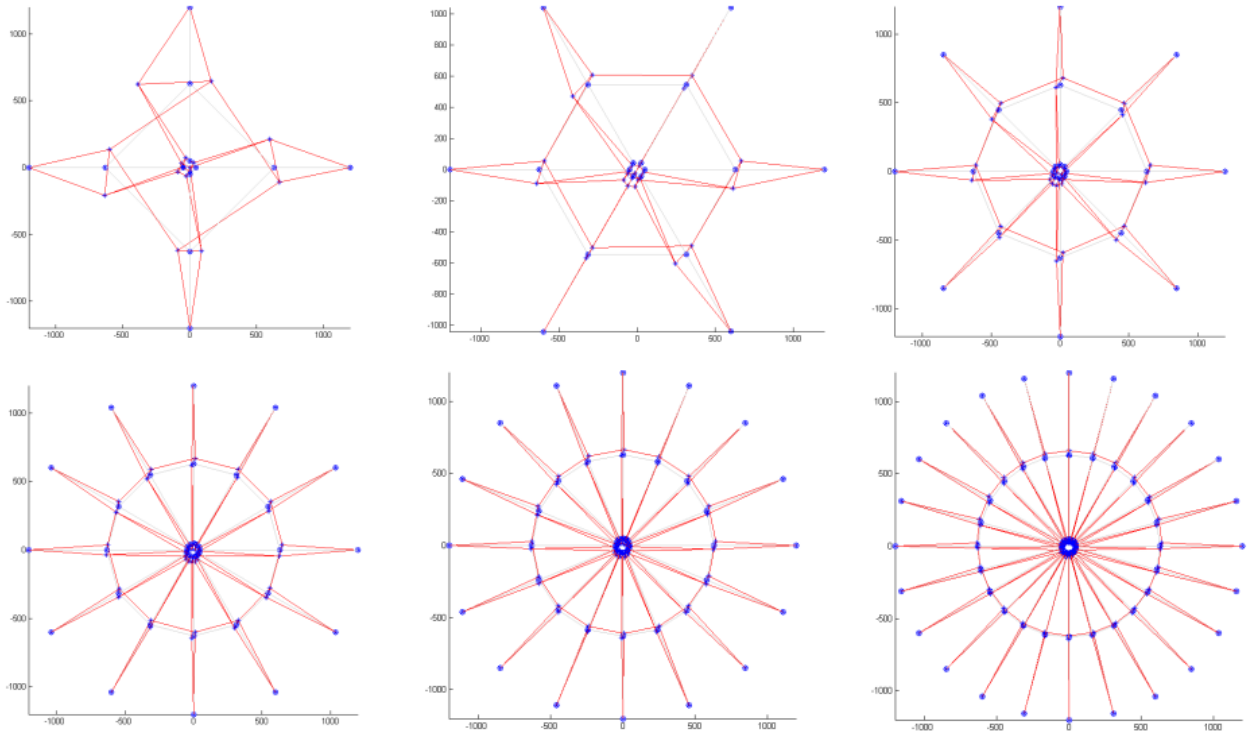

Figure 6.9 Torsional distortions in plan view for domes with n = 4, 6, 8, 12, 16, and 24

For the domes investigated, it can be concluded that large cable domes with flexible roof membrane must be designed with a minimum number of 16 polygon sides. As such, the palette for parametric studies has been reduced to n=16 and n=24 domes.

6.4 Summary

The cable-strut structures examined in this chapter gave valuable insights about the trend in member behavior under the action of gravity and uplift forces. The forces in the diagonal and the hoop cables kept increasing with increase in gravity loads. While this was happening, there was a reduction in the ridge cable tensions, to the extent that some ridge cables went slack. Essentially, the hoop and the diagonal cables resist the majority of gravity loads through catenary action. This is especially evident from the two-strut cable truss. The analysis results of the three-dimensional structure emphasized the torsional softness that may exist in domes with fewer polygon sides. This sets up the basis for the study of larger cable domes.

CHAPTER 7 LIMIT STATES IN CABLE DOME DESIGN

This chapter is devoted to the study of dome behavior both in the elastic and inelastic range of the materials. The trend in member behavior is first understood from an elastic analysis. Inelastic analysis is done to evaluate the limit states and thereby to know the potential source for dome instability and demise. The structural behavior of twelve 400 ft. span domes with different depth-to-span ratios is discussed in Section 7.1. The domes were subject to the action of both symmetric and asymmetric loads. In Section 7.2, the limit states of strut buckling and serviceability are evaluated. To gain further insight into the progressive yielding of cable members, a displacement-controlled analysis was used. The analysis showed that cable rupture may never be the cause for collapse of domes that are well-designed.

7.1 Geometric Nonlinear Behavior

For practical considerations such as serviceability, cable domes are designed to ensure that the member stresses are within the elastic range of the materials. The analysis type is nonlinear elastic – nonlinear due to large displacement or geometrical effects. The elastic range for the steel strands is defined at a strain value of 0.011 with the corresponding yield stress as 243 ksi. Consider the sample *N*1:*n*16:*L*400:*r/L*0.083:*d/L*0.14 dome (Figure 5.4).

The analysis showed that the behavior of the *N*1:*n*16 dome under gravity loading is catenary-like (Figure 7.1) with the diagonal cables and the hoop cables as the principal load-resisting members. The ridge cables relax due to the downward movement of the dome and as a result, there is a reduction in their tension forces.

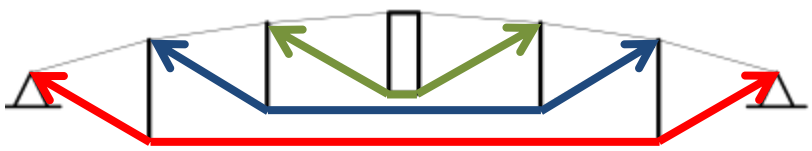

Figure 7.1 Catenary-type load path in cable-trusses

Under uniform gravity loading, LC-2a (Table 3-2) for this analysis, the behavior of the ridge cables is interesting in the sense that not all ridge cables behave alike. As the live load is increased, the central tension ring hub deflects downward, causing the ridge cables attached to the ring to relax, i.e. lose tension. This is the first sign of departure from a stable structure as the inner vertical strut begins to have large displacements due to partial restraint at its top end. The inner ridge cables in all the domes examined, i.e., *N*1:*n*16, *N*2:*n*16 and *N*3:*n*16, lose tension with continuous increase in loading. Eventually, these cables go slack. Any small residual tension is because of their self-weight (Figure 7.2).

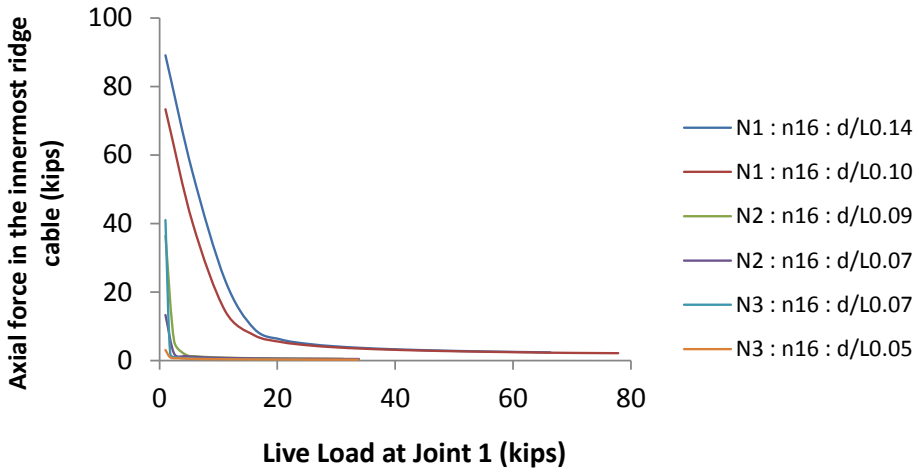

Figure 7.2 Geometric Nonlinear Analysis: Inner ridge cable force versus live load in *n*16 domes

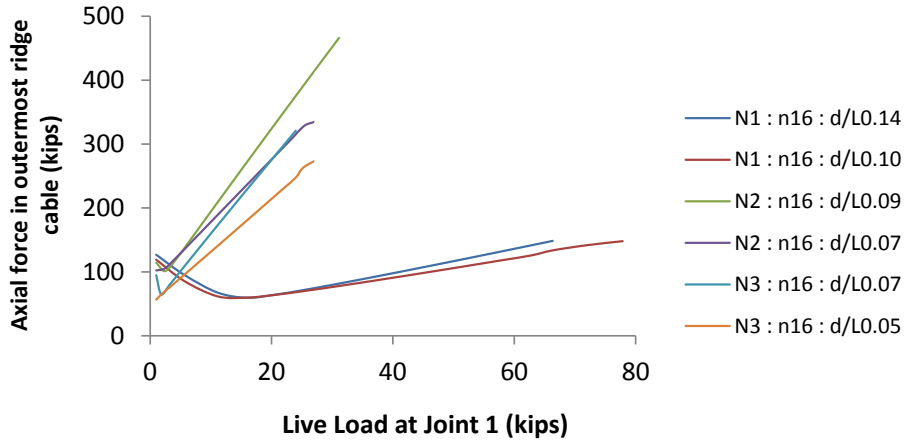

Figure 7.3 Geometric Nonlinear Analysis: Outer ridge cable force versus live load in *n*16 domes

The outer ridge cables initially lose tension under the action of gravity loads. However, these cables begin to regain tension to balance the increasing compressive forces in the struts (Figure 7.3). The ridge and valley cables are the primary load-resisting members for suction forces while the other cables serve ancillary purposes. The valley cables, in fact, resist most of the uplift forces. There will be no instability, and the structure may fail only by overcoming the tensile strength of the ridge cables. This should be a more ductile failure than that caused by column instability. When cable domes are designed for hurricane-prone regions such as Florida coasts, higher prestressing force levels may be required to ensure that no cables will go slack. Moreover, some means to tie down the structure may be necessary.

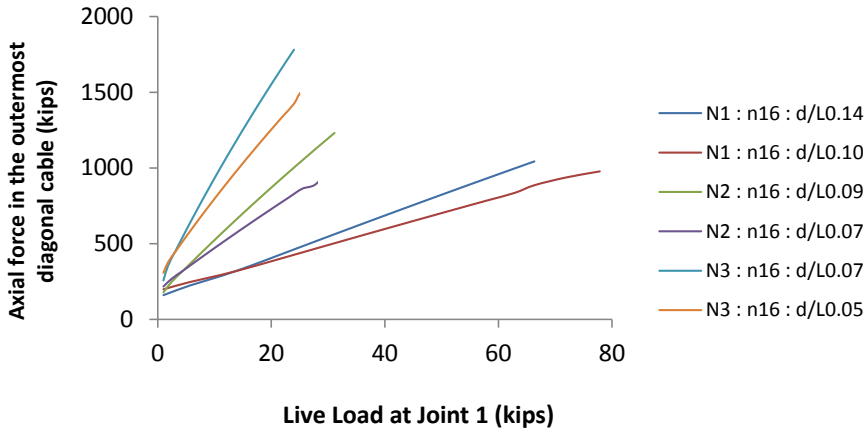

Figure 7.4 Geometric Nonlinear Analysis: Outer diagonal force versus live load in *n*16 domes

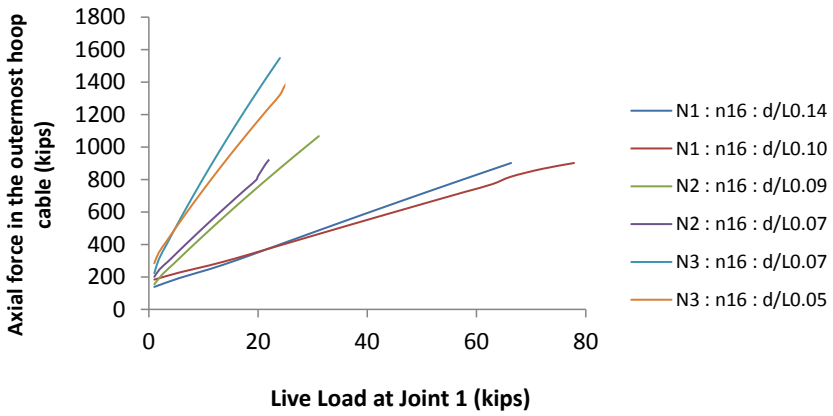

Figure 7.5 Geometric Nonlinear Analysis: Hoop cable force versus live load in *n*16 domes

For the *n*16 domes in subject, the outermost diagonal and hoop cable forces were observed to increase with increase in live loads (Figures 7.4 and 7.5). Although at the prestressed state, the tension in the cables for all domes are not very different, the cable tensions increase at a faster rate for *N*3 domes as compared to *N*2 followed by *N*1. Moreover, for the same *N*, domes that are shallow (smaller *d/L*) show a slower rate of increase in tension as compared with deeper domes.

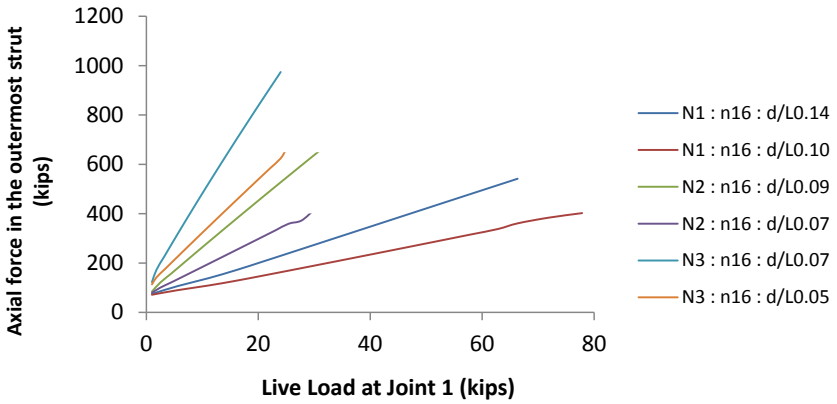

Figure 7.6 Geometric Nonlinear Analysis: Outermost strut force versus live load in *n*16 domes

The forces in the struts are relatively small (Figure 7.6) compared to the diagonal and hoop cable forces. Similar to the cable tensions, the compression in the struts increase at a faster rate for *N*3 domes as compared to *N*2 followed by *N*1.

Under the action of asymmetric snow loads, a portion of the dome deflects downward and part of the structure is lifted up. As a consequence, the ridge cables in the portion lifted up gain tension. This effect is further magnified by wind suction (Figure 7.7). Ridge cable design is therefore governed by the asymmetric load case LC-4d (Table 3-2).

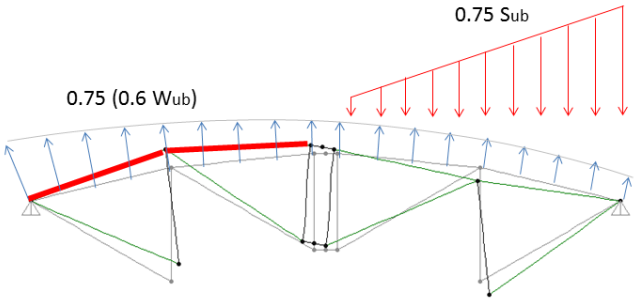

Figure 7.7 Magnifying effect caused by action of asymmetric snow and wind suction

Although LC-2a (symmetric snow load case) causes maximum internal forces in critical members, it cannot be deemed as the governing case for design of members that attract compressive forces in the *N*1:*n*16:*r/L*0.083:*d/L*0.14 dome. The design must be checked for wind uplift loads that may cause cable compression (Figures 7.8). Prestressing force levels may then be adjusted accordingly.

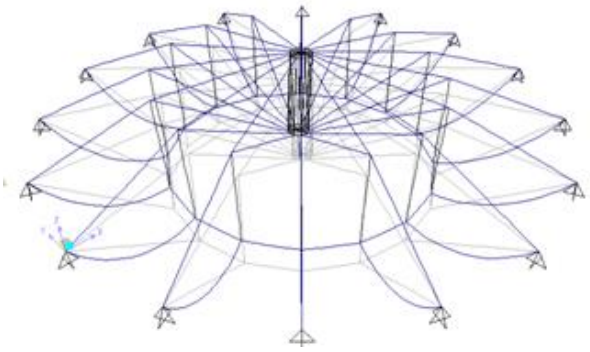

Figure 7.8 Cable slackening due to wind uplift

A good practice is to increase the prestressing force levels uniformly across the span of a dome, i.e., linearly in all diagonal cables. This ensures proper control of the structure's stiffness.

7.2 Limit States

The following limit states define the capacity of a dome, namely: 1) strut buckling (stability), 2) serviceability (stiffness), and 3) cable rupture (strength). The results of the elastic analysis revealed that the limit states 1 and 2 occurred well within the elastic range of the materials. A dome may not be considered usable after the buckling of struts. That said, the structure may still be subjected to increasing loads after limit states-1 and 2 have happened. To capture the full path of the structure's response, the inelastic behavior of the dome was examined.

Beyond the elastic limit of the material, the structural response was nonlinear both with respect to material properties and geometrical effects. The behavior of cables can become highly nonlinear when slackening and inelastic tensile strains intervene. Such nonlinearities affect the constitutive laws of the cable members (Maier and Contro, 1975). A bi-linear material model for the cables was considered (Figure 7.9a). The ultimate strain ε_u of the steel strands is 0.04, corresponding to a breaking stress at 270 ksi. The strand yield strain, ε_y, was taken as 0.011 corresponding to a yield stress equal to 90% of the ultimate stress, i.e. 243 ksi.

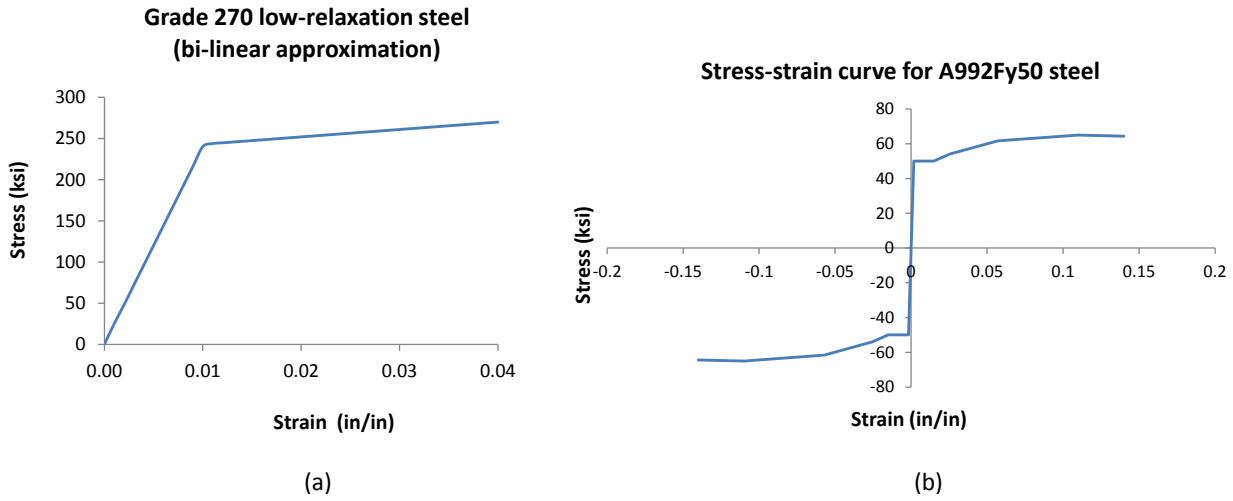

Figure 7.9 (a) Material model (bi-linear approximation) used for steel strands; and (b) Material model for structural steel used for struts

To simulate the inelastic behavior using SAP2000, discrete "yielding links" were assigned at mid-spans of all members. The nonlinear behavior of a member was concentrated at the links. The yield stress and yield strain were selected as scaling factors. Therefore, the yield point B is assigned a value of 1.0 and the ultimate point E was assigned a value of the ratio of the ultimate stress and the yield stress, which equals 1.11 (Figure 7.10). The corresponding strain ratio at ultimate is 3.64. Intermediate points C and D may be used as performance criteria per the designer's discretion.

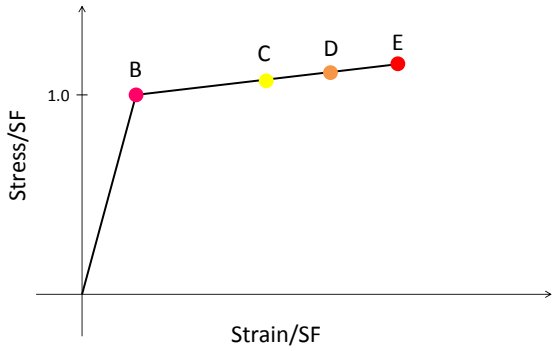

Figure 7.10 "Yielding link" data used for inelastic analysis

The static nonlinear analysis capabilities for both material and geometrical effects are fully integrated into the SAP2000 program and allows for efficient implementation of the analysis procedure. A displacement-controlled static nonlinear analysis is used wherein the load at all the roof nodes is incrementally (and linearly) increased until a target nodal displacement is reached.

The target displacement is set to five times the permissible deflections (span/180) in order to note the progressive yielding of members. Knowing which member would fail first will enable a designer to redesign the structure in order to ensure a ductile behavior, i.e. yielding of cables.

For academic curiosity, the inelastic response was examined to see how cables would respond to increasing live load. An *N*1:*n*16 dome was loaded until the first cable ruptured. The behavior was monitored at intermittent load-steps. The summary of results for the sample domes *N*1:*n*16:*L*400:*r/L*0.083:*d/L*0.14 and *N*1:*n*16:*L*400:*r/L*0.083:*d/L*0.10 has the limit states and the corresponding live loads W_1 and W_2 highlighted (Tables 7-1 and 7-2). The member stresses are listed only for the hoop and outer diagonal, as they yield and rupture before other cable members, leading to potential collapse of the dome.

The struts do not develop their full capacity. Clearly, it would take substantial enhancement in the prestressing force and strut sizes to cause rupture of the cables to occur before buckling of struts (Tables 7-1, 7-2 and 7-3). The same was evident in *N*2 and *N*3 domes as well (Tables C-1 through C-4, Appendix C).

Table 7-1 Summary of results for *N*1:*n*16:*L*400:*r/L*0.083:*d/L*0.14 dome

(Live) Load Step	Vert. Defl.		Live Load		Member Forces						Member Stresses	
	at Joint 1	at Joint 5	at Joint 1	at Joint 5	Diagonal Cables		Hoop Cable	Ridge Cables		Strut	Hoop Cable	Outer Diagonal
	Δ_1 in.	Δ_5 in.	W_1 kips	W_2 kips	F_{D1} kips	F_{D2} kips	T_H kips	T_{R1} kips	T_{R2} kips	C_{S1} kips	σ_H	σ_{D2}
Prestressed	17.3	5.60	1	6.0	39.6	160	139	89.1	127	-75.0	37.4	36.8
1	13.3	2.60	5.6	33.9	43.6	223	194	54.8	95.4	-107	52.2	51.4
2	9.3	-0.40	11.1	67.2	48.0	286	248	23.4	67.5	-139	66.9	65.9
3	4.8	-3.40	16.0	96.8	54.9	350	303	9.30	59.5	-171	81.7	80.6
4	0.0	-6.40	20.6	124	63.3	413	358	6.15	64.3	-204	96.6	95.3
5	-4.8	-9.40	25.1	152	72.0	477	414	4.87	71.3	-238	112	110
6	-9.5	-12.4	29.6	179	80.8	542	469	4.15	79.0	-271	127	125
7	-14.3	-15.4	34.2	207	89.7	606	525	3.68	87.3	-305	141	140
8	-19.1	-18.4	38.9	235	98.7	671	581	3.34	95.8	-339	157	155
9	-23.9	-21.4	43.6	263	108	735	637	3.08	105	-374	172	169
10	-28.6	-24.4	48.3	292	117	800	693	2.88	114	-409	187	184
11	-33.3	-27.4	53.1	321	126	866	749	2.71	123	-444	202	200
12	-38.1	-30.4	57.9	350	135	931	805	2.57	132	-480	217	215
13	-42.8	-33.4	62.8	379	145	997	862	2.45	142	-516	232	230
14	-46.1	-35.5	66.3	400	151	1043	902	2.37	149	-542	243	240
15	-51.4	-38.9	71.9	434	162	1117	965	2.27	160	-583	260	257
16	-57.0	-42.5	77.9	470	173	1195	1033	2.17	171	-627	278	275

Color Code	Limit State
	Strut buckling
	Serviceability
	Cable yielding
	Cable rupture

Table 7-2 Summary of results for *N*1:*n*16:*L*400:*r*/*L*0.083:*d*/*L*0.10 dome

(Live) Load Step	Vert. Defl.		Live Load		Member Forces						Member Stresses	
	at Joint 1	at Joint 5	at Joint 1	at Joint 5	Diagonal Cables		Hoop Cable	Ridge Cables		Strut	Hoop Cable	Outer Diagonal
	Δ_1 in.	Δ_5 in.	W_1 kips	W_2 kips	F_{D1} kips	F_{D2} kips	T_H kips	T_{R1} kips	T_{R2} kips	C_{S1} kips	σ_H	σ_{D2}
Prestressed	16.7	3.6	1	6.0	45.8	198.6	184	73.3	119	-71.6	49.6	45.8
1	12.6	0.6	3.8	22.9	46.4	246.0	228	40.1	85.7	-90.3	61.4	56.7
2	8.3	-2.4	7.3	44.1	48.4	293.7	272	14.5	61.6	-109	73.3	67.7
3	3.2	-5.4	10.1	61.1	53.7	341.7	316	7.4	59.7	-128	85.2	78.7
4	-2.0	-8.4	12.8	77.1	59.9	389.9	361	5.4	64.0	-148	97.2	89.8
5	-7.2	-11.4	15.4	93.2	66.4	438.3	405	4.5	69.6	-168	109	101
6	-12.4	-14.4	18.1	109.5	73.1	487.0	450	3.9	75.8	-188	121	112
7	-17.6	-17.4	20.9	126.1	79.8	536.0	495	3.5	82.4	-209	134	124
8	-22.8	-20.4	23.7	142.8	86.6	585.2	541	3.2	89.1	-229	146	135
9	-28.0	-23.4	26.5	159.9	93.5	634.7	586	3.0	96.1	-251	158	146
10	-33.1	-26.4	29.4	177.2	100.4	684.5	632	2.8	103	-272	170	158
11	-38.2	-29.4	32.3	194.8	107.5	734.5	678	2.6	111	-294	183	169
12	-43.3	-32.4	35.2	212.6	114.6	784.7	725	2.5	118	-316	195	181
13	-48.4	-35.4	38.2	230.8	121.7	835.2	771	2.4	126	-338	208	192
14	-53.4	-38.4	41.3	249.2	129.0	886.0	818	2.3	134	-361	220	204
15	-58.5	-41.4	44.4	267.9	136.3	937.0	865	2.2	142	-384	233	216
16	-62.4	-43.8	46.9	282.9	142.1	977.5	902	2.1	148	-402	243	225
17	-69.1	-47.8	51.1	308.6	152.0	1046.2	965	2.0	159	-434	260	241
18	-76.2	-52.1	55.7	336.3	162.7	1119.1	1032	2.0	171	-468	278	257

Color Code	Limit State
	Strut buckling
	Serviceability
	Cable yielding
	Cable rupture

With reference to Table 7-3, *N*1 domes failed by buckling of the outermost strut under half the service load. The buckling capacity of the outermost strut for *N*1 domes can be calculated from Euler's formula $\frac{\pi^2 EI}{(kL)^2}$ as 98.9 kips (for *d*/*L*=0.14) and 154 kips (for *d*/*L*=0.10), where *EI* = 29000 ksi x 299.2 in^4 = 8.677 x 10^6 k.in^2 is the flexural stiffness of the strut, *L* = 77.6 ft. (for *d*/*L*=0.14) and 62.1 ft. (for *d*/*L*=0.10) and *k* =1 for hinged ends. Of course, their slenderness is unreasonable to begin with, with the tallest strut height = 77.6 ft. Such a failure is sudden and premature (brittle-type), and should be avoided.

In comparison, *N*2 and *N*3 domes became unserviceable before full service loads were applied. Of the *N*3 domes, it did not take much of a load to make the shallower domes where *d*/*L* = 0.05 unserviceable (Table 7-3, and Tables C-1 through C-4 in Appendix C). The allowable deflection was calculated as span/180 = 400 ft./180 = 26.7 in. However, this limit on deflections is not a code requirement, but rather estimated from observation of existing domes under service loads. In practice, the serviceable limits are determined by the structural and mechanical engineers so as to ensure positive drainage of water from the roof. The remedy to enhance the stiffness and limit the

deflections is to increase the prestressing force assigned to the diagonal members. As a consequence, the ridge cables have a higher initial tension which help to restrain the movement of the strut joints. Another remedy to control vertical deflections is to provide more hoop cable area.

Table 7-3 Limit states for cable domes

Dome designation	Load factor (times the full service snow load) at which the outermost strut buckles	Load factor (times the full service snow load) at which the dome becomes unserviceable	Load factor (times the full service snow load) at which the outermost hoop cable ruptures
*N*1:*n*16:*d/L* 0.14	0.33	2.34	6.15
*N*1:*n*16:*d/L* 0.10	0.44	1.43	4.40
*N*2:*n*16:*d/L* 0.09	1.86	1.25	5.65
*N*2:*n*16:*d/L* 0.07	1.97	0.51	3.99
*N*3:*n*16:*d/L* 0.07	0.89	0.68	4.24
*N*3:*n*16:*d/L* 0.05	1.52	0.21	2.93
*N*1:*n*24:*d/L* 0.14	0.57	1.98	4.04
*N*1:*n*24:*d/L* 0.10	0.60	1.20	2.81
*N*2:*n*24:*d/L* 0.09	1.69	0.99	3.56
*N*2:*n*24:*d/L* 0.07	1.82	0.40	2.48
*N*3:*n*24:*d/L* 0.07	0.99	0.51	2.77
*N*3:*n*24:*d/L* 0.05	1.65	0.16	1.97

Assuming that the struts are stiffened adequately such that cable rupture happens first; it was the outermost hoop cable that yielded and ruptured before other cables in all of the domes examined. This is because of the significantly high tension force in the outermost hoop cables, which essentially resisted much of the applied loads along with the outermost diagonal cables.

In terms of the number of polygon sides, the hoop cables in *n*24 were flexible compared to those of the *n*16 domes (Figure 5.3). Therefore, despite the lower loads on an *n*24 dome compared with an *n*16 dome, the load carrying capacity reduced as the number of polygon sides increased.

7.3 Summary

An *N*1:*n*16 dome was used an a representative example to describe its behavior under loads. The behavior of cable domes is non-linear, primarily due to the magnitude of the dimensional changes under load. The structure resists loads by changing its shape, thereby taking advantage of the flexibility of cables which conventional steel structures do not benefit from. They resist loads by losing tension in the ridge cables and gaining tension in the diagonals and hoop cables. As such, the ridge cables must be tensioned such that under applied external loading, the change in internal force is not large enough to cause them to go slack. The diagonal and hoop cables must be adequately sized to carry the initial prestress and the additional tension due to applied loading. The geometry of the dome has an effect on the prestressing force levels and plays an important role in the structural behavior.

The following observations were made with respect to the relationship between applied loads and member forces.

1. The outermost sets of diagonal cables, hoop cables, and struts were the critical members for gravity loads. This met the anticipated results, as the outermost diagonal and hoop members behaved like a catenary in resisting the full load from the roof.
2. For the *N*1, *N*2 and *N*3 domes investigated, symmetric load cases governed the design of the critical members, i.e., outermost hoop, diagonal and strut. For domes in high wind-prone regions, adequate prestressing force levels had to be provided, which along with dead weight can overcome wind uplift forces. The remaining load cases were checked mainly for design of ancillary members and details.
3. Under the action of gravity loads, the ridge, diagonal and hoop cables responded differently to the applied loading. The tension in the ridge cables reduced with increase in gravity loading. The loads in the outermost hoop and diagonal cables continuously increased with applied load. The rate of increase in cable tension was greatest for the outermost hoop cables and diagonal cables.
4. When loads were increased beyond design loads, the set of ridge cables attached to the central cage were the first to go slack. The outer sets of ridge cables initially lost tension. And as the central hub deflected downward, the outer ridge cables started to regain tension to equilibrate the compressive forces building in the struts. Evidently, the external forces were carried to the supports by reduction in ridge cable tension and increase in diagonal and hoop cable tensions.

5. The struts resisted small forces when compared to the diagonals and hoops.

An inelastic analysis showed that significant enhancement of strut sizes and prestressing forces were required, in order to force cable rupture to happen before a strut buckled or serviceability limit state could be reached. This observation justifies the use of elastic design, which has been the standard practice for cable domes.

CHAPTER 8 CRITICAL DESIGN PARAMETERS

Since the structural behavior of a cable dome is greatly influenced by the prestressing force levels and geometry, understanding the effects of the force and shape parameters is paramount. Needless to say, prestressing force is the fundamental design parameter for cable domes, as without prestress a dome does not have a defined geometry, let alone its capacity to resist loads. In Section 8.1, the influence of prestressing force in the structural design of cable domes is discussed. The influence of the geometrical parameters, namely, the number of sectors (n), hoop radii (R), number of hoops (N) and depth-to-span ratio (d/L) are described in Sections 8.2 and 8.3. Reference is made to the expressions that were derived for the two-dimensional model (Eqs. 5.13, 5.17 and 5.18) for making some of the observations. Knowing the influence of the aforementioned parameters, structural engineer can make prudent decisions at the preliminary design stages.

8.1 Influence of Prestressing Force

Prestress is *sine qua non* to the existence of cable domes. They provide the necessary initial stiffness to stabilize the dome. Adequate prestressing force levels are necessary to resist external loads and to control vertical and lateral movements of a dome. The level of prestress is not only a function of the superimposed loading, but is also directly related to the topology of the structure. Essentially, the prestressing force levels must ensure that no cables go slack under any loading condition. This is a necessary condition, but not sufficient, especially considering the limit states of serviceability and strut buckling. A higher initial prestressing force reduces the vertical deflection under gravity loads. The increment in cable tensions with applied load also becomes smaller.

Prestressing forces are related to the structural depth (d) of the dome as well as the number of polygon sides (n). Greater the depth, greater will be the vertical component of the assigned prestressing force. As such, a smaller prestressing force will be required to lift the dome to a certain elevation when compared to a dome with a smaller depth. Similarly, a larger n will reduce the loads on each truss and the prestressing force demand will be lower.

The $N$1:n16:$L$400:r/L0.083:d/L0.14 dome in Section 3.2.2 was analyzed for various prestressing

force levels until yielding of the first cable. A higher prestressing force increases the initial stiffness of the dome significantly (Figure 8.1) which helps to limit the vertical defelection of the dome. This in turn would delay the slackening of the ridge cable attached to the tension ring.

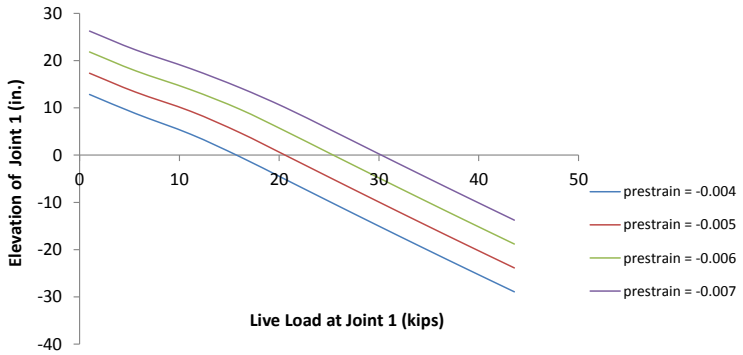

Figure 8.1 Nonlinear Elastic Analysis: Vertical deflection at joint-1 versus live load in *N*1:*n*16:*L*400:*r/L*0.083:*d/L*0.14 dome for different prestressing force levels

Lower than optimum prestressing force levels may make a dome flexible and more prone to becoming unserviceable. Therefore, optimal prestressing force levels must be determined to increase the structure's stiffness and load carrying capacity, without using more than necessary cable capacity.

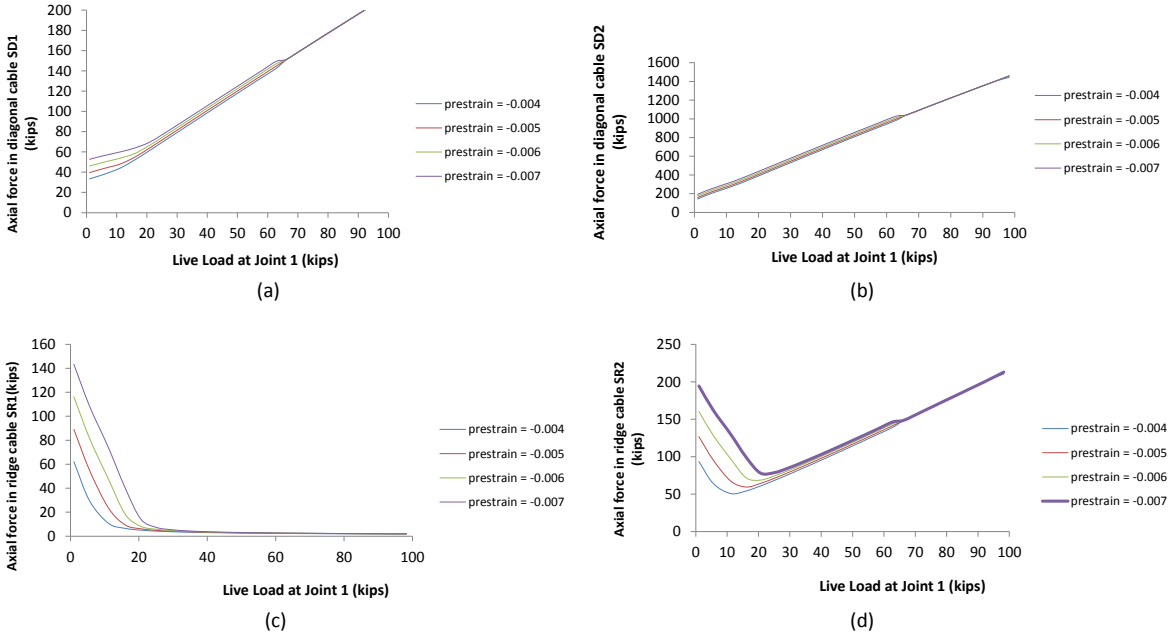

Figure 8.2 Nonlinear Elastic Analysis: Diagonal and ridge cable force variations in *N*1:*n*16:*L*400:*r/L*0.083:*d/L*0.14 dome for various prestressing force levels

Higher prestressing forces, while providing the necessary initial stiffness do not seem to affect the final tension force in the cable members (Figure 8.2 a,b,c and d). This is good as the cable capacity is utilized efficiently.

Another point to keep in mind is the possible loss of tension in cables over time, after the dome has been in service. This may be due to cable relaxation, damage or some accident. In such a case, additional prestress may be required to stiffen the dome. An efficient means to provide additional prestress can be found from an influence coefficient analysis. For this, a prescribed prestress (in the form of unit shortening) is given to the diagonals of the prestressed dome and the corresponding internal member forces are determined. This is done for one set of diagonals (outer or inner) at a time.

Consider two cases; in Case- I, only the inner diagonal is prestressed and in Case- II, only the outer diagonal is prestressed. The internal forces generated as a result of the two separate cases are listed in Table 8-1. The change in member forces for the two cases is normalized with respect to the change in member force of the additionally prestressed diagonals.

Normalizing the force values with respect to the force in the outer diagonal D_2, we notice that tensioning of the exterior cables produces all the expected results, i.e., cables are tensioned and the struts are compressed. Also, while the force in the outer diagonal is 1.0, the forces in the ridges are greater than 1.0, and the forces in all other components are less than one.

Tensioning the inner diagonal D_1 produced some unexpected results, in that the influence coefficients were greater than 1.0 in the ridge, diagonal and hoop cables. That being the case, its influence was definitely important as a source of additional tension to an already-tensioned bottom cable as well as ridge cable. Moreover, tensioning the inner diagonals was the best way to re-tension the ridge cables because of inner diagonals' large influence on the ridge cable forces.

Table 8-1 Influence Coefficients

		Case I: Additional prestress applied only to diagonal D_1		Case II: Additional prestress applied only to diagonal D_2	
Member	**Member force (kips) at prestressed state (LC-1)**	**Increase in member force (kips)**	**Normalized force**	**Increase in member force (kips)**	**Normalized force**
Diagonal D_2	160	3.2	2.13	9.3	1.00
Diagonal D_1	39.6	1.5	1.00	3.3	0.35
Hoop H	139	2.7	1.80	8.0	0.86
Ridge R_2	127	6.8	4.53	18	1.94
Ridge R_1	89.1	5.5	3.67	14.9	1.60
Strut S_1	17.1	0.9	0.60	2.2	0.24
Strut S_2	74.9	1.7	1.13	5.1	0.55
Tension Ring (top)	88.3	5.4	3.60	14.7	1.58
Tension Ring (bottom)	34.8	1.3	0.87	2.9	0.31

8.2 Influence of Number of Sectors (*n*) and Hoop Radius (*R*)

The number of sectors *n* will depend on column spacing. As the number of polygon sides *n* increases, the loads on each truss will be smaller, leading to more reasonable prestressing force levels and member sizes.

The most important influence of *n* can be recognized in the term $2\sin\left(\frac{\pi}{n}\right)$ that affects the forces and stiffness of the dome (Eqs. 5.13, 5.17, and 5.18). From Eq. 5.18, $T = \frac{T_R}{2\sin\left(\frac{\pi}{n}\right)}$, indicates that a higher *n* increases the hoop cable tensions *T*. To transfer *T* across the castings below the struts, heavier connections will be required.

Another influence of *n* is on hoop stiffness. The relationship between the radial (two-dimensional) and hoop (three-dimensional) stiffness was derived in Section 5.2. The dimensionless ratio of the

stiffnesses was found to be: $\frac{K_R}{\left(\frac{AE}{R}\right)} = 2\sin\left(\frac{\pi}{n}\right)$. The recurrence of $2\sin\left(\frac{\pi}{n}\right)$ now as the measure of the hoop stiffness in a dome indicates the significance of this parameter. The hoop stiffness was reduced to half when n was doubled. Likewise, the hoop stiffness was halved when the hoop radius R was doubled (Eq. 5.12).

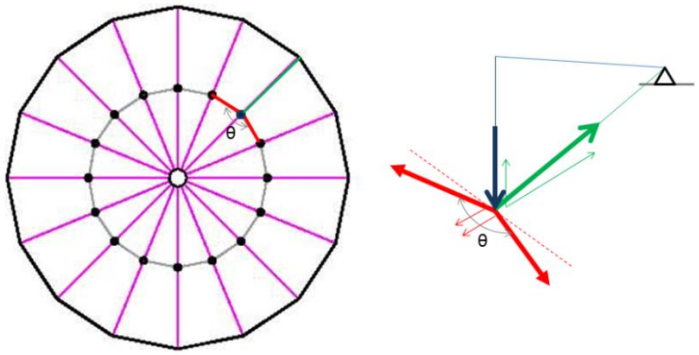

(a) (b)

Figure 8.3 (a) Schematic plan of *N*1:*n*16 dome showing the angle between hoop segments; and (b) equilibrium of forces at a critical node

In circular cable domes with larger n (Figure 8.3a), the hoop segments become almost collinear. This is detrimental as the hoop cable segments do not provide a significant radial component to balance the diagonal cable force. As a result, the forces in the hoop cables will be significantly large. That said, the lateral movements in a dome due to asymmetric loads are pronounced for domes whose n is small (Figure 6.9). In lieu of the above, the selection of n requires careful judgment as there will be expected design trade-offs.

The number of sectors n also has a direct impact on fabric stresses. The fabric span which will be larger for a higher number of sectors n will increase the stresses in the fabric. As a result, the fabric thickness will be greater, leading to more weight and cost.

8.3 Influence of Number of Hoops (*N*) and Depth-to-Span Ratio (*d/L*)

The hoop cables along with the inclined diagonal cables resist much of the applied gravity loads and help to reduce vertical displacements. In a radial cable dome, hoops are the only members to provide resistance to torsional movements caused by asymmetrical loading. The stiffness of the

hoop must therefore be adequate as a flexible hoop may cause large vertical deflections even for small loads.

More circumferential hoops will make the diagonal cable lengths shorter and thereby increase their stiffness. For the same rise and same diagonal inclinations, more hoop rings will raise the centroid of hoop tensions, thus reducing the effective structural depth and moment resistance (Figure 8.4b). Also, more hoop rings will lead to greater number of struts and connections. This will increase the weight and, therefore, the cost of the structure.

The depth-to-span ratio *d/L* is important for several reasons. A higher *d/L* ratio helps to increase the structural depth of the system by keeping the outermost hoop deeper with respect to the compression ring, thereby increasing the moment capacity of a dome (Figure 8.4a). A higher *d/L* ratio will provide a larger vertical component of the pretension force. It will therefore be easier to prop a dome higher with a smaller prestressing force.

Table 8-2 Self-weights of domes

Dome	Self-weight (kips)	Normalized Self-weight
*N*1:*n*16:*L*400:*r/L*0.083:*d/L*0.14	232	1.00
*N*1:*n*16:*L*400:*r/L*0.083:*d/L*0.10	202	0.87
*N*2:*n*16:*L*400:*r/L*0.083:*d/L*0.09	261	1.12
*N*2:*n*16:*L*400:*r/L*0.083:*d/L*0.07	230	0.99
*N*3:*n*16:*L*400:*r/L*0.083:*d/L*0.07	357	1.54
*N*3:*n*16:*L*400:*r/L*0.083:*d/L*0.05	323	1.39

Domes with two or more hoops *N* and smaller *d/L* ratios will be better suited in high wind-prone regions. With their greater self-weight (Table 8-2) compared to *N*1 domes, *N*2 and *N*3 domes should offer better resistance to wind uplift forces.

The number of hoops and the depth-to-span ratio may easily affect the stability of a cable dome. Stability is an important concern partly due to the relative flatness of the roof and increase in dead weight with span. The following observations can be made with regard to the role of hoop tensions, dome depth, and loss of tension in the ridge cables on the global stability of a dome structure.

1. In conventional trusses, the structural depth is the overall depth between the center-lines of the top and bottom chords. In cable-trusses, however, the relevance of structural depth requires more careful consideration. The moment arm for resistance is developed between the radial tension (T_{CR}) at the perimeter ring and the resultant hoop cable tensions (T_{ri}). The structural depth is taken as the vertical distance between T_{CR} and T_{ri}. For the overall system stability and strength, the centroid of hoop tensions must therefore fall below the perimeter compression ring (Figure 8.4a). Domes with small diagonal inclinations (or d/L) may be susceptible to overall system instability (Figure 8.4b). Since the lowermost hoop will experience greatest tension, it should be kept as low as possible to prevent such instability.

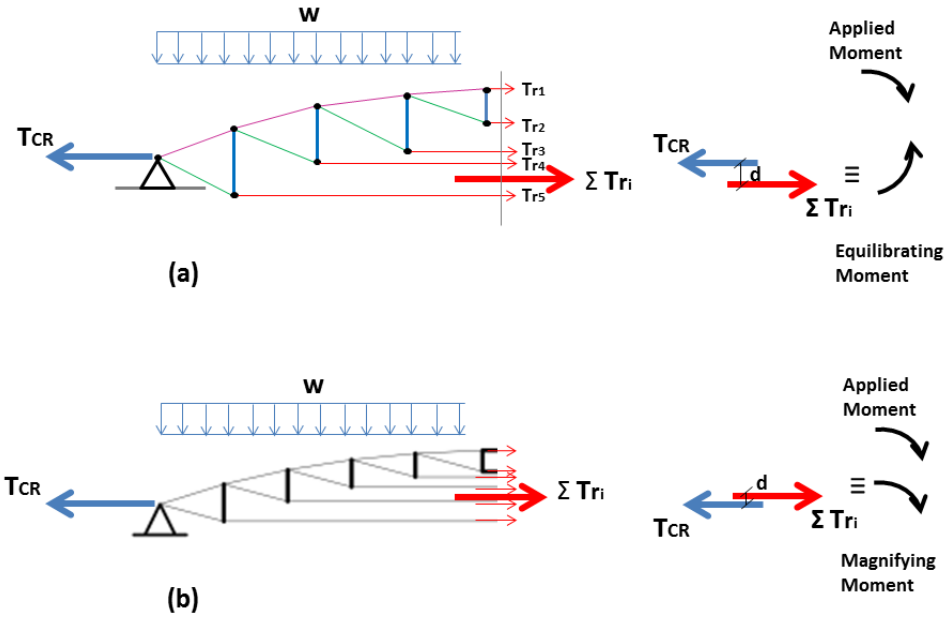

Figure 8.4 (a) A stable cable dome; and (b) an unstable cable dome

2. Progressive loss of tension in the ridge cables may cause in-plane (Figure 8.5a) and out-of-plane (Figure 8.5b) displacements of the top end of the struts. With increase in gravity loading, the cables closest to the central cage go slack and do not recover. With further increase in loads, the outer sets of ridge cables lose tension. Instability of struts will ensue with more ridge cables losing tension. Unless the struts have another source of lateral support, they will buckle just as double-hinged struts would do if one of their ends loses lateral support. For viability of design, it is, therefore, most important to keep the ridge cable in tension at all times and for all possible

loading conditions. This is achieved by providing adequate prestressing forces to the diagonal cables.

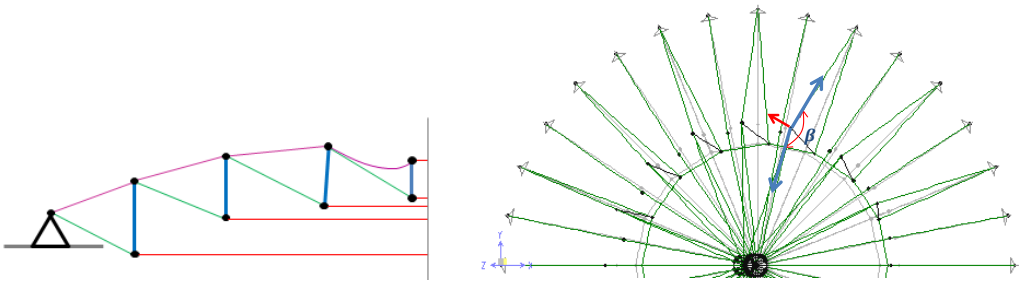

(a) (b)

Figure 8.5 (a) Slackening of ridge cables causing in-plane instability; (b) Restraining force for out-of plane displacements

3. The cable dome is a sensitive structure and relatively large vertical deflections may take place in response to any change in loading. The top of the struts therefore does move in response to changes in the load. This movement is limited by the fixed length bridge ropes not only in the radial direction but also circumferentially, although not to a great degree. Any change in loading of the membrane roof results in forces that tend to move the mast toward its theoretically desired position. These out-of-plane displacements will cause the ridge cables to re-tension and thereby create a restraining force (Figure 8.5b, in red) to hold back the struts. The struts, as such, regain stability and further lateral displacements are restricted. This restraining force can be calculated as $F = 2T_R \ sin\beta$, where T_R is the ridge cable force (Figure 8.5b, in blue) and β is the angle by which the ridge has rotated from its original position, measured at the compression ring. Although T_R will not vary by much, the angle β will be reduced as necessary to restore column equilibrium. This torsional instability is more pronounced when *n* is less than 16. The solution is to increase the overall prestress of the system; i.e., linearly increase prestress in all sets of diagonals.

8.4 Summary

Needless to say, the force and geometric parameters in a cable dome have a direct influence on their stability and efficiency. Prestressing supplies the required initial stiffness to a dome to carry its own weight and also to support the applied loads. A higher number of polygon sides and higher

depth-to-span ratio reduce the required amount of prestressing force. Despite a difference in the initial prestressing force, the final cable tensions end up being the same. In case of loss of tension in cables, additional prestress may be given to the interior diagonals because of its higher influence on other members.

The hoop stiffness is given as $K_R = 2\frac{AE}{R}\sin\left(\frac{\pi}{n}\right)$ indicating that fewer hoops with small radii will enhance the stiffness of hoops. This will help to control both, the vertical and lateral displacements. More hoops will raise the centroid of the hoop tensions, and thereby reduce its moment resistance. A higher *d/L* ratio will increase the moment capacity of a dome and also will provide a larger vertical component of the pretension force to elevate it in the form-finding process.

CHAPTER 9 USE OF PRESTRESSED CABLE-STAYED STRUTS

It would not be prudent to design cable domes that will fail prematurely due to strut buckling. A way has to be found to enhance the critical load of the vertical struts. In Section 9.1, the use of prestressed cable stays is proposed as a design strategy to delay the buckling of struts. With adequate prestressing force, the stays will stiffen the struts and increase their buckling capacity. The buckling load was calculated using the Stiffness-Probe Method (Gurfinkel, Miller and Robinson, 2009). The method is described with numerical examples in Section 9.2, first using a simple HSS column followed by cable-stayed struts with different prestressing force levels.

9.1 Prestressed Cable-Stayed Struts

Simple struts made of Hollow Steel Sections (HSS) or pipes have been typically used in cable domes. The buckling capacity of such struts can be increased by selecting larger diameter and thicker HSS sections with adequate bending stiffness. As an alternate design strategy, the use of prestressed cable-stays (Figure 9.1a) is recommended. A prestressed cable-stayed strut is made of an HSS section with cross-arms welded at intermediate locations. In this study, four cross-arms are welded at mid-height (Figure 9.1b). The stay cables connect the ends of the cross-arms to the ends of the strut. The stays are prestressed sufficiently before being placed in a cable dome.

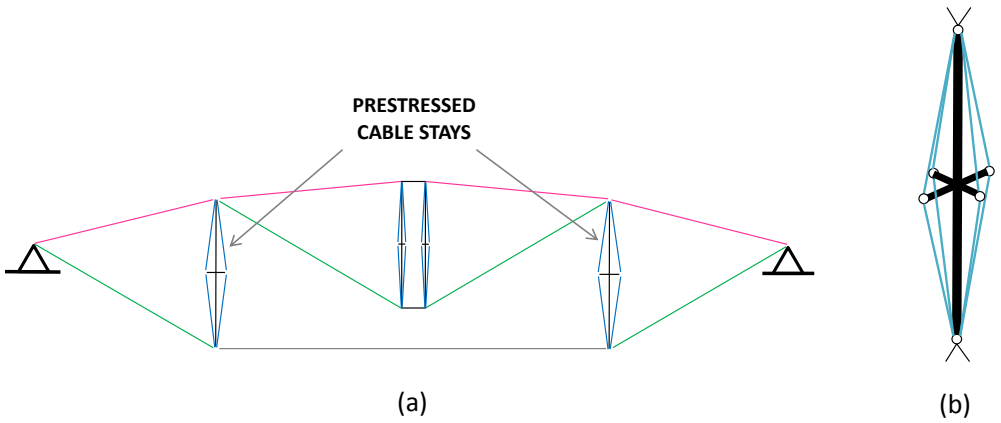

Figure 9.1 (a) Cable dome with prestressed cable-stayed struts in place of simple HSS struts; and (b) Three-dimensional model of prestressed cable-stayed strut

Before discussing the behavior of a prestressed cable-stayed strut, consider the conventional design of cable domes using simple HSS sections only (Figure 9.2a). The critical load or elastic buckling load P_{cr} of the strut may be computed using Euler's formula. Because the ends of the strut are restrained at the bottom by the diagonal and hoop cables, and at the top by the ridge cable (disregarding the contribution of the roof membrane in providing restraint), it may seem unlikely that the strut will be able to freely rotate about its vertical axis. However, a quick study showed that very tall struts may not be capable of developing the restraint at the top ends where the joint stiffness reduces with reduction in ridge cable tensions under gravity loading. As such, the struts will have to be braced in the circumferential direction in order to achieve k = 1.0. With this assumption, as the axial load on the strut is increased, the transverse deformations increase, and at $P_a = P_{cr}$, transverse deformations grow rapidly eventually reducing the strut stiffness to zero. At this stage, the strut is said to have buckled. For cable domes with one or two hoop rings, the strut lengths may be significant. Their high slenderness makes them buckle at very small loads. To overcome this limitation, prestressed cable stayed struts are used. The cross-arms and prestressed stays restrain the transverse displacement of the HSS strut. The enhanced system is expected to increase the strut's buckling capacity. The configuration of the strut used in this study is a four cross-arm strut (Figure 9.1b).

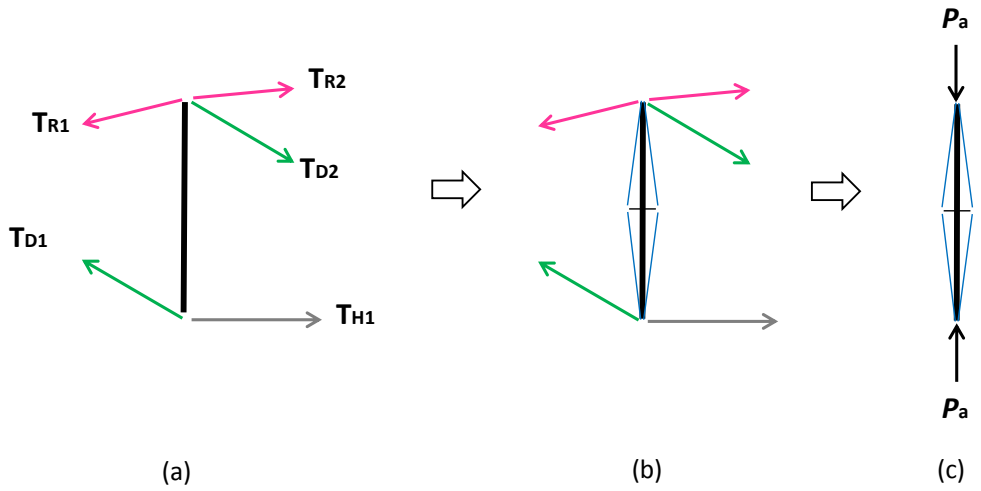

Figure 9.2 (a) simple strut; (b) cable-stayed strut; (c) compressive force on cable-stayed strut

Before its placement in the cable dome network, the strut already has internal forces due to prestressing of the stays. Then, as the dome is erected, the prestress applied to the diagonal cables further increases the compression in the vertical strut (Figure 9.2b). Let the resulting compressive

force induced at the strut ends at the completion of the erection process be called P_a (Figure 9.2c). As a consequence, the strut will shorten and there will be reduction in stay tension due to shortening of the stays. As the applied (live) load is increased, there is a load at which the cable-stayed strut will buckle. This critical load will be determined using a perturbation analysis in conjunction with the stiffness-probe method. But first, this procedure will be demonstrated on a simple pin-ended column.

Consider a 77.6 ft. tall simple steel strut made of HSS 12 x 0.5in. The Euler elastic buckling load is computed as 98.9 kips. The strut is subjected to an axial load P_a and a small transverse perturbation force F = 0.1 kip acting at mid-height (Figure 9.3). The Young's Modulus of steel is 29,000 ksi with a yield stress of 42 ksi. When the applied load is close to the buckling load, the deformations become unrealistic when compared to the strut length. This awkwardness, when the stiffness becomes close to zero, is overcome using the stiffness-probe method with an augmenting spring.

9.2 Stiffness-Probe Method

The Stiffness-Probe Method, developed by Gurfinkel, Miller and Robinson (2009), uses perturbation analysis for calculating the instability of columns. A small lateral perturbing force is applied at an appropriate joint of a straight column to generate an initial deviation from an otherwise perfectly straight line. A spring with a reasonable stiffness = 0.2 kip/in. is assigned to the same node as the perturbing force (Figure 9.3). The spring provides some lateral stability in order to ensure that the lateral deflections close to the buckling load are reasonable.

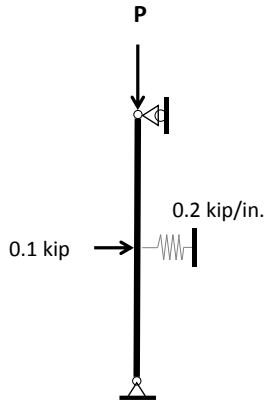

Figure 9.3 Analytical model of a simple column used for the stiffness-probe method with an augmenting spring

The stiffness of the augmented system is calculated as the perturbation force divided by the displacement along the perturbation force at the spring location. The stiffness K is a function of the compression force P and is maximum at P=0. With increase in the applied load, the stiffness of the column gradually reduces to zero, the state at which the column is said to have buckled.

The difference between the stiffness of the augmented system and the spring stiffness is equal to the stiffness of the strut. The load at which the stiffness reduces to zero is the elastic buckling load of the strut. The buckling load was found to be 98.7 kips. A plot of the variation of stiffness and applied load is shown in Figure 9.4. The buckling load P_{cr} corresponds to the value of K=0. The small difference between this value and the Euler buckling load (98.9 kips) is due to the fact that Euler's formula neglects the axial and shear deformations in a column, while the stiffness-probe method includes those effects.

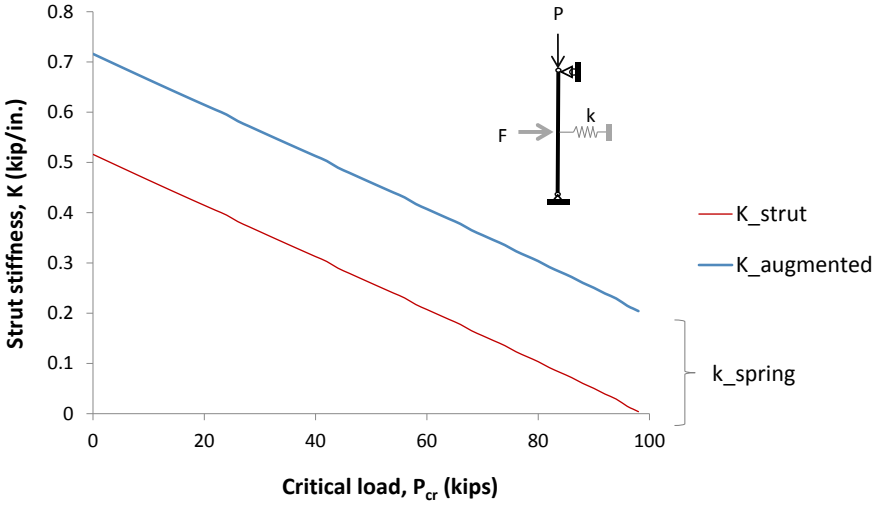

Figure 9.4 Stiffness variation versus applied load

The stiffness-probe procedure is now applied to the same HSS 12 x 0.5in. strut but with cross-arms at mid-height and stayed cables (Figures 9.1 and 9.5). The lengths of the strut L = 77.6 ft., stays l_s =39 ft. and cross-arms l_{ca} = 4 ft. The cross-arms are made of HSS 6 x 0.5in. The cable material has a Young's Modulus of 24,000 ksi with a cross-sectional area of 1.0 in^2. An initial prestrain of -0.003 is assigned to the cables; this is equivalent to a prestressing force of 72 kips. The prestressing force causes compressive forces in the strut and the cross-arms, and tensile force in the cables.

The following assumptions are made in the modeling and analysis of the cable-stayed struts:

1. A bilinear stress-strain curve for the cable stays (Figure 7.9a) with an initial Modulus of Elasticity E = 24000 ksi and Poisson's ratio v = 0.3;
2. The cross-arms are rigidly connected to the central strut.
3. The connections between the cable-stays and strut ends, and between the cable-stays and cross-arms are hinged.
4. A small perturbation load is used to generate an initial deviation from a straight line. The load is kept small so as not to affect the deformations significantly.

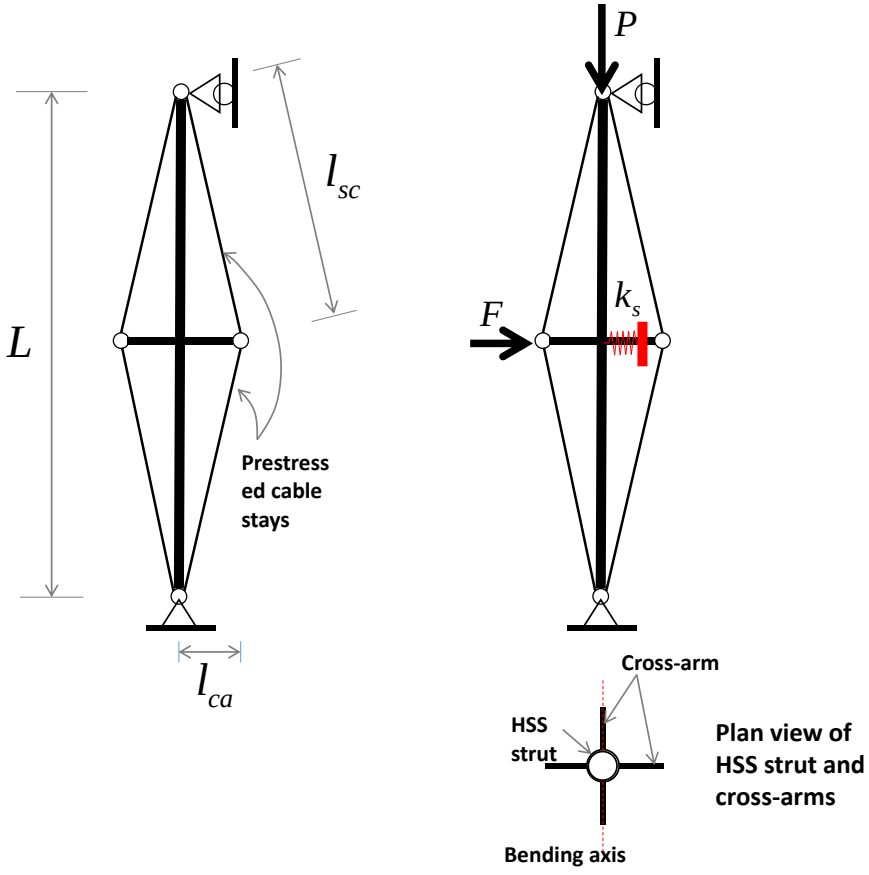

Figure 9.5 Analytical model of a prestressed cable-stayed strut

There may be three possible limit states for cable-stayed struts, namely (a) yielding of strut, (b) buckling[4] of the stayed column, and (c) yielding of stays. The yield stress for the strut and cable-

[4] Buckling load is defined as the load at which the stiffness of a cable-stayed strut becomes zero.

stays are 42 ksi and 243 ksi, respectively. The buckling load is determined using the stiffness-probe method.

To determine the axis about which the critical load is smallest, two models were considered – Case A and Case B. In Case A, the bending axis is at 90˚, and in Case B, the bending axis is at 45˚ (Figure 9.6a). The cable locations for the two models are shown in Figure 9.6b and c. The prestrain provided to the cables is -0.003 (corresponding to a prestress of 72 ksi, which is less than one-third the yield stress). The stiffness-probe procedure is applied to the enhanced system that comprises the HSS strut, the cross-arms, stay cables and the spring at mid-height of the strut.

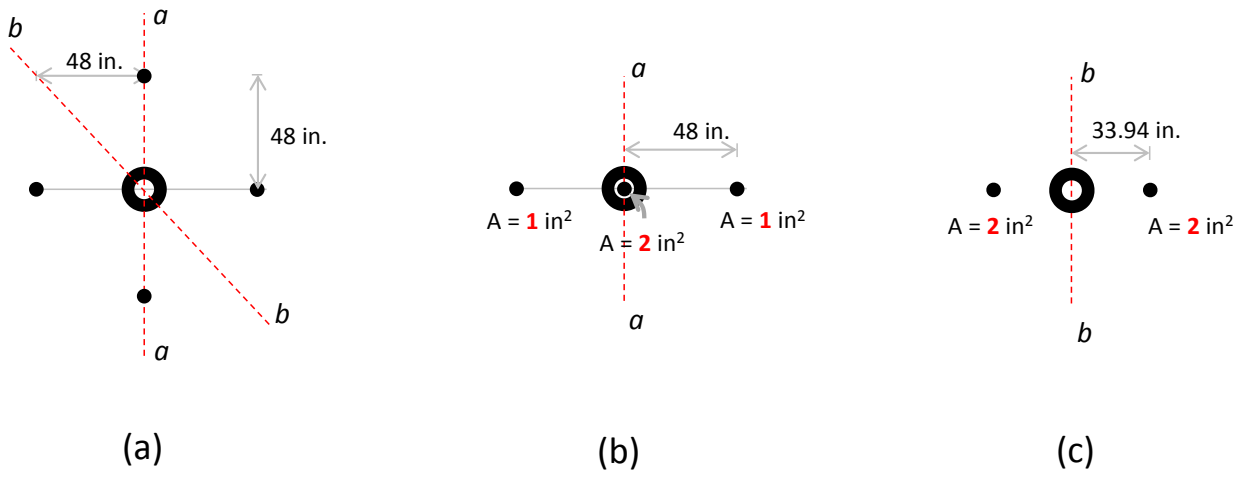

Figure 9.6 (a) Plan showing central strut and cable stays (b) Case A: Plan of planar model showing bending axis a-a; and (c) Case B: Plan of planar model showing bending axis b-b

The analysis of the two cases showed that the critical load was 323.15 kips for Case-A (Table D-1, Appendix D) and 390.6 kips for Case-B (Table D-2, Appendix D). This can be explained from the initial stiffness of the column, i.e., at P=0. The initial stiffness of the column in Case-A is 1.89 kips/in. while the initial column stiffness in Case-B is 2.56 kips/in. The stiffer column will obviously have a higher critical load. Thus, it can be concluded that the bending axis at 90 degrees from the horizontal governs the computation of critical loads.

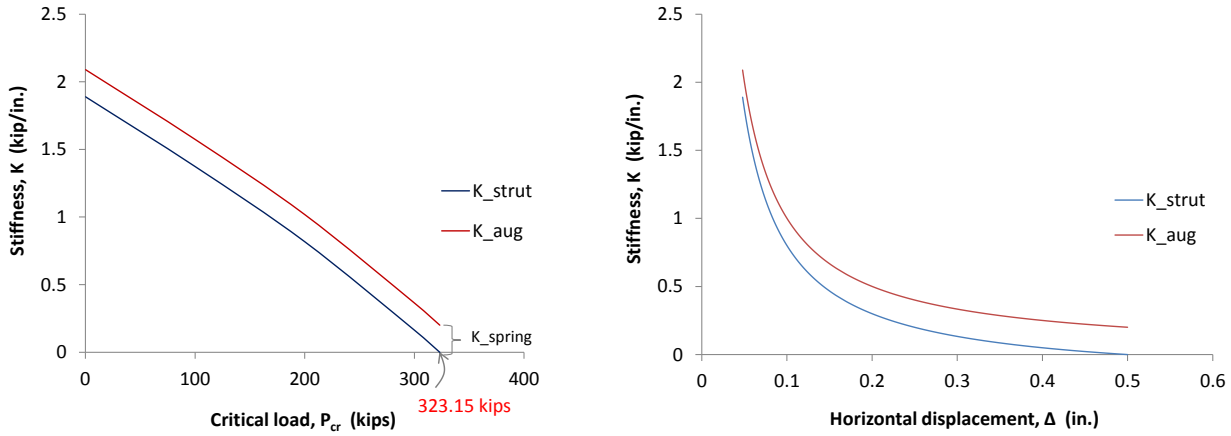

Figure 9.7 (a) Case A: Plot of Stiffness versus applied load; and (b) Case A: Plot of Stiffness versus horizontal displacement

For the benefit of the reader, the combined (axial + bending) stresses at the strut ends and at mid-height are listed for the two cases (Tables D-1 and D-2, Appendix D), to check how the actual member stresses compare with the yield stress. Figures 9.7a and 9.8a show the variation of stiffness versus applied load for the columns. Figures 9.7b and 9.8b show the exponentially decreasing stiffness with increase in applied loads. The plots verify the usual expectation in physical behavior of the strut under increasing loading.

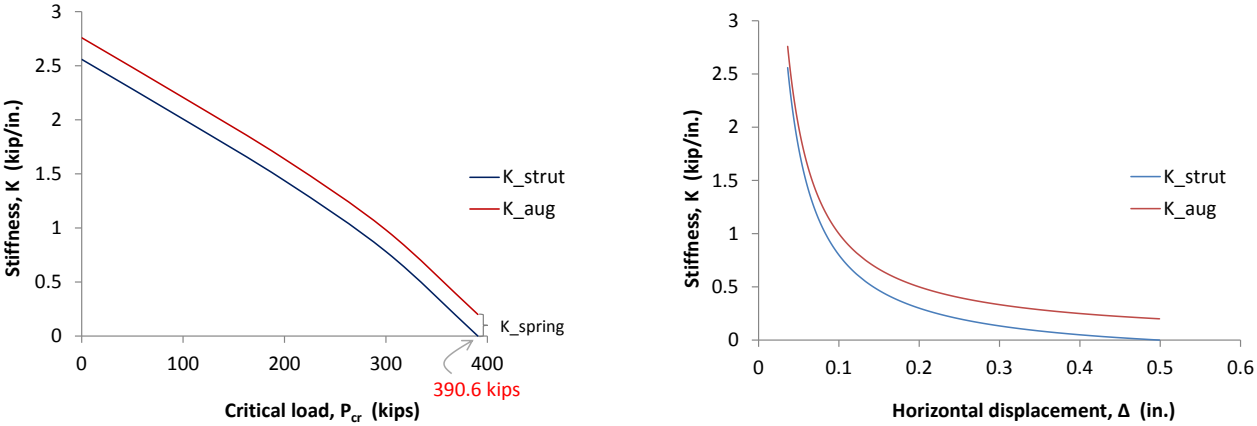

Figure 9.8 (a) Case B: Plot of Stiffness versus applied load; and (b) Case B: Plot of Stiffness versus horizontal displacement

The effects of varying the prestressing force in cable-stays is examined next. The different prestressing forces assigned to the stays are 9.6 kips, 24 kips, 48 kips, 72 kips and 96 kips. The analysis results using the stiffness-probe procedure are listed in Table 9-1, and the variation of stiffness versus applied load is plotted in Figure 9.9. The results show that at very low prestressing force levels (prestrain = -0.0004, prestressing force = 9.6 kips), the tension in the stays gradually reduce with an increase in load. A reduction in the stay tensions leads to slackening of the stays. Lateral or rotational restraint is lost and the stiffness abruptly drops to zero. The buckling load of 230 kips for this prestressing force is still more than two times the buckling load of a simple strut. For prestrain = -0.001, the strut buckling load is enhanced to 455 kips. This is a significant gain in capacity when compared to HSS strut alone.

Table 9-1 Summary of results for varying prestressing force in stays

Prestrain in stays	Corresp. prestress force in stays	Strut buckling load	Axial Stress in HSS strut at buckling	Axial Stress in left stay **at P=0**	Axial Stress in left stay **at P=Pcr**	Axial Stress in right stay **at P=0**	Axial Stress in right stay **at P=Pcr**
	(kips)	(kips)	(ksi)	(kips)	(ksi)	(kips)	(ksi)
0 (HSS only)	-	98.7	5.43	-	-	-	-
-0.0004	9.6	230	15.2	7.94	0	8.32	1.77
-0.001	24	455	30.3	20.1	0.256	20.5	5.48
-0.002	48	392	31.5	40.4	22.8	40.9	28.7
-0.003	72	323	31.8	60.7	45.9	61.2	51.2
-0.004	96	254	32.3	81	69.0	81.6	74.1
-0.005	120	184	32.9	101	91.9	102	97.2

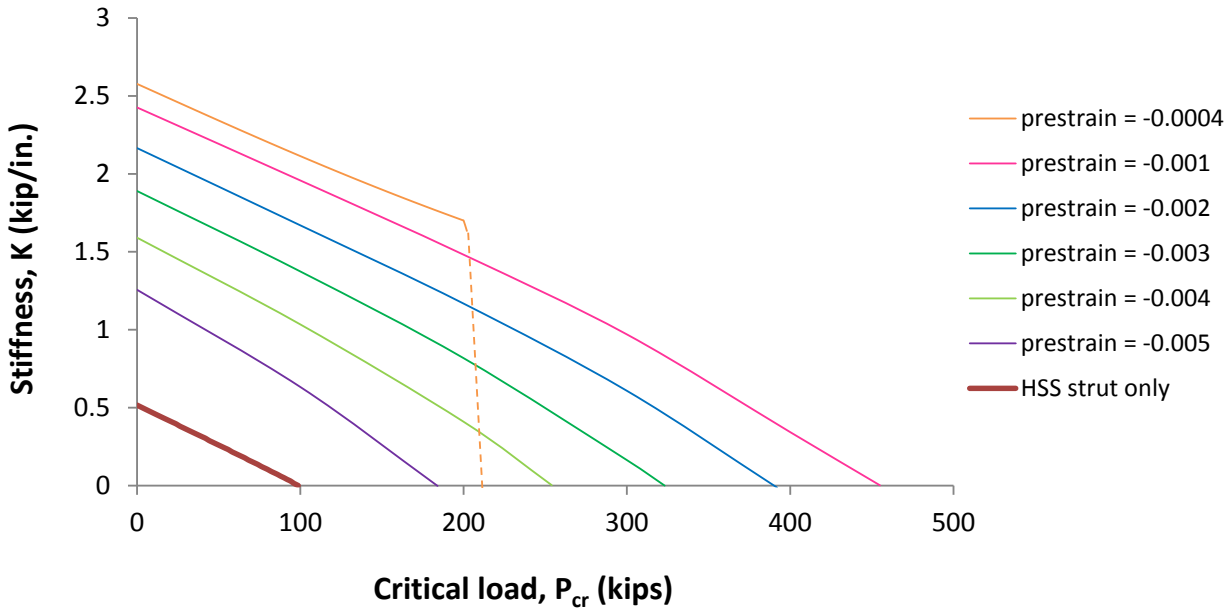

Figure 9.9 Stiffness versus applied load for the stayed column at various prestressing force levels

However, as the prestressing force in the stays is increased, there is a reduction in the buckling capacity of the strut (Figure 9.10). This can be attributed to the loss of compression capacity caused by higher initial compression induced by prestressing. It must be noted that at buckling, the cable stays have a residual tension. The larger the initial prestressing force, the larger are the residual tension in the stay cables. Neither the strut nor the stays yielded for the cases presented.

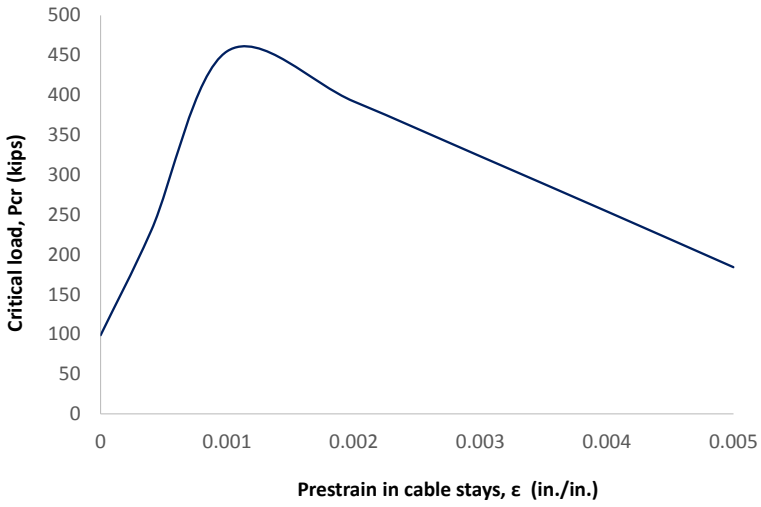

Figure 9.10 Stiffness versus applied load for the stayed strut at various prestressing force levels

Next, the buckling loads obtained from the Stiffness-Probe Method are compared with the results from SAP2000. The procedure in SAP is an iterative approach that implements PΔ and large-displacement effects. A plot of applied load versus joint displacement (Figure 9.11) shows a softening behavior, indicating the onset of buckling and the ensuing instability (CSI Analysis Reference Manual for SAP 2000). The comparative results are in good agreement (Table 9-2).

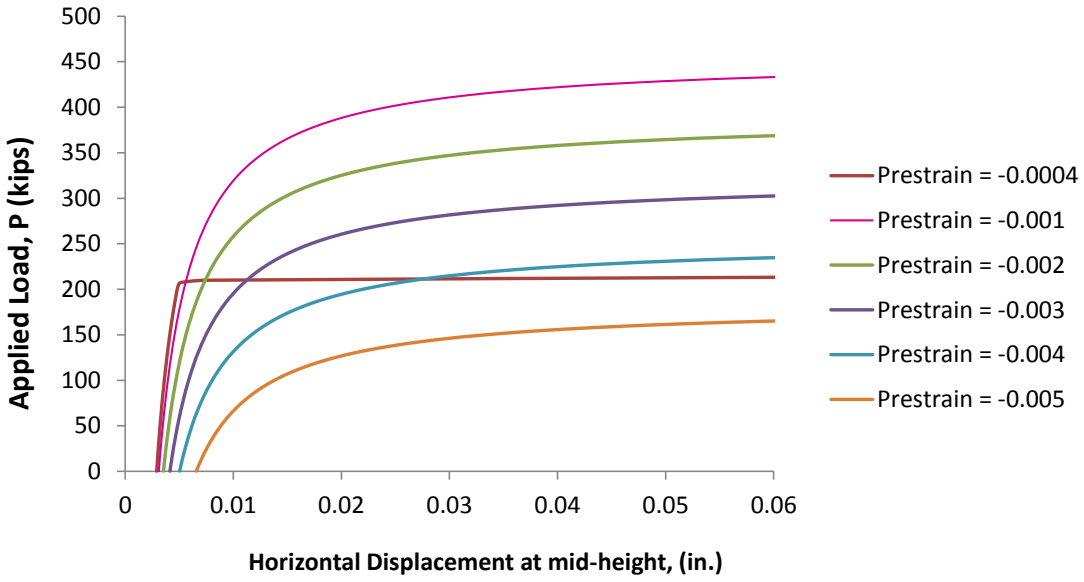

Figure 9.11 SAP2000 plot of applied load versus joint displacement for a prestrain = -0.001

Table 9-2 Buckling Load Comparison

	Stiffness-Probe Method	**Eigenvalue Analysis (using SAP2000)**
Prestrain in stays	Strut buckling load (kips)	Strut buckling load (kips)
0 (HSS only)	98.7	98.8
-0.0004	210	210
-0.001	455	453
-0.002	392	388
-0.003	323	322
-0.004	254	252
-0.005	184	183

Clearly, the buckling capacity of the struts can be increased to several times that of the HSS strut, by using cable-stays set at appropriate levels of prestressing force. For the case where prestrain = -0.001, the buckling capacity of the strut is 455 kips. For a strut alone to be able to achieve this capacity, the outer diameter would have to be increased to 20 in. (originally 12 in.).

The weight of a 20 in. dia. (1/2 in. thick) strut can be found as:

$$W = \gamma_t A_t L \tag{9.1}$$

where γ_t is the density of the strut material, A_t is the cross-sectional area and L is the length of the strut. For γ_t = 490 pcf, A_t = 30.63 in^2 and L = 77.6 ft, Eq. 9.1 gives W = 8088 lb.

Now, for a cable-stayed strut, the weight of the system can be computed as:

$$W = \gamma_t A_t L + 4\gamma_{ca} A_{ca} l_{ca} + 8\gamma_{sc} A_{sc} l_{sc} \tag{9.2}$$

For γ_t = 490 pcf, A_t = 18.06 in^2, L = 77.6 ft, γ_{ca} = 490 pcf, A_{ca} = 18.06 in^2, l_{ca} = 4 ft, γ_{sc} = 490 pcf, A_{sc} = 1 in^2, l_{sc} = 39 ft, Eq. 9.2 gives W = 4768.8 + 983.3 + 1061.7 = 6814 lb.

The comparative weights show that an HSS strut with stays would weigh less than the strut without stays, to achieve the same buckling capacity. Furthermore, using a smaller cross-section for the stays and a larger prestrain will give the same enhanced buckling capacity for a strut (Eq. 5.19). Doing so will result in considerable reduction of a dome's weight. The use of cable-stayed struts, therefore, provides a good alternative design solution to enhance a strut's buckling load by using an appropriate prestressing force in the stays, thereby resulting in a lighter structure.

Now, let's consider the variation of forces in members with applied load. The rate of increase in strut force is smaller for the stayed-struts as compared to the simple strut (without stays). This is because the cables resist a portion of the applied axial load. Clearly, the higher the initial prestressing force in the stays, the higher is the initial compression occurring in the strut (Figure 9.12). That said, at all of the prestressing force levels examined, the rate of increase of strut force was always nearly the same.

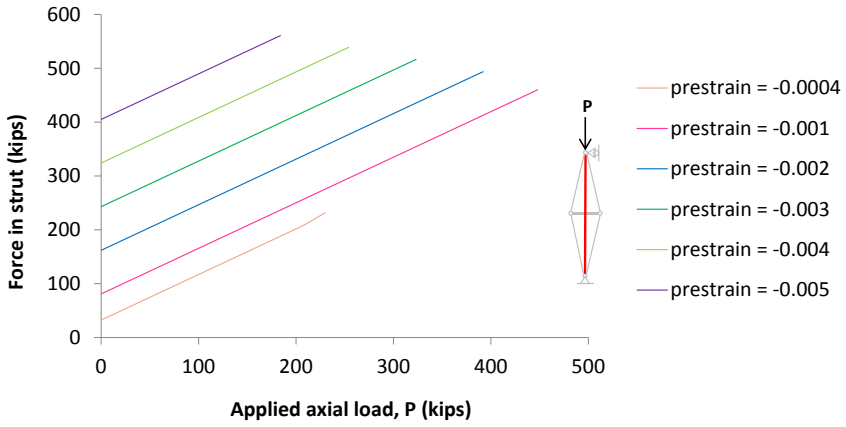

Figure 9.12 Strut force versus applied load for stayed column at various prestressing force levels

Consider the action of the applied load *P* and the perturbation force. The resulting *P-Δ* effect on the strut makes the column move to the right. This causes a reduction in tension in the left stays (Figure 9.13a). At the same time, the strut is pushed downward as *P* increases. This downward deflection also causes the stay on the right to relax. As such, all the stays experience a reduction in tension.

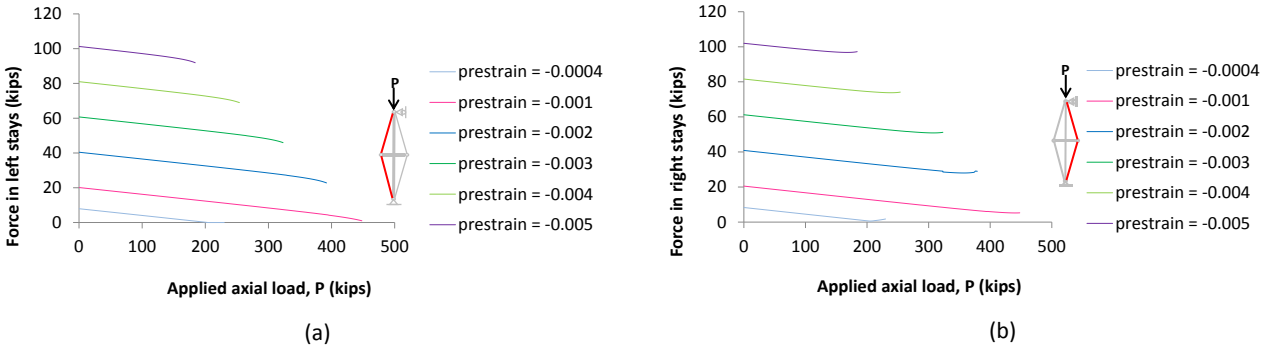

Figure 9.13 (a) Force in the left stays versus applied load P; and (b) Force in the right stays versus applied load P

While it may seem that the transverse movement of the strut would increase the tension in the right stays, the plots show a reduction in tension (Figure 9.13b). This is because the downward movement of the strut relaxes the tensions in the right stay cables. From the same plot, clearly, the right stays do completely lose tension for any of the prestress levels. However, the tension in the left stay may become zero at small prestressing force levels.

9.3 Summary

An alternative design solution has been proposed for domes that abruptly fail due to strut buckling. The use of prestressed cable-stayed struts is found to be an efficient way to increase strut capacity (Table 9-3), depending on the amount of prestressing force given to stay cables. For some cases, the solution may likely change the limit state from one of stiffness/stability of struts to strength failure of struts or stay cables and ensure a ductile behavior. As a consequence of this new design, the domes will have an improved load carrying capacity.

The Stiffness-Probe Method was used for determining the buckling load for the cable-stayed struts. The method proved to be valuable for the following reasons:

1. The method gives a physical understanding of the ensuing instability due to loss of stiffness of a compression member.
2. The user does not have to go through differential equations and numerical schemes for solving for the critical load.
3. The method generates reasonable values of transverse deflections of a column because of the lateral stability provided by the spring. In the absence of a spring, the deflections are unrealistic (10 or more times the length of the column) when the column is close to the buckled state.

CHAPTER 10 SUMMARY AND CONCLUSIONS

10.1 Summary

In this dissertation, the structural behavior of radial-type cable domes under various loading conditions was investigated using a series of (12) 400 ft. span domes with different geometries. The three possible limit states for a cable dome were evaluated, namely 1) buckling of struts, 2) serviceability, and 3) rupture of cables, and an improved design has been recommended to enhance the load carrying capacity of cable domes. Two-dimensional model parameters were derived to replace the three-dimensional hoop and tension ring members of a cable dome. The nonlinear elastic analysis was streamlined using influence surface analysis to identify the governing load combinations for member design.

The two-dimensional model is adequate for the design of domes governed by axisymmetric snow loads. Domes vulnerable to wind uplift could be readily identified using the influence surface analysis. Prestressing force levels were accordingly adjusted to ensure that all cables remained in tension under all loading conditions.

The important force and geometrical parameters, namely, prestressing forces (p), the number of sectors (n), the number of hoop rings (N), hoop radii (R), rise-to-span ratio (r/L), and depth-to-span ratio (d/L) must be carefully determined at the conceptual design stage for design of efficient domes.

For a well-designed cable dome, i.e. whose cables remain in tension under all loading conditions, and for the same rise-to-span ratios, it was found that the struts in a one-hoop ($N1$) domes buckle at half the service load. Two-hoop ($N2$) domes with small d/L ratio = 0.07 and $N3$ domes became unserviceable before the full service load could be supported. Overall, $N2$ domes with d/L ratio = 0.09 performed well for all limit states.

Inelastic analysis using a displacement-controlled procedure was done to determine how much load it takes for the cables to rupture. Clearly, the strut sizes and prestressing forces would have to be substantially increased to allow the cables to yield before the strut buckles of the displacements could exceed the allowable limit. The findings justify the use of an elastic design for cable domes.

To enhance the buckling capacity of the struts, the use of prestressed cable-stays to support the HSS struts was recommended as an alternative solution. Doing so, in turn, increases the load carrying capacity of the domes. The buckling load for stayed struts was found using the Stiffness Probe Method (Gurfinkel, Miller and Robinson, 2009). The method gave a clear understanding of the loss of strut capacity without the need for using differential equations and numerical schemes.

On comparing the member forces due to loads, it was recognized that the struts attracted the least amount of forces. Using this to advantage and considering that erection costs make up approximately 40% of the project cost, an efficient and low-cost prestressing method has been proposed for the erection of cable domes in future research. The prestressed configuration can thus be achieved by prestressing the vertical struts instead of the traditional approach of prestressing the diagonal cables.

The eventual objective of this research is to develop an *American Society of Civil Engineers* (ASCE) Standard for the structural design of prestressed domes. As a prelude towards that effort, design guidelines for cable domes are presented in Appendix-A.

10.2 Conclusions

Based on the design and analysis of the 12 domes, the following conclusions can be drawn:

1. A two-dimensional model is sufficient for the design of cable domes governed by axisymmetric load combinations, thus not requiring complicated and time-consuming three-dimensional analysis. Further, intuitive understanding and valuable insights can be gained efficiently from parametric studies using a two-dimensional model.
2. Findings from an influence surface analysis serve as a good preliminary indicator of the adequacy of the prestressing forces assigned to a dome. The analysis identifies the governing load combinations for critical members and shall be used to minimize the load cases that need to be checked.
3. Prestressing force levels assigned to the diagonal cables must be large enough to keep all cables in tension under the various loading cases and to provide the necessary stiffness to meet the serviceability requirements. While prestressing forces impart the necessary initial stiffness to a dome, they do not affect the final tensions in the cable members. Excessive prestressing forces must be avoided to reduce the demand on the supporting structure.

4. The geometrical parameters play a critical role in the stability of cable domes and their resistance to applied loads. Torsional movements may be minimized by using a polygon with more sides (n). For an efficient design with minimal prestress, it is advisable to use a minimum of n=24 for large span domes. Domes with more hoops (N) will be heavier mainly because of the increase in the number of members, joints and connections. While the additional dead weight may be helpful against uplift forces, more hoops may raise the centroid of hoop tensions which may impact the global stability of a dome. Domes with smaller d/L ratios require more prestressing force to achieve a desired elevation (shape) than those with a higher d/L ratio. Smaller d/L ratios lead to larger horizontal end reactions that may significantly increase the size of the supporting perimeter beam and walls.
5. The outermost diagonal and hoop cables are the critical members in resisting the applied loads, as they experience the largest internal force. The ridge cables are essential stiffening members and generally experience a reduction in tension. The outer ridge cables have a unique behavior; they regain tension under increased gravity loading to maintain the equilibrium at the strut ends and to prevent the tension-ring hub from collapsing. The valley cables contribute significantly to resisting wind uplift forces. They also help to maintain the prestress in the fabric membrane. The stiffened profile of valley cables being arch-shaped, they offer no resistance to gravity loads.
6. The global stability of a cable dome is greatly dependent on the position of the centroid of the hoop tension forces. Structural instability will ensue if the centroid of hoop cable tensions lies too close to or above the elevation of the perimeter beam. Thus, lower the centroid of hoop tension forces below the perimeter beam, larger will be the moment-arm and greater will be the moment resistance and overall stability of a dome.
7. Buckling of struts and/or large displacements are the controlling limit states for a cable dome. These limit states were found to be compromised well within the elastic range of the members. As such, an elastic design is fully justified for the design of cable domes.
8. For domes vulnerable to strut buckling, enhanced capacity can be achieved by stiffening the struts using prestressed cable-stays. Depending on the amount of prestress assigned and section properties of the struts, cables and cross-arms, the addition of the stays may change the limit state from one of stiffness/stability of struts to a strength failure of struts or stay cables. The Stiffness-Probe Method provided an efficient means to compute the critical loads for

prestressed stayed struts. The method gave a physical insight into the loss of capacity of the struts with increase in applied loads.

9. Strut buckling (rigid body buckling) due to ridge cables going slack may happen at higher loads. This in-plane instability may be avoided by ensuring that prestressing force levels are adequate to retain tension in all cables under any loading condition. Increasing the overall prestress in the system uniformly across the span helps to better control the stiffness of the structure. Prestressing force may be increased to control transverse (or torsional) movements of the ridge nodes which can get larger under asymmetric loading. In the case that some cables lose tension due to relaxation or damage, tensioning the interior diagonal cables is the best way to impart additional tension to the already-tensioned diagonal cables as well as ridge cables.
10. For domes that became unserviceable due to large deflections, increasing the initial prestressing forces in the diagonal cables and providing more hoop cable area will stiffen the domes against vertical deflections.

It can be concluded that for a successful cable dome design, the designer must carefully select the various parameters (geometric and prestress), knowing well how they affect the overall structural requirements of strength, stiffness and stability. Prestressing force levels equal to 50% of the strand yield stress is a reasonable initial value. The designer shall use a two-dimensional model and influence surface analysis to check the adequacy of the prestressing force levels. As an enhancement to the conventional structural design of cable domes, the design shall incorporate prestressed cable-stayed struts in place of simple struts as an alternative to increase the critical load of the strut. From a practical point-of-view, the limit states will be reached well within the elastic range. This endorses elastic design as the methodology for cable dome design.

10.3 Future Research

Future research on cable domes may be exciting, both as a creative endeavor for developing new forms and for finding cost-effective construction methods. Exploring the following areas will serve to advance the current literature in cable dome research:

10.3.1 Experimental research

A. Parametric investigation of cable dome behavior

This study has shown that practical requirements keep the design of cable domes within the elastic range. The primary objective of experimental studies of small-scale domes will be to match test results with calculated response from SAP2000 and verify if a good correlation exists between the measured and calculated results.

The specific goals of the experiments shall be to:

1. Identify the various limit states within the elastic range.
2. Study the effect of loss in cable tension on the strength and stiffness of a cable dome.

Because space constraints and expense in testing full-scale domes are generally prohibitive, it will be reasonable to construct and test models to $1/10^{th}$ scale. As there are several critical parameters in cable-dome design, the experiments shall be focused to a few parametric variations. The analysis results from this study showed that *N*2 domes performed well to satisfy the limit states. Two models shall be tested as part of the experimental verification. In Model-1, prestressing forces and *d/L* ratios shall be varied for an *N*2:*n*24:*r/L*0.083 domes. In Model-2 the number of hoops shall be varied (*N* = 2 and 3). The latter will be useful for studying the effectiveness of struts for different *N*. The domes shall be investigated for static loads, both symmetric and asymmetric. The uplift forces due to wind may be simulated from an internal pressure test using high-power fans/blowers.

B. Prestressed cable-stayed struts.

Prestressed cable-stays offer great potential as an alternative for stiffening compression members. The findings from this thesis have shown that the critical load can be increased significantly by appropriately prestressing the stays. The goal will be to evaluate the experimental response of these prestressed steel columns and compare them with the results of computer simulations using SAP2000, for two different configurations, namely one and two cross-armed struts (Figure 10.1).

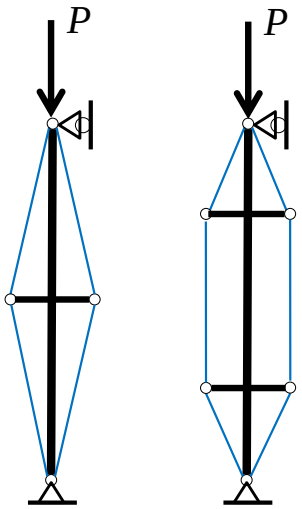

Figure 10.1 (a) One-arm cable-stayed strut; (b) Two-arm cable-stayed strut

The potential benefits of using prestressed cable-stayed struts to enhance the buckling capacity shall be examined further for the following objectives:

a. To determine the buckling load for various prestressing forces in the stays.
b. To determine the effect of multiple cross-arms along the height of a strut on the limit state of the strut. The limit states to be observed in the tests are slackening of the cable-stays, crushing of the HSS tube, and yielding or rupture of cable-stays.
c. Investigating the strength and stiffness interaction of the two stayed-strut configurations in subject.

A quarter-scale two-dimensional model of pin-ended stayed struts, shown in Figure 10.1, shall be used for experiments. The material and members properties will be the same as that used in the computer analysis. An initial imperfection would have to be introduced to initiate the bending of the struts under loads. The models will be tested for different prestressing force in the stays, namely $0.25f_y$, $0.33f_y$ and $0.5f_y$, where f_y = 243 ksi is the yield stress of the strands.

10.3.2 Design of asymmetrical cable domes

Many stadia and performing arts facilities have plans that are asymmetrical. Cable dome forms that follow the function of the space to be roofed may generate interesting and expressive structures. Asymmetrical circular (Figure 10.2a) and asymmetrical elliptical cable domes (Figure 10.2b) have not been built to date. Departure from a symmetrical layout of cables, struts and

supporting structure has structural implications. Consider the following two configurations: i) Circular cable dome with an eccentric tension ring; and ii) Elliptical cable dome with a concentric tension ring. The cable forces will not be the same, even under a uniform pressure field. This arrangement results in large out-of-balance horizontal forces at the perimeter beam. The large bending moments will require a massive and expensive supporting structure.

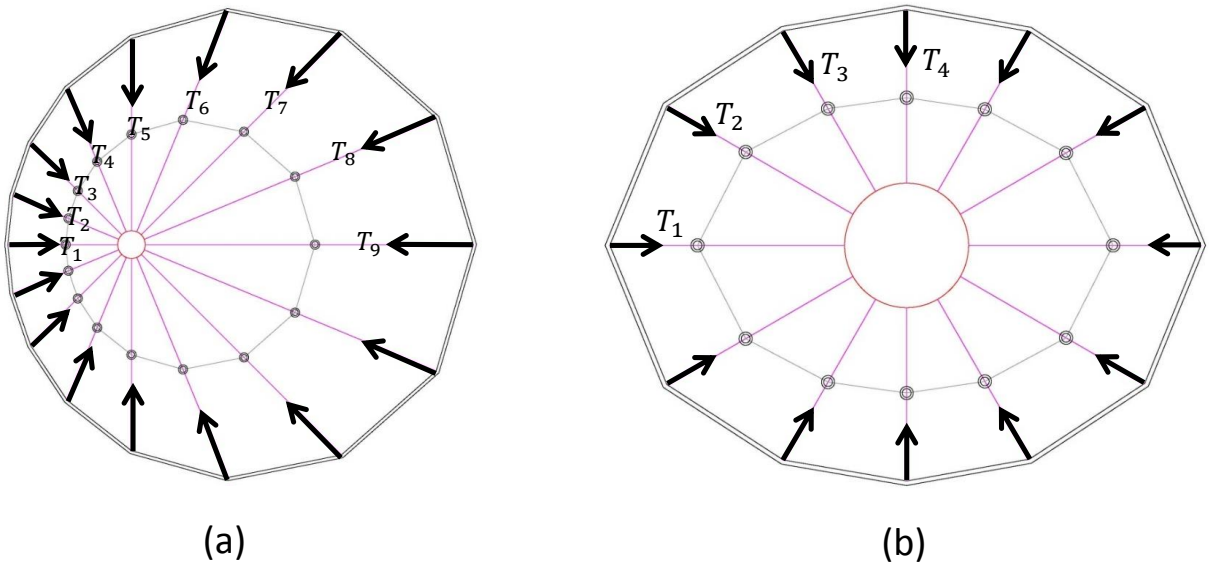

Figure 10.2 (a) Circular cable dome with an eccentric tension ring; and (b) Elliptical cable dome with concentric tension ring

The intellectual challenge in the design of asymmetrical cable domes is to minimize the structural implications of asymmetry. An iterative computer program may be written to determine cable tensions such that the perimeter beam is theoretically moment-less.

10.3.3 Erection method using prestressing of struts

Conventional practice (Figure 10.3, Stages 1-4) calls for cable domes to be erected by first hanging the ridge cables and struts from the outer compression ring. Once this is done, diagonal and hoop cables are attached sequentially from the compression ring side to the tension ring side. Diagonals are prestressed in a sequential manner, from outside to inside. This approach involves many workers on the job prestressing the diagonal cables simultaneously to induce only equal radial forces in order to keep bending moments from being induced in the compression ring. After all diagonals are prestressed, the dome acquires the desired geometry. Prestressing force levels are adjusted one last time to ensure radial force balance. The entire process involves many workers

and proper coordination. The erection costs are approximately 40% of the total cost of design and construction.

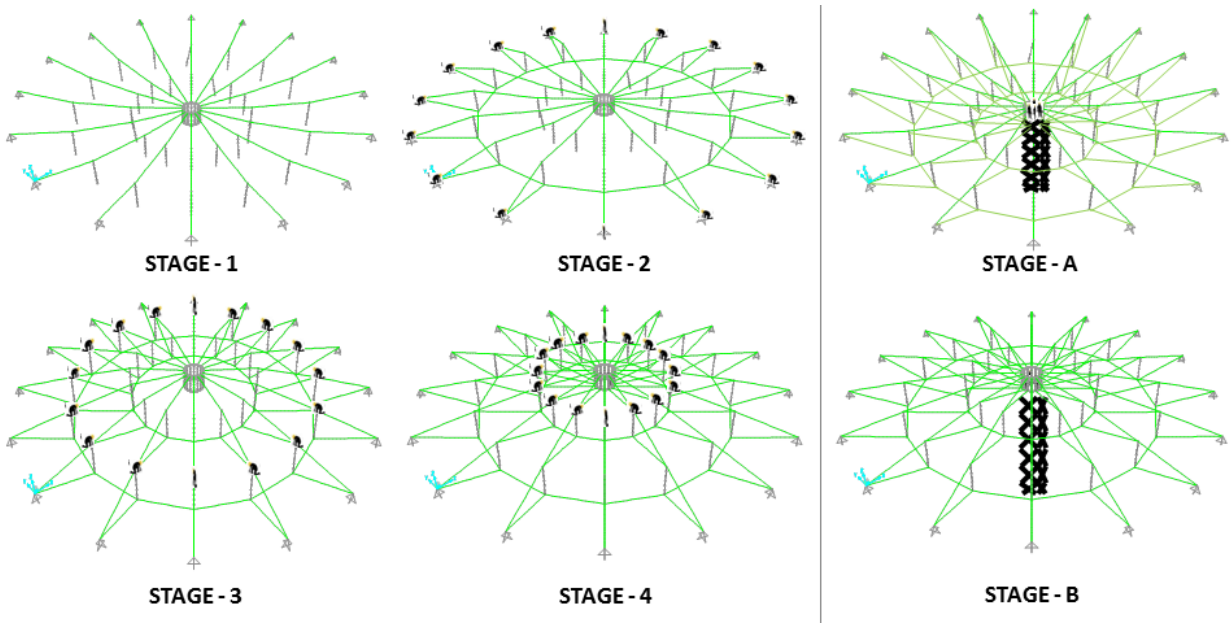

Figure 10.3 Traditional method of erection (Stages 1-4)
Proposed method of erection (Stages A and B)

In lieu of the above and taking advantage of the smaller forces in the struts, a smaller prestress in the struts may yield the same desired dome geometry as a large prestress in the diagonals. In this suggested alternative method for erection, all essential operations can be done from the central cage (Figure 10.3, Stages A and B). All members will be assembled on ground and hoisted up at the central hub. The ends of the outer ridge and diagonals will then be connected to the compression ring. Once the web is formed, the central hub can be hoisted further until the crown reaches the desired elevation. At this stage, the hoisting system will be locked and prestressing of vertical struts will commence at the central hub. Prestressing may be done by telescoping the struts. A feasibility and cost-benefit of this erection method may lead to significant cost-savings for contractors. The aforementioned method may be used advantageously for cable domes to be erected in between locked topography or urban spaces, i.e., in between rock hills or in between existing buildings, where site-presented constraints will not allow for the conventional method of prestressing of the diagonal cables.

APPENDIX A

DESIGN GUIDELINES

This document provides guidelines for the design of cable domes based on the findings of this research and industry practices. The ASCE/SEI 19-10 for design of cables in buildings and the ASCE/SEI 55-10 provisions for design of tensile and membrane structures are broad and provide useful guidelines for tensile structures in general. Design of cable domes requires specialized engineering knowledge. An ASCE/SEI Standard developed exclusively for cable dome design to include radial, triangulated and other prestressed cable domes will serve as a valuable design guide. Based on the findings of this research and industry practices, the following guidelines are intended to organize current knowledge and the findings of this research on radial-type cable domes in order to help structural engineers make informed design decisions.

1. Codes and Standards

The diagonal, hoop and ridge cables shall be designed using the ASCE Standard 19-10 "Structural Applications of Steel Cables for Buildings" and the membrane must be designed per the ASCE/SEI Standard 55-10 "Tensile Membrane Structures." Both Standards follow the ASCE 7-10 Code "Minimum Design Loads for Buildings and Other Structures."

2. Material Specifications

Steel and reinforced concrete are the basic materials used for the construction of cable domes. The struts shall be made of standard steel pipes; they shall possess sufficient bending stiffness for a higher buckling capacity and shall be designed per AISC specifications. Steel strands and ropes shall be used for the diagonal, hoop and ridge cables. They shall be designed in accordance with ASCE 19-10. The steel ropes and strands shall be pre-stretched by repeated loading and unloading cycles with traction values equal to approximately 50 percent of their fracture load to elevate the elastic modulus and thereby eliminate cable relaxation or creep.

Strand is covered by ASTM A416 "Steel Strand, Uncoated Seven-Wire for Prestressed Concrete." There are seven wires, with six of them helically wound around a straight center wire which is slightly larger than the outer wires. Strands are available in two grades: Grade 250 (f_{pu} = 250 ksi)

and Grade 270 (f_{pu} = 270 ksi) and in two types of material: "low-relaxation" and "stress-relieved (normal relaxation)". The low-relaxation type Grade 270 has been the grade of choice for cable domes (Table A-1).

Table A-1 Properties of ASTM A416, Seven-Wire Strand, Grade 270

Diam. **in.**	Weight lb./1000ft	Area in^2	Tensioning Load lb., at 202.5 ksi	Strength lb., at 270 ksi
3/8	290	0.085	17,200	23,000
7/16	390	0.115	23,300	31,000
1/2	520	0.153	31,000	41,300
0.6	740	0.217	43,900	58,600

Wire is covered by ASTM A421. Several sizes are available. Table A-2 lists the available choices. The stress-strain characteristics are similar to those of strand, except that Young's Modulus should be a little higher since the wire is a solid bar. The strengths are a little lower than that of strand because of cooling rate differences during manufacturing.

Table A-2 Properties of a Wire

Diameter* (in.)	**Area** (in^2)	**Min. yield stress** (ksi)	**Rupture Stress** (ksi)
0.192	0.02895	200	250
0.196	0.03017	200	250
0.250	0.04909	192	240
0.276	0.05983	188	235

* Other sizes and types exist

The perimeter ring beam shall be made of reinforced concrete and shall be designed in accordance with ASCE 318. This may be polygonal or circular, depending on the number of sides used.

Fabric membrane shall be made of polytetrafluoroethylene (PTFE) to provide both strength and self-cleansing properties. Newer materials with better architectural properties shall be considered; for example, ETFE and UltraLUX. The strength and durability of any new material shall be comparable to or better than those of PTFE. Membrane physical properties shall be determined in accordance with ASTM D485.

3. Connections

Membrane to cable, cable-to-cable, cable-to-steel and cable to perimeter beam connections shall be designed to transfer all applied and internal forces and moments as required by the analysis. Environmental effects, cable relaxation and movements caused by large deflections and rotations of the structure shall be accounted for. Corrosion protection shall be provided for durability of connections.

4. Structural Design

Cable domes experience loads similar to conventional building structures, except for their prestressing force which is part of the resistance. They shall be designed for the combined effects of gravity and wind uplift forces that may produce the most unfavorable effects.

Loads

Prestress

Appropriate prestressing forces shall be provided to ensure adequate structural stiffness. Prestressing force levels shall be considered satisfactory if on application of external loads, no cables go slack and the deflections are within permissible limits. Initial prestressing force levels shall be kept within 50% of the yield stress of the strands.

Dead and Live Loads

The dead load shall include self-weight of fabric, struts, strands, cables, tension ring, and cast steel connections. A load case with a single concentrated load of 100 kips shall be applied in the gravity direction at a single outer hoop to a strut connection node. The superimposed dead load shall be taken as 8 psf. The domes shall be designed for a minimum live load of 12 psf.

Rain Loads

Rain loads (if applicable) must be included depending on the roof geometry where ponding is a possibility. Sections 7.10 and 7.11 of ASCE/SEI 7-10 (ASCE 2010c) shall apply.

Snow Loads

Symmetric and asymmetric loads shall be determined from Section 7.6.2 and Figure 7-3 of ASCE/SEI 7-10 (ASCE 2010c, p. 37). Due to low-rise, the slope at the eaves is less than 30°. Thus, Case-1 from Figure 7-3 in ASCE 2010c shall be used to determine the distribution of snow loads. Depending on the rise of the dome, appropriate values for C_s shall be assumed. For domes with $r/L \leq 0.083$, C_s =1.0 is acceptable. Depending on the ridge profile, the snow may slide towards the compression ring because of the slope. As the slope of ridge varies in elevation, the snow loads shall be modified in accordance with Sec. 7.6.3 of ASCE/SEI 7-10 (ASCE 2010c, p. 32). Besides the geometry of the roof, other factors such as formation of ice dams shall be considered. The slickness of roof surface, insulation and cold bridges may have a significant influence. Some of the aforementioned factors for cold and warm roofs are addressed in Figure 7-2a and Sec. 7.9 of ASCE/SEI 7-10 (ASCE 2010c, p. 36). The provisions for asymmetric loads as applied to curved roofs shall be applicable to cable domes. Figure 7-3 of ASCE/SEI 7-10 (ASCE 2010c, p. 37) illustrates the variation of asymmetric loads.

Wind Loads

The Main Wind Force Resisting System (MWFRS) shall be designed for wind pressures as obtained by the Directional Procedure (Chapter 27, ASCE7-10c). The ASD load factor of 0.6 for wind loads will reduce the peak wind loads obtained from the Directional Procedure to service load value. Design wind pressures (psf) shall be specified for the design of the fabric membrane as well as wall claddings of the superstructure per Figure 30.4-7 of ASCE/SEI 7-10 (ASCE 2010c, p. 344). Special consideration shall be given to local effects of wind turbulence and vibrations, especially near the eaves of the dome.

Other Loads

Earthquake loads and other loads such as thermal effects, cable relaxation and construction loads shall be appropriately considered.

Load Combinations

The design of members should be based on the load combination causing the most unfavorable effect, keeping in mind that in some cases, this effect may occur when one or more loads are not acting. The load combinations selected are similar to the Allowable Stress Design (ASD) load combinations from ASCE 19-10, except for LC-6 which is given a factor of 0.6 on prestress for safety. The rationale for all combinations is explained in Section 3.2.

Table A-3 Allowable Stress Design Load Cases and Load Combinations

Load Case	Load Combinations
LC-1	D + P
LC-2a.	D + P + S_s (Snow on full span)
LC-2b.	D + P + S_{as} (Snow on half span)
LC-3a.	D + P + 0.6W_s (Suction on full span)
LC-3b.	D + P + 0.6W_{as} (Suction on half span)
LC-4a.	D+ P + 0.75(0.6W_s) + 0.75 S_s
LC-4b.	D+ P + 0.75(0.6W_{as}) + 0.75 S_s
LC-5a.	D+ P + 0.75(0.6W_s) + 0.75 S_{as}
LC-5b.	D+ P + 0.75(0.6W_{as}) + 0.75 S_{as}
LC-6	0.6D + 0.6P +0.6W_s
LC-7	D + P + C_n

Structural engineers shall adopt the LRFD procedure after further research regarding combinations of prestressing forces and factored loads, and understanding of geometric nonlinearities.

Influence Surface Analysis

The design process shall be made efficient by using the influence surface analysis. The findings from the influence surface analysis shall be used to identify the governing load combinations for critical members of the dome. They shall also inform the designer about the adequacy of the prestressing force levels.

Layout and Sizing

For domes with span equal to or greater than 400 ft., a designer shall use a minimum of n = 24 with a d/L=0.14. This will result in reasonable prestressing force levels and internal forces. Torsional movements will also be restricted, and the horizontal end reactions will also be small. The hoop stiffness reduces by half when either n or R is doubled (Figure 5.3). Therefore, use small R to increase the effectiveness of the hoop cables which is one of the principal members of a cable dome.

The preliminary member areas of cables and struts shall be based on the analysis of a two-dimensional truss model (i.e., a truss in which the ridge cables are replaced by two-force members) using full axisymmetric snow loads on the structure. The compression in the top chord members can be overcome by prestressing the diagonal members. After the ridge members are sufficiently tensioned (5-10% of the rupture stress), the members shall be sized using the internal forces and the allowable member stresses.

Use of Two-dimensional Model

An equivalent two-dimensional model (Chapter 5) shall be used for efficient design and to gain insights about behavior via parametric studies. For domes in snow-prone regions, a two-dimensional analysis will be sufficient for the design of circular axisymmetric cable domes.

Structural Modeling and Analysis

A nonlinear finite element algorithm that accounts for large displacements shall be developed. Alternatively, commercial programs such as SAP2000, Abaqus or ANSYS may be used. The analysis type shall be nonlinear with large displacement and P-Δ effects. Inelastic analysis shall be performed using an approximate bilinear material model for the steel strands (Figure 7.9a).

Assumptions for modeling and analysis shall include:

i. Large displacement and small strain.
ii. Uniaxial loading.
iii. Cables are tension-only members.
iv. Roof membrane has negligible bending stiffness.
v. Snow loads are applied as point loads at the top nodes of the struts.
vi. Rigid perimeter beam.

Other Design Considerations and Concerns

The limit states criteria for a cable dome will depend on the governing load combination. Strut buckling, serviceability and cable rupture are possible limit states. The following design criteria and provisions shall be used:

1. Under any loading conditions, no cables shall go slack. Under asymmetric load conditions, few cables going slack would be acceptable near the maximum design loads only. They shall not go slack at less than 80% of the design load. More than 10% of cables going slack shall not be acceptable. Wind loadings cause cable slackening; this must be addressed in the design process.

2. Prestrain given to the diagonal cables shall be kept at 50% of $\varepsilon_y = \frac{\sigma_y}{E} = \frac{243\,ksi}{24,000\,ksi} = 0.01$, i.e. 0.005. Keeping the prestrain level at 0.005 ensures enough tensile capacity needed for the cables to resist applied loads.

3. The maximum tensile stress in cables shall not exceed $\frac{\sigma_{rupture}}{2.2}$. To ensure that there is enough residual tension in the ridge cables, a minimum internal stress of $\sigma_{\min} = \frac{\sigma_{\max}}{10}$ shall be maintained in all cables.

4. The vertical deflections in built cable domes are observed to be approximately equal to span/180. The limit shall be the designer's judgment such that proper positive drainage in the roof is provided despite large displacements. Levy (1991) mentions a stringent deflection criterion of *L*/250 for live load in triangulated domes.

5. The net horizontal displacement of the nodes can be given a more stringent limit of $h/240$, where h is the strut height. This will ensure both structural integrity and aesthetics.
6. Use fewer hoops to minimize the number of members and connections.
7. Diagonal cable inclinations shall be 30° or greater to keep the prestressing force levels and member forces reasonable.
8. Prestressed cable-stayed struts shall be used as an alternative to HSS struts alone, for very slender members.

5. Fabrication and Erection

Detailed shop drawings shall be produced for the fabrication of all components of a cable dome structure. The drawings shall comply with the requirements of the respective standards of the component members, i.e., ASCE 19-10 for cables, AISC for struts, and ASCE 55-10 for fabric membrane.

Cable domes shall be erected by diagonal prestressing, which is the traditional and tested approach. The suggested new method (Section 10.3) for erecting cable domes by prestressing the struts shall be evaluated by the contractors for feasibility and cost-benefit. Success with the latter can be advantageously used for erecting cable domes in locations where the conventional method of prestressing is not viable. In either case, the erection procedure shall include a detailed numerical analysis of the stages involved in erection of the cable dome.

APPENDIX B

INFLUENCE SURFACE ANALYSIS RESULTS FOR *N*2:*N*16 AND *N*3:*N*16 DOMES

Results from the influence surface analysis for *N*1 dome were presented in Section 3.2.2. This appendix complements Section 3.2.2 to include results from *N*2 and *N*3 domes.

The significance of influence coefficients can be best understood from the illustrations in Figure B.1. The vertical deflections in the illustrations are the influence coefficients for the vertical loads applied at those nodes. Using the numerical values of the influence coefficients and Eq. 3.13, the member forces are obtained for the various load combinations. Clearly, the outermost hoop cables, diagonal cables and struts will experience maximum internal forces due to a symmetric loading condition (F_{D3}, T_{H2}, C_{S3} in Figure B.1). The innermost members F_{D1}, C_{S1}, and T_{R1} are governed by asymmetric wind loading conditions. Some of the inner member designs and the ridge cable designs are governed by wind suction forces.

Table B-1 Internal member forces found using influence coefficients for the *N*2:*n*16:*d*/*L*0.09 dome

LC - #	ASD LOAD COMBINATIONS	F_{D3}	F_{D2}	F_{D1}	T_{H2}	T_{H1}	C_{S3}	C_{S2}	C_{S1}	T_{R3}	T_{R2}	T_{R1}
LC - 1	D + P	185	71.0	24.0	411	158	89.7	32.3	11.5	116	50.8	29.4
LC – 2a.	D + P + S_b	537	254	87.9	1189	564	268	125	43.3	92	-133	-209
LC – 2b.	D + P + S_{ub}	323	144	23.5	730	331	140	48.5	0.90	180	44.7	25.7
LC – 3a.	D + P + 0.6 W_b	141	113	15.8	314	252	67.5	53.4	7.40	151	47.1	33.0
LC – 3b.	D + P + 0.6 W_{ub}	155	98.0	24.4	348	216	68.3	52.7	7.30	136	47.6	25.6
LC – 4a.	D + P + 0.75 (0.6 W_b) + 0.75 S_b	416	240	65.8	922	533	207	117	32.3	124	-89.7	-146
LC – 4b.	D + P + 0.75 (0.6 W_{ub}) + 0.75 S_{ub}	427	229	72.3	948	506	207	117	32.2	113	-89.3	-152
LC – 4c.	D + P + 0.75 (0.6 W_{ub}) + 0.75 S_b	256	157	17.5	578	358	110	60.3	0.50	190	43.5	29.3
LC – 4d.	D + P + 0.75 (0.6 W_b) + 0.75 S_{ub}	266	145.8	24.0	603	331	111	59.7	0.40	179	43.9	23.7
LC – 5a.	0.6D + 0.6P + 0.6W_b	83.3	90.7	7.1	185	201	38	44.0	3.1	104	21.3	14.9
LC – 5b.	0.6D + 0.6P + 0.6W_{ub}	97.1	75.4	15.7	219	165	38.8	43.3	3.0	88.7	21.9	7.5

Clearly, the prestressing force levels assigned are not adequate, as two sets of ridge cables (except for outermost) went slack under LC-2a (full symmetric snow loads) and under LC-4a and 4b. The influence surface analysis is therefore a good indicator of the adequacy of prestressing force levels for a dome.

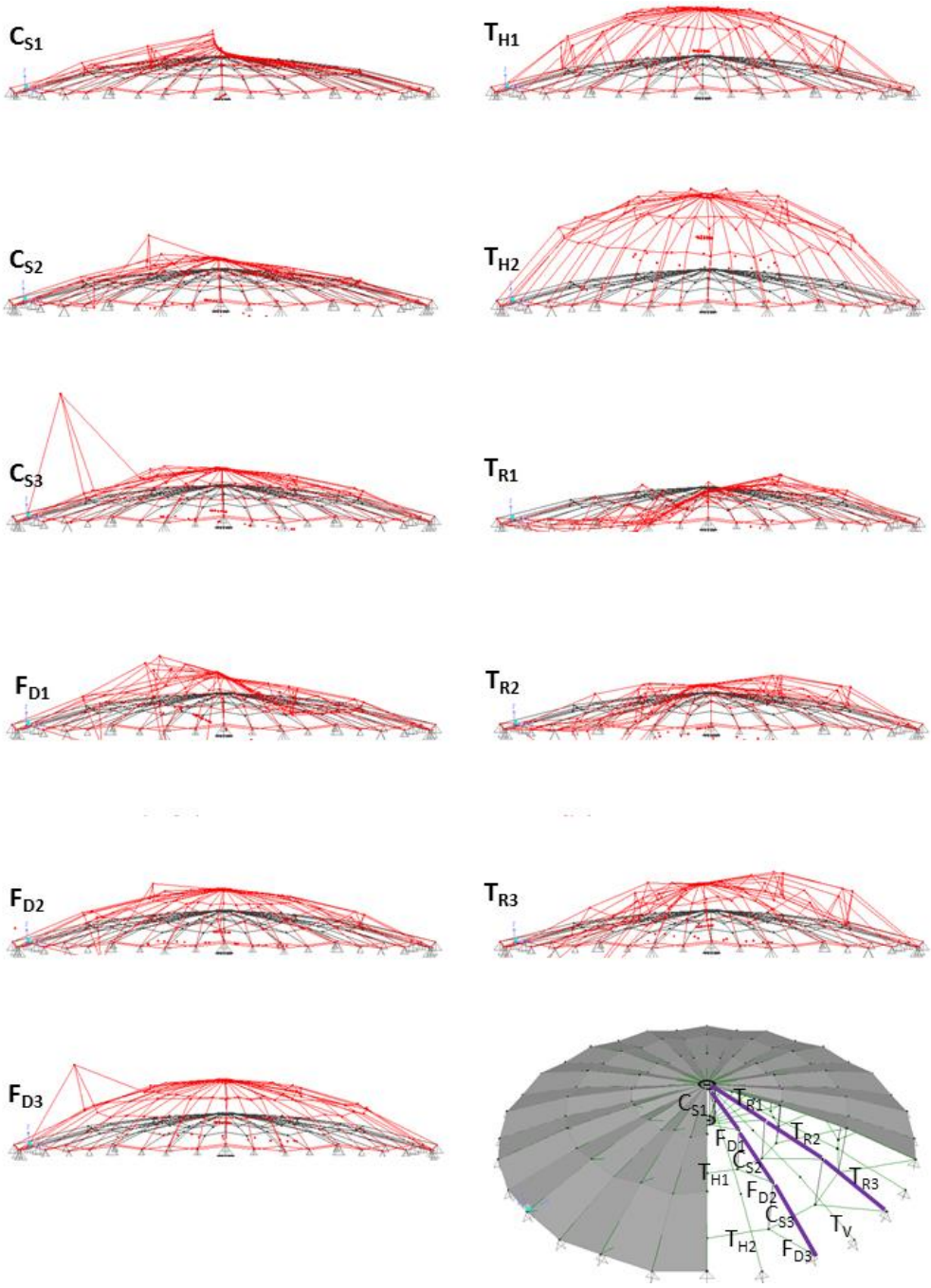

Figure B.1 Influence surface for the various members of an *N*2:*n*16:*d*/*L*0.09 dome (Scale = 2000)

The influence surfaces for the various members in an *N*3:*n*16 dome are shown in Figure B.2. Clearly, the outermost members, i.e., hoop T_{H3}, diagonal F_4 and strut C_4 experienced the maximum internal forces due to applied gravity loads (Table B-2) due to full axisymmetric snow load, LC-2a. The innermost members F_{D1}, C_{S1}, and T_{R1} are governed by wind loadings. It must be noted that under the action of reduced dead load and wind uplift forces, the outermost diagonal members are almost going into compression. They further instruct a designer about the load combinations to use that the largest downward nodal forces and the largest net uplift forces. Some of the inner diagonal cable and ridge cable designs are governed by the effect of wind suction forces. When compared to *N*2:*n*16 and *N*1:*n*16, the internal member forces are much higher under gravity loads. The prestressing force levels are not adequate to resist snow loads.

Table B-2 Internal member forces found using influence coefficients for the *N*3:*n*16:*d/L*0.07 dome

LC - #	ASD LOAD COMBINATIONS	F_{D4}	F_{D3}	F_{D2}	F_{D1}	T_{H3}	T_{H2}	T_{H1}	C_{S4}	C_{S3}	C_{S2}	C_{S1}	T_{R4}	T_{R3}	T_{R2}	T_{R1}
LC - 1	D + P	260	117	48.1	15.6	577	259	107	126	55.6	22.6	7.3	204	95.1	51.6	37.8
LC – 2a.	D + P + S_b	468	196	66.7	8.8	1036	435	148	232	95.9	32.1	4.1	171	-7.1	-65.2	-72.4
LC – 2b.	D + P + S_{ub}	335	147	55.5	4.9	757	333	126	147	60.5	20.7	0.70	189	49.5	-0.50	-4.20
LC – 3a.	D + P + 0.6 W_b	99.5	59.1	36.6	21.3	222	132	81.5	44.0	26.3	16.7	10.1	233	175	140	121
LC – 3b.	D + P + 0.6 W_{ub}	157	80.9	41.1	13.3	361	185	93.9	59.5	29.5	15.0	5.0	220	139	99.9	88.0
LC – 4a.	D + P + 0.75 (0.6 W_b) + 0.75 S_b	296	133	53.4	14.8	655	295	119	144	63.8	25.3	7.0	201	78	30.2	17.2
LC – 4b.	D + P + 0.75 (0.6 W_{ub}) + 0.75 S_{ub}	339	150	56.8	8.80	759	336	128	156	66.3	24.0	3.10	191	51.0	0.20	-7.20
LC – 4c.	D + P + 0.75 (0.6 W_{ub}) + 0.75 S_b	196	96.1	45.0	11.9	446	219	102	80.0	37.3	16.7	4.4	215	121	78.8	68.3
LC – 4d.	D + P + 0.75 (0.6 W_b) + 0.75 S_{ub}	239	112	48.4	5.90	550	259	112	91.7	39.7	15.4	0.60	204	93.4	48.7	43.9
LC – 5a.	0.6D + 0.6P + 0.6W_b	0.80	15.0	17.5	14.2	3.2	32.2	39.2	-3.80	5.10	7.80	6.80	162	145	127	114
LC – 5b.	0.6D + 0.6P + 0.6W_{ub}	58.4	36.7	22.1	6.20	142	85.9	51.6	11.7	8.3	6.0	1.60	149	109	87.2	81.6

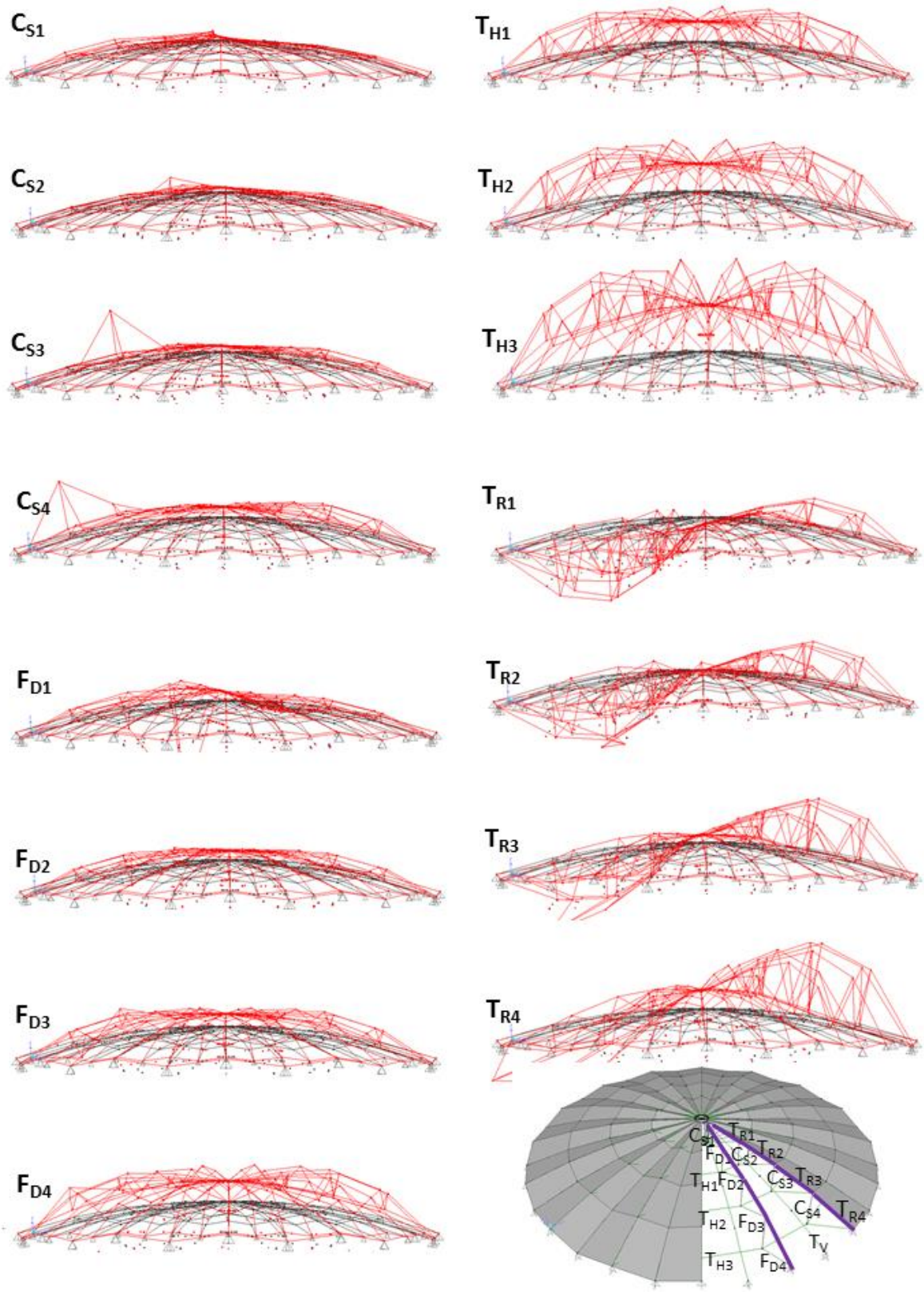

Figure B.2 Influence surface for the various members of an *N*3:*n*16:*d/L*0.07 dome (Scale = 1000)

APPENDIX C

NONLINEAR ANALYSIS RESULTS: *N*2 AND *N*3 DOMES

This section provides a comparison of member forces and displacements for *N*2 and *N*3 domes, each with two different *d/L* ratios. The results provide an insight into the limit state of each of the domes. Tables C-1 and C-2 present the results for *N*2:*n*16:*L*400:*r/L*0.083:*d/L*0.09 dome and *N*2:*n*16:*L*400:*r/L*0.083:*d/L*0.07 dome. The former failed simultaneously in serviceability and strut buckling, while the latter clearly failed in serviceability.

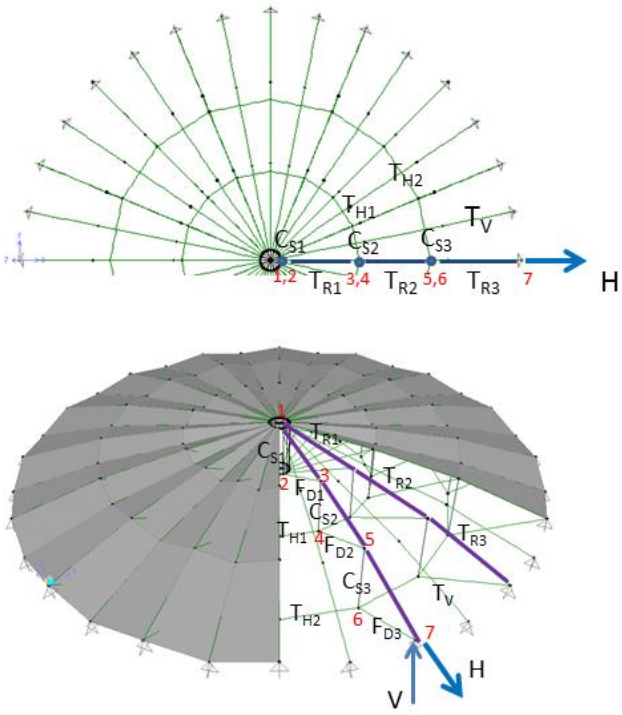

Figure C.1 *N*2 dome node and member labels

The ridge cable cross-sectional areas (inner to outer) provided are 1.67 in^2, 2.97 in^2 and 5.58 in^2 respectively, the diagonal cable areas are 1.30 in^2, 2.60 in^2 and 5.21 in^2, respectively; and the hoop cable areas are 6.04 in^2 and 11.25 in^2 respectively. The struts areas (inner to outer) are 14.9 in^2, 18.1 in^2 and 18.1 in^2. The buckling capacity of the outermost strut calculatedd from Euler's formula as 204 kips (for *d/L*=0.09) and 313 kips (for *d/L*=0.07), where *EI* = 29000 ksi x 299.2 in^4 = 8.677 x 10^6 $k.in^2$ is the flexural stiffness of the strut, *L* = 54 ft. (for *d/L*=0.09) and 43.7 ft. (for *d/L*=0.07) and *k* =1 for hinged ends.

Table C-1: Inelastic analysis: Summary of results for *N*2:*n*16:*L*400:*r*/*L*0.083:*d*/*L*0.09 dome

	Vert. Defl. at Joint 1	at Joint 5	at Joint 9	Live Load at Joint 1	at Joint 5	at Joint 9	Member Forces Diagonal Cables			Hoop Cables		Ridge Cables			Strut			
	Δ_1 in.	Δ_5 in.	Δ_9 in.	W_1 kips	W_5 kips	W_9 kips	D_1 kips	D_2 kips	D_3 kips	T_1 kips	T_2 kips	R_1 kips	R_2 kips	R_3 kips	C_1 kips	C_2 kips	Stress_T_2	Stress_D_3
0	15.1	7.1	2.0	1	5.3	9.8	19.1	65.7	178.3	57.1	154.8	36.4	53.4	114.4	-30.3	-84.7	35.3	34.2
1	9.06	2.1	-0.7	2.5	13.2	24.2	18.2	86.9	249.2	75.5	216.3	5.6	21.8	101.3	-41.0	-120.8	49.3	47.9
2	1.28	-3.3	-3.4	4.4	23.7	43.4	21.2	110.5	320.4	95.9	278.0	1.7	20.7	121.7	-53.1	-157.4	63.4	61.5
3	-6.66	-8.7	-6.1	6.4	34.0	62.3	24.8	134.5	391.9	116.7	340.0	1.2	23.5	146.7	-65.5	-194.6	77.5	75.2
4	-14.5	-14.2	-8.8	8.3	44.5	81.6	28.5	158.7	463.7	137.7	402.3	1.0	26.8	172.4	-78.2	-232.3	91.7	89.0
5	-22.4	-19.6	-11.5	10.3	55.2	101.2	32.2	183.1	535.8	158.9	464.8	0.9	30.3	198.6	-91.1	-270.5	105.9	102.9
6	-30.1	-25.0	-14.2	12.4	66.1	121.1	36.0	207.7	608.2	180.2	527.5	0.8	33.9	225.2	-104.2	-309.4	120.2	116.8
7	-37.8	-30.4	-16.9	14.4	77.2	141.5	39.9	232.5	680.9	201.6	590.5	0.7	37.7	252.2	-117.6	-348.7	134.6	130.8
8	-45.5	-35.8	-19.6	16.6	88.5	162.2	43.7	257.5	754.0	223.3	653.8	0.7	41.6	279.7	-131.2	-388.6	149.0	144.8
9	-53.0	-41.1	-22.3	18.7	100.1	183.3	47.7	282.6	827.3	245.1	717.4	0.6	45.6	307.5	-145.1	-429.1	163.5	158.9
10	-60.6	-46.5	-25.0	20.9	111.8	204.8	51.6	308.0	901.0	267.0	781.2	0.6	49.7	335.8	-159.2	-470.1	178.1	173.0
11	-68.0	-51.8	-27.7	23.1	123.7	226.7	55.6	333.6	974.9	289.2	845.2	0.6	53.9	364.5	-173.5	-511.6	192.7	187.2
12	-75.4	-57.1	-30.4	25.4	135.9	249.0	59.7	359.4	1049.2	311.4	909.5	0.5	58.2	393.6	-188.1	-553.7	207.3	201.5
13	-82.8	-62.4	-33.1	27.7	148.3	271.6	63.8	385.4	1123.7	333.9	974.1	0.5	62.7	423.1	-202.9	-596.4	222.0	215.8
14	-90.1	-67.7	-35.8	30.1	160.8	294.7	67.9	411.5	1198.5	356.5	1038.9	0.5	67.2	453.1	-217.9	-639.6	236.8	230.1
15	-93.3	-70.0	-37.0	31.1	166.4	304.9	69.8	423.1	1231.4	366.5	1067.4	0.5	69.2	466.3	-224.6	-658.7	243.3	236.4
16	-101.5	-75.9	-40.1	33.8	180.9	331.4	74.5	452.8	1315.8	392.2	1140.4	0.5	74.6	500.7	-241.8	-708.1	259.9	252.6
17	-112.3	-83.8	-44.2	37.5	200.6	367.4	80.9	492.5	1428.1	426.5	1237.7	0.4	81.8	547.0	-265.2	-774.6	282.1	274.2
18	-119.3	-89.0	-46.9	40.0	213.8	391.7	85.1	519.2	1503.1	449.5	1302.6	0.4	86.8	578.4	-281.0	-819.4	296.9	288.6
19	-126.4	-94.2	-49.6	42.5	227.3	416.5	89.5	546.0	1578.2	472.7	1367.8	0.4	91.9	610.1	-297.1	-864.8	311.8	303.0
20	-132.7	-98.9	-52.0	42.4	226.6	439.3	93.5	570.5	1646.9	493.9	1427.2	0.4	96.6	639.4	-311.8	-906.5	325.3	316.2

Color Code	Limit State
	Strut buckling
	Serviceability
	Cable yielding
	Cable rupture

Table C-2: Inelastic analysis: Summary of results for *N*2:*n*16:*L*400:*r/L*0.083:*d/L*0.07 dome

	Vert. Defl.			Live Load			Member Forces											
	at Joint 1	at Joint 5	at Joint 9	at Joint 1	at Joint 5	at Joint 9	Diagonal Cables			Hoop Cables		Ridge Cables			Strut			
	Δ_1 in.	Δ_5 in.	Δ_9 in.	W_1 kips	W_5 kips	W_9 kips	D_1 kips	D_2 kips	D_3 kips	T_1 kips	T_2 kips	R_1 kips	R_2 kips	R_3 kips	C_1 kips	C_2 kips	Stress_T_2	Stress_D_3
0	11.7	3.1	-0.6	1	5.3	9.8	17.9	73.5	217.2	68.1	201.1	13.3	30.3	102.2	-25.9	-79.5	45.8	41.7
1	3.4	-2.5	-3.3	1.2	6.7	12.2	18.2	88.8	269.0	82.3	249.0	2.0	19.3	105.8	-32.0	-100.3	56.8	51.7
2	-5.8	-8.4	-6.0	2.3	12.3	22.5	20.6	105.4	321.2	97.6	297.3	1.3	20.9	123.7	-38.8	-121.5	67.8	61.7
3	-14.9	-14.2	-8.7	3.4	18.0	33.1	23.1	122.2	373.7	113.2	345.9	1.0	23.1	142.5	-45.7	-143.2	78.8	71.8
4	-23.9	-20.0	-11.4	4.5	23.9	43.9	25.6	139.2	426.6	128.9	394.8	0.9	25.6	161.7	-52.9	-165.4	90.0	81.9
5	-32.7	-25.8	-14.1	5.6	30.0	55.0	28.2	156.4	479.9	144.8	444.1	0.8	28.2	181.3	-60.2	-188.0	101.2	92.1
6	-41.5	-31.5	-16.8	6.8	36.3	66.4	30.8	173.8	533.5	160.9	493.7	0.7	30.9	201.3	-67.8	-211.1	112.5	102.4
7	-50.1	-37.2	-19.5	8.0	42.7	78.1	33.5	191.4	587.5	177.2	543.6	0.7	33.7	221.6	-75.5	-234.6	123.9	112.8
8	-58.6	-42.9	-22.2	9.2	49.2	90.2	36.2	209.2	641.8	193.7	593.8	0.6	36.6	242.3	-83.4	-258.6	135.4	123.2
9	-67.1	-48.5	-24.9	10.5	56.0	102.6	39.0	227.2	696.5	210.3	644.4	0.6	39.6	263.4	-91.6	-283.1	146.9	133.7
10	-75.4	-54.1	-27.6	11.8	62.9	115.2	41.8	245.4	751.5	227.1	695.3	0.6	42.7	284.8	-99.9	-308.1	158.5	144.3
11	-83.6	-59.7	-30.3	13.1	70.0	128.3	44.7	263.8	806.8	244.1	746.5	0.5	45.9	306.6	-108.4	-333.6	170.2	154.9
12	-91.7	-65.3	-33.0	14.5	77.3	141.6	47.6	282.3	862.5	261.3	798.0	0.5	49.2	328.7	-117.1	-359.5	181.9	165.6
13	-95.8	-68.0	-34.4	15.2	81.0	148.4	49.1	291.7	890.5	269.9	823.9	0.5	50.8	339.9	-121.6	-372.6	187.8	171.0
14	-109.8	-77.7	-39.1	17.6	94.3	172.8	54.3	324.9	989.1	300.6	915.1	0.5	56.9	380.0	-137.5	-419.5	208.6	189.9
15	-117.6	-83.2	-41.8	19.1	102.2	187.2	57.4	344.1	1045.9	318.4	967.7	0.5	60.5	403.4	-146.8	-447.0	220.6	200.8
16	-125.3	-88.6	-44.5	20.6	110.2	201.9	60.5	363.5	1103.0	336.4	1020.6	0.4	64.2	427.2	-156.4	-475.0	232.6	211.8
17	-138.3	-97.7	-49.1	23.2	124.1	227.4	65.8	396.6	1199.5	367.0	1110.1	0.4	70.7	468.0	-172.9	-522.9	253.0	230.3
18	-146.9	-103.9	-52.1	25.0	133.8	245.1	69.5	419.3	1265.1	387.9	1170.9	0.4	75.2	496.2	-184.4	-556.1	266.9	242.9
19	-153.8	-108.8	-54.6	26.5	141.7	259.7	72.5	437.6	1318.0	404.9	1219.9	0.4	78.9	519.2	-193.8	-583.1	278.1	253.1

Color Code	Limit State
	Strut buckling
	Serviceability
	Cable yielding
	Cable rupture

Tables C-3 and C-4 present the results for *N*2:*n*16:*L*400:*r/L*0.083:*d/L*0.09 dome and *N*2:*n*16:*L*400:*r/L*0.083:*d/L*0.07 dome. Both domes failed in serviceability.

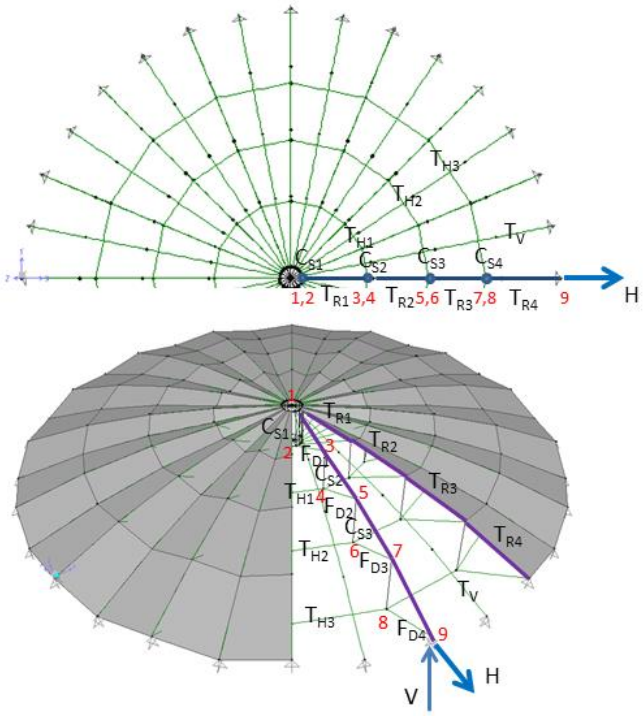

Figure C.2 *N*3 dome node and member labels

The ridge cable cross-sectional areas (inner to outer) provided are 1.67 in^2, 2.97 in^2, 5.58 in^2 and 10.8 in^2; respectively; the diagonal cable areas are 1.30 in^2, 2.60 in^2, 5.21 in^2 and 9.11 in^2 respectively; and the hoop cable areas are 11.25 in^2, 13.85 in^2 and 16.45 in^2 respectively. The struts areas (inner to outer) are 14.9 in^2, 18.1 in^2, 18.1 in^2 and 18.1 in^2. The buckling capacity of the outermost strut calculated from Euler's formula as 334 kips (for *d/L*=0.07) and 502 kips (for *d/L*=0.05), where *EI* = 29000 ksi x 299.2 in^4 = 8.677 x 10^6 $k.in^2$ is the flexural stiffness of the strut, *L* = 42.2 ft. (for *d/L*=0.07) and 34.5 ft. (for *d/L*=0.05) and *k* =1 for hinged ends.

Table C-3: Inelastic analysis: Summary of results for *N*3:*n*16:*L*400:*r/L*0.083:*d/L*0.07 dome

	Vert. Defl.				Live Load				Member Forces																
	at Joint 1	at Joint 5	at Joint 9	at Joint 13	at Joint 1	at Joint 5	at Joint 9	at Joint 13	Diagonal Cables				Hoop Cables			Ridge Cables				Strut				
	Δ_1 in.	Δ_5 in.	Δ_9 in.	Δ_{13} in.	W_1 kips	W_5 kips	W_9 kips	W_{13} kips	D_1 kips	D_2 kips	D_3 kips	D_4 kips	T_1 kips	T_2 kips	T_3 kips	R_1 kips	R_2 kips	R_3 kips	R_4 kips	C_1 kips	C_2 kips	C_3 kips	Stress_T_3	Stress_D_4
0	16.5	9.7	4.3	1.0	1	4.8	8.8	12.7	13.5	46.1	114.4	256.8	40.0	99.4	223.0	41.0	53.1	94.9	202.0	-20.6	-53.2	-123.0	34.7	28.2
1	7.7	2.6	-0.4	-1.4	1.8	8.7	16.0	23.2	12.8	57.3	153.7	355.3	49.8	133.5	308.5	1.9	13.4	64.8	207.4	-26.4	-73.3	-173.5	48.1	39.0
2	-3.6	-5.4	-5.4	-3.8	3.2	15.2	27.7	40.2	15.2	72.2	196.3	454.2	62.8	170.4	394.3	0.9	14.5	79.2	261.4	-34.1	-95.3	-224.8	61.4	49.8
3	-14.8	-13.3	-10.4	-6.2	4.5	21.7	39.6	57.6	17.7	87.5	239.4	553.6	76.0	207.8	480.7	0.7	16.6	95.3	317.6	-42.1	-117.9	-277.1	74.9	60.7
4	-25.7	-21.2	-15.3	-8.6	5.9	28.4	51.9	75.4	20.3	103.0	282.9	653.5	89.4	245.6	567.4	0.6	19.0	111.9	374.9	-50.4	-141.0	-330.3	88.4	71.7
5	-36.5	-29.0	-20.2	-11.0	7.4	35.3	64.5	93.7	22.9	118.7	326.8	753.9	103.1	283.7	654.5	0.5	21.5	128.8	433.1	-58.9	-164.7	-384.3	102.0	82.7
6	-47.1	-36.7	-25.2	-13.4	8.8	42.4	77.5	112.6	25.6	134.6	371.1	854.7	116.8	322.1	742.1	0.4	24.2	146.2	492.2	-67.7	-188.8	-439.3	115.6	93.8
7	-57.5	-44.3	-30.1	-15.8	10.4	49.7	90.9	132.0	28.3	150.6	415.9	955.9	130.8	361.0	830.0	0.4	26.9	164.0	552.2	-76.6	-213.5	-495.2	129.3	104.9
8	-67.8	-51.9	-34.9	-18.2	11.9	57.2	104.6	151.9	31.0	166.9	461.1	1057.7	144.9	400.2	918.4	0.4	29.8	182.2	613.2	-85.8	-238.8	-551.9	143.1	116.0
9	-77.9	-59.4	-39.8	-20.6	13.5	64.9	118.6	172.3	33.8	183.4	506.7	1159.8	159.3	439.8	1007.2	0.4	32.8	200.8	675.1	-95.2	-264.5	-609.6	156.9	127.3
10	-87.9	-66.8	-44.6	-23.0	15.2	72.8	133.0	193.3	36.7	200.1	552.7	1262.4	173.8	479.8	1096.4	0.3	35.9	219.7	738.0	-104.8	-290.8	-668.1	170.8	138.5
11	-97.7	-74.2	-49.4	-25.4	16.8	80.9	147.8	214.7	39.6	217.1	599.1	1365.4	188.5	520.1	1186.0	0.3	39.2	239.1	801.8	-114.7	-317.6	-727.5	184.8	149.8
12	-107.4	-81.5	-54.3	-27.8	18.6	89.2	163.0	236.7	42.5	234.2	646.0	1468.8	203.3	560.8	1276.0	0.3	42.5	258.9	866.7	-124.8	-344.9	-787.9	198.8	161.2
13	-117.0	-88.8	-59.0	-30.2	20.3	97.7	178.5	259.3	45.5	251.6	693.3	1572.7	218.4	601.9	1366.4	0.3	45.9	279.2	932.5	-135.1	-372.7	-849.1	212.9	172.6
14	-126.5	-96.0	-63.8	-32.6	22.1	106.4	194.4	282.3	48.6	269.1	741.0	1676.9	233.7	643.4	1457.1	0.3	49.5	299.8	999.3	-145.6	-401.1	-911.2	227.0	184.0
15	-135.8	-103.2	-68.6	-35.0	24.0	115.3	210.6	305.9	51.6	286.9	789.2	1781.5	249.2	685.2	1548.3	0.3	53.2	320.9	1067.1	-156.4	-430.0	-974.2	241.2	195.5
16	-142.1	-108.0	-71.8	-36.7	25.3	121.4	221.8	322.2	53.8	299.1	822.0	1852.4	259.7	713.8	1610.2	0.3	55.7	335.5	1113.6	-163.9	-450.0	-1017.4	250.9	203.3
17	-155.9	-118.7	-78.9	-40.3	28.2	135.4	247.3	359.2	58.5	326.4	895.5	2010.6	283.5	777.7	1748.1	0.3	61.6	368.4	1218.5	-180.6	-494.8	-1114.3	272.4	220.6
18	-164.9	-125.6	-83.6	-42.7	30.2	144.9	264.6	384.4	61.8	344.9	944.8	2115.9	299.5	820.6	1840.1	0.3	65.6	390.9	1289.4	-192.1	-525.3	-1179.8	286.7	232.2
19	-180.3	-137.8	-91.8	-46.9	33.7	161.9	295.8	429.6	67.5	377.5	1031.6	2300.1	327.9	896.3	2001.1	0.2	72.9	431.0	1415.5	-212.7	-579.7	-1296.1	311.8	252.4
20	-180.8	-138.1	-92.1	-47.0	33.8	162.5	296.8	431.0	67.7	378.5	1034.4	2305.9	328.8	898.7	2006.1	0.2	73.1	432.3	1419.5	-213.2	-581.3	-1299.6	312.6	253.0

Color Code	Limit State
	Strut buckling
	Serviceability
	Cable yielding
	Cable rupture

Table C-4: Inelastic analysis: Summary of results for *N*3:*n*16:*L*400:*r*/*L*0.083:*d*/*L*0.05 dome

	Vert. Defl. at Joint 1 Δ_1 in.	at Joint 5 Δ_5 in.	at Joint 9 Δ_9 in.	at Joint 13 Δ_{13} in.	Live Load at Joint 1 W_1 kips	at Joint 5 W_5 kips	at Joint 9 W_9 kips	at Joint 13 W_{13} kips	Member Forces Diagonal Cables D_1 kips	D_2 kips	D_3 kips	D_4 kips	Hoop Cables T_1 kips	T_2 kips	T_3 kips	Ridge Cables R_1 kips	R_2 kips	R_3 kips	R_4 kips	Strut C_1 kips	C_2 kips	C_3 kips	Stress_T_3	Stress_D_4
0	10.6	3.9	-0.2	-1.7	1	4.8	8.8	12.7	11.0	45.1	123.9	307.3	41.8	114.8	284.6	3.1	13.4	56.5	179.0	-15.2	-44.0	-113.7	44.3	33.7
1	-3.5	-5.4	-5.6	-4.1	0.7	3.4	6.1	8.9	12.3	54.4	152.1	378.1	50.4	140.9	350.1	0.9	12.4	64.5	214.8	-19.0	-55.5	-142.4	54.5	41.5
2	-17.3	-14.6	-10.9	-6.5	1.4	6.7	12.3	17.8	13.9	64.1	180.9	449.4	59.4	167.5	416.1	0.7	13.9	75.2	254.0	-23.1	-67.4	-172.0	64.8	49.3
3	-30.7	-23.7	-16.2	-8.9	2.1	10.2	18.7	27.1	15.5	74.0	210.0	521.2	68.5	194.5	482.7	0.5	15.4	86.4	294.1	-27.4	-79.8	-202.2	75.2	57.2
4	-43.8	-32.6	-21.5	-11.3	2.9	13.9	25.4	36.8	17.1	84.0	239.5	593.6	77.9	221.8	549.7	0.5	17.0	97.9	335.0	-31.9	-92.6	-233.2	85.7	65.1
5	-56.4	-41.3	-26.7	-13.7	3.7	17.7	32.3	46.9	18.8	94.3	269.5	666.6	87.4	249.6	617.3	0.4	18.8	109.7	376.7	-36.6	-105.8	-265.0	96.2	73.1
6	-68.8	-50.0	-31.9	-16.1	4.5	21.6	39.5	57.4	20.5	104.7	299.8	740.1	97.0	277.7	685.4	0.4	20.7	121.9	419.2	-41.4	-119.4	-297.5	106.8	81.2
7	-80.8	-58.4	-37.1	-18.5	5.4	25.8	47.1	68.4	22.2	115.3	330.6	814.1	106.8	306.2	754.0	0.4	22.6	134.3	462.4	-46.2	-133.3	-330.8	117.5	89.3
8	-92.5	-66.8	-42.2	-20.9	6.2	30.0	54.8	79.7	24.1	126.1	361.8	888.6	116.9	335.1	823.2	0.4	24.7	147.2	506.6	-51.4	-147.8	-364.8	128.3	97.5
9	-104.0	-75.1	-47.3	-23.3	7.2	34.4	62.9	91.4	25.9	137.1	393.3	963.7	127.1	364.4	892.8	0.3	26.8	160.4	551.7	-56.7	-162.6	-399.6	139.1	105.7
10	-115.2	-83.2	-52.4	-25.7	8.1	39.0	71.3	103.5	27.8	148.3	425.3	1039.2	137.5	394.1	962.9	0.3	29.1	174.0	597.6	-62.3	-177.9	-435.1	150.0	114.0
11	-126.2	-91.2	-57.4	-28.1	9.1	43.7	79.9	116.1	29.8	159.8	457.8	1115.3	148.1	424.2	1033.6	0.3	31.4	187.9	644.4	-68.0	-193.7	-471.4	161.0	122.4
12	-137.0	-99.2	-62.4	-30.5	10.1	48.6	88.8	129.0	31.8	171.4	490.6	1191.9	158.9	454.7	1104.7	0.3	33.9	202.2	692.1	-73.9	-209.8	-508.5	172.1	130.8
13	-147.5	-107.0	-67.4	-32.9	11.2	53.7	98.0	142.4	33.8	183.2	523.9	1269.0	170.0	485.7	1176.3	0.3	36.4	216.9	740.7	-80.0	-226.4	-546.3	183.3	139.2
14	-157.9	-114.7	-72.4	-35.3	12.3	58.9	107.6	156.2	35.9	195.2	557.6	1346.5	181.2	517.0	1248.5	0.3	39.1	232.0	790.3	-86.2	-243.4	-584.9	194.5	147.7
15	-168.1	-122.4	-77.3	-37.7	13.4	64.2	117.4	170.5	38.0	207.5	591.7	1424.5	192.6	548.8	1321.1	0.3	41.8	247.6	840.8	-92.8	-260.9	-624.3	205.8	156.3
16	-178.1	-130.0	-82.2	-40.1	14.5	69.8	127.5	185.1	40.2	220.0	626.3	1503.1	204.3	580.9	1394.2	0.3	44.7	263.4	892.3	-99.4	-278.7	-664.5	217.2	164.9
17	-187.9	-137.5	-87.1	-42.5	15.7	75.5	137.9	200.2	42.5	232.7	661.3	1582.0	216.1	613.5	1467.9	0.3	47.6	279.7	944.7	-106.2	-297.0	-705.4	228.7	173.6
18	-197.6	-144.9	-92.0	-44.9	16.9	81.3	148.6	215.8	44.8	245.6	696.7	1661.5	228.2	646.6	1542.0	0.3	50.6	296.4	998.1	-113.2	-315.8	-747.1	240.2	182.3
19	-200.0	-146.7	-93.2	-45.5	17.2	82.8	151.3	219.7	45.3	248.8	705.6	1681.4	231.2	654.9	1560.7	0.3	51.5	300.9	1012.2	-115.0	-320.6	-757.8	243.2	184.5
20	-213.9	-157.4	-100.3	-49.0	18.4	88.4	167.6	243.5	48.8	268.2	758.3	1798.3	249.3	704.1	1669.8	0.2	56.1	326.0	1091.9	-125.8	-349.1	-820.5	260.2	197.3
21	-216.4	-159.4	-101.6	-49.7	19.5	93.5	170.8	248.1	49.5	272.0	768.4	1820.6	252.8	713.5	1690.5	0.2	56.8	330.6	1106.8	-127.6	-354.3	-832.2	263.4	199.8

Color Code	Limit State
	Strut buckling
	Serviceability
	Cable yielding
	Cable rupture

APPENDIX D

STAYED COLUMN ANALYSIS RESULTS

The stayed column in Section 9.2 was analyzed for two cases of planar models. In Case A, the bending axis was at 90º, and in Case B, the bending axis was at 45º with respect to the horizontal axis of the section in plan view (Figure D.1). The complete results from the analyses are presented in Tables D-1 and D-2.

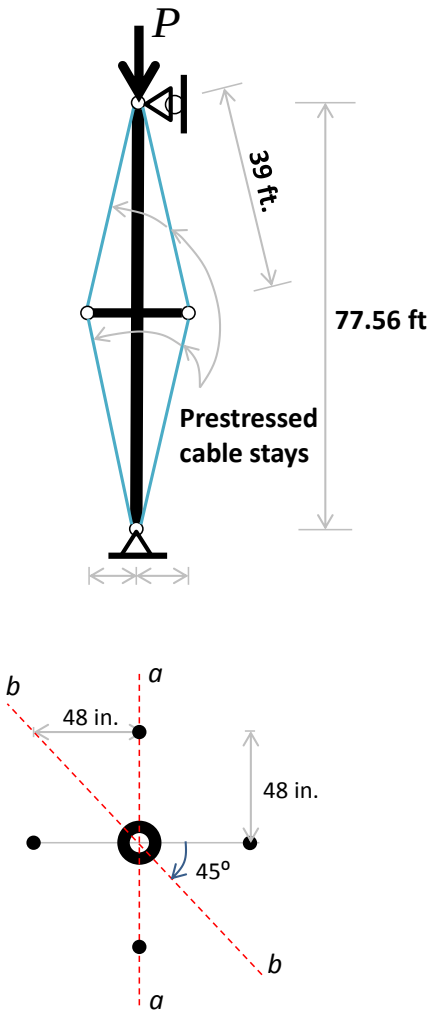

Figure D.1 Bending axes for Cases A and B at 90º and 45º respectively

Table D-1 Stayed Column: Summary of Results for Case A

	Prestrain = -0.003				Left Stay		Right Stay		Central cable		Strut		
P	**Δ**	**K_aug**	**K_spr**	**K_col**	**Force**	**Strain**	**Force**	**Strain**	**Force**	**Strain**	**Force**	**Stress (at ends)**	**Stress (at mid-ht.)**
	(in.)	(kip/in.)	(kip/in.)	(kip/in.)	(kips)		(kips)				(kips)	(ksi)	(ksi)
0	0.04785	2.089864159	0.2	1.889864159	60.73	0.002530	61.23	0.002551	121.73	0.0025361	243.03	13.454	13.454
2	0.048085	2.079650619	0.2	1.879650619	60.65	0.002527	61.15	0.002548	121.58	0.0025329	244.72	13.547	13.549
4	0.048323	2.069407942	0.2	1.869407942	60.57	0.002524	61.08	0.002545	121.42	0.0025296	246.41	13.641	13.645
6	0.048563	2.059180858	0.2	1.859180858	60.49	0.002520	61.00	0.002542	121.27	0.0025264	248.11	13.735	13.740
8	0.048805	2.048970392	0.2	1.848970392	60.41	0.002517	60.93	0.002539	121.11	0.0025231	249.80	13.828	13.836
10	0.04905	2.038735984	0.2	1.838735984	60.34	0.002514	60.85	0.002536	120.96	0.0025199	251.49	13.922	13.932
20	0.050313	1.987557888	0.2	1.787557888	59.95	0.002498	60.48	0.00252	120.18	0.0025038	259.95	14.390	14.411
30	0.051638	1.936558349	0.2	1.736558349	59.55	0.002481	60.10	0.002504	119.41	0.0024876	268.41	14.859	14.890
40	0.053025	1.885902876	0.2	1.685902876	59.16	0.002465	59.72	0.002488	118.63	0.0024715	276.88	15.327	15.370
50	0.054474	1.83573815	0.2	1.63573815	58.77	0.002449	59.35	0.002473	117.86	0.0024553	285.34	15.796	15.850
100	0.063544	1.573712703	0.2	1.373712703	56.81	0.002367	57.48	0.002395	113.98	0.0023745	327.64	18.138	18.265
150	0.076633	1.304920857	0.2	1.104920857	54.82	0.002284	55.63	0.002318	110.10	0.0022938	369.95	20.480	20.710
200	0.098249	1.017822064	0.2	0.817822064	52.79	0.002200	53.82	0.002243	106.22	0.0022130	412.26	22.822	23.216
250	0.139558	0.716547959	0.2	0.516547959	50.65	0.002111	52.12	0.002172	102.35	0.0021322	454.57	25.164	25.864
300	0.274843	0.363844086	0.2	0.163844086	48.02	0.002001	50.92	0.002122	98.46	0.0020512	496.86	27.505	29.159
310	0.34009	0.294039813	0.2	0.094039813	47.29	0.001971	50.88	0.00212	97.68	0.0020349	505.31	27.973	30.087
312	0.357258	0.279909757	0.2	0.079909757	47.12	0.001964	50.89	0.00212	97.52	0.0020316	507.00	28.067	30.302
314	0.376331	0.265723525	0.2	0.065723525	46.95	0.001956	50.91	0.002121	97.36	0.0020284	508.69	28.160	30.530
316	0.397646	0.25147996	0.2	0.05147996	46.76	0.001948	50.95	0.002123	97.20	0.0020251	510.38	28.253	30.773
318	0.42162	0.237180399	0.2	0.037180399	46.55	0.001940	51.00	0.002125	97.04	0.0020218	512.06	28.347	31.036
320	0.448781	0.222825833	0.2	0.022825833	46.33	0.001931	51.06	0.002128	96.89	0.0020184	513.75	28.440	31.320
322	0.480025	0.208322483	0.2	0.008322483	46.09	0.001920	51.15	0.002131	96.72	0.0020151	515.43	28.533	31.633
322.2	0.483379	0.206876577	0.2	0.006876577	46.064	0.001919	51.158	0.002132	96.71	0.0020148	515.60	28.543	31.666
322.4	0.486781	0.205431612	0.2	0.005431612	46.038	0.001918	51.168	0.002132	96.69	0.0020144	515.77	28.552	31.699
322.6	0.490232	0.203985884	0.2	0.003985884	46.012	0.001917	51.178	0.002132	96.68	0.0020141	515.94	28.561	31.733
322.8	0.493734	0.20253985	0.2	0.00253985	45.986	0.001916	51.189	0.002133	96.66	0.0020137	516.11	28.571	31.767
323	0.497288	0.201089907	0.2	0.001089907	45.96	0.001915	51.2	0.002133	96.64	0.0020134	516.28	28.580	31.801
323.05	0.498185	0.20073066	0.2	0.00073066	45.953	0.001915	51.203	0.002133	96.64	0.0020133	516.32	28.582	31.810
323.1	0.499084	0.200368678	0.2	0.000368678	45.946	0.001914	51.205	0.002134	96.64	0.0020132	516.36	28.585	31.818
323.15	0.499988	0.200004	0.2	4.00008E-06	45.939	0.001914	51.208	0.002134	96.63	0.0020131	516.40	28.587	31.827
323.2	0.500894	0.199644633	0.2	-0.000355367	45.933	0.001914	51.211	0.002134	96.63	0.0020131	516.44	28.589	31.836

Table D-2 Stayed Column: Summary of Results for Case B

Prestrain = -0.003					Left Stay		Right Stay		Strut		
P	**Δ**	**K_aug**	**K_spr**	**K_col**	**Force**	**Strain**	**Force**	**Strain**	**Force**	**Stress (at ends)**	**Stress (at mid-ht.)**
	(in.)	(kip/in.)	(kip/in.)	(kip/in.)	(kips)		(kips)		(kips)	(ksi)	(ksi)
0	0.036243	2.75915349	0.2	2.55915349	121.6	0.00253271	122.13	0.00254433	243.01	13.453	13.453
2	0.036386	2.74830979	0.2	2.54830979	121.4	0.00252946	121.98	0.00254115	244.71	13.546	13.548
4	0.036531	2.73740111	0.2	2.53740111	121.3	0.00252623	121.82	0.00253796	246.40	13.640	13.643
6	0.036677	2.72650435	0.2	2.52650435	121.1	0.002523	121.67	0.00253477	248.09	13.734	13.738
8	0.036824	2.71562025	0.2	2.51562025	120.9	0.00251975	121.52	0.00253158	249.78	13.828	13.833
10	0.036973	2.70467639	0.2	2.50467639	120.8	0.00251652	121.36	0.0025284	251.48	13.921	13.929
20	0.037734	2.65012986	0.2	2.45012986	120.0	0.00250033	120.60	0.00251244	259.94	14.390	14.405
30	0.038526	2.59564969	0.2	2.39564969	119.2	0.00248415	119.83	0.00249652	268.40	14.858	14.881
40	0.039349	2.54136064	0.2	2.34136064	118.5	0.00246796	119.07	0.00248058	276.86	15.327	15.358
50	0.040204	2.4873147	0.2	2.2873147	117.7	0.00245175	118.30	0.00246467	285.33	15.795	15.835
100	0.045314	2.2068235	0.2	2.0068235	113.8	0.00237063	114.49	0.00238517	327.64	18.137	18.228
150	0.051702	1.93416115	0.2	1.73416115	109.9	0.00228929	110.68	0.00230588	369.95	20.480	20.635
200	0.061077	1.63727753	0.2	1.43727753	106.0	0.00220746	106.90	0.00222708	412.26	22.822	23.067
250	0.076194	1.3124393	0.2	1.1124393	102.0	0.00212473	103.16	0.00214919	454.57	25.164	25.546
300	0.101894	0.98141206	0.2	0.78141206	97.9	0.00204027	99.50	0.002073	496.88	27.507	28.120
350	0.181597	0.55066989	0.2	0.35066989	93.5	0.00194713	96.26	0.00200544	539.19	29.849	31.123
360	0.213541	0.46829414	0.2	0.26829414	92.4	0.0019259	95.74	0.00199448	547.65	30.317	31.858
370	0.260732	0.38353558	0.2	0.18353558	91.3	0.00190219	95.33	0.00198594	556.11	30.785	32.720
380	0.337634	0.2961787	0.2	0.0961787	89.9	0.00187367	95.14	0.0019821	564.56	31.253	33.826
382	0.35922	0.27838094	0.2	0.07838094	89.6	0.00186694	95.15	0.00198233	566.25	31.346	34.098
384	0.384109	0.26034277	0.2	0.06034277	89.3	0.00185969	95.19	0.00198306	567.93	31.440	34.398
386	0.412717	0.24229678	0.2	0.04229678	88.9	0.00185181	95.25	0.00198438	569.62	31.533	34.728
388	0.446159	0.22413534	0.2	0.02413534	88.5	0.00184315	95.35	0.00198646	571.30	31.626	35.098
390	0.485767	0.20586001	0.2	0.00586001	88.007	0.00183348	95.50	0.0019895	572.99	31.719	35.519
390.2	0.490133	0.20402625	0.2	0.00402625	87.957	0.00183244	95.51	0.00198988	572.99	31.719	35.555
390.4	0.494581	0.20219135	0.2	0.00219135	87.907	0.0018314	95.53	0.00199025	572.99	31.719	35.592
390.6	0.499113	0.20035543	0.2	0.00035543	87.856	0.00183033	95.55	0.00199065	572.99	31.719	35.629
390.65	0.500259	0.19989645	0.2	-0.0001035	87.843	0.00183006	95.56	0.00199075	572.99	31.719	35.639

APPENDIX E

DESIGN WIND PRESSURES FOR ROOF

This section provides a step-by-step calculation for wind pressure on the roof that was summarized in this dissertation's Section 3.1.5. The procedure for wind load calculations as described in Mehta & Coulbourne's book, "*Wind Loads: Guide to the Wind Load Provisions of ASCE 7-10*" is adapted for cable domes. The Directional Procedure for design of the main wind force resisting system (MWFRS) as per Chapter 27 of ASCE/SEI 7-10 (ASCE 2010c) is followed. The ASD load factor of 0.6 for wind loads reduces the peak wind loads obtained from the Directional Procedure to service load value. Only the MWFRS is considered in the analysis.

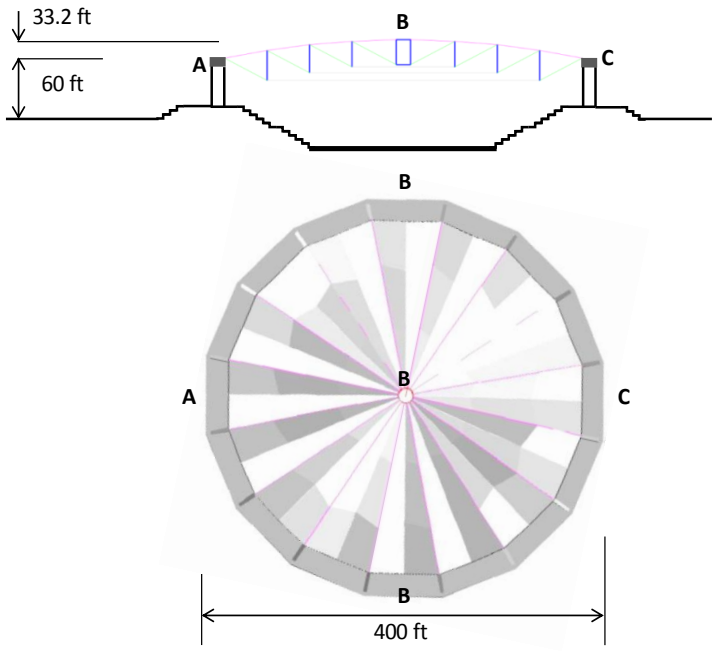

Figure E.1 Geometry and dimensions of cable dome in reference

Domed Roof Pressures

For special structures such as cable domes, whose roof is pleated and membrane is flexible, a more accurate estimate of wind forces must be obtained from wind tunnel tests. Wind tunnel studies have shown that a shallow folded roof has very little impact on the Main Wind Force Resisting System. As such, Figure 27.4-2 of ASCE/SEI 7-10 (ASCE 2010c, p.265) is applicable. It has been found that

there is very little pressure on the roof on the windward side. This is because of the low rise. The distribution of wind pressure coefficients on the roof is therefore taken as negative throughout the roof. The coefficients C_p generally depend on the shape of the structure, the wind direction and position on the roof.

The roof pressure coefficients for a domed roof are taken from Figure 27.4-2 of ASCE/SEI 7-10 (ASCE 2010c, p.265). The height from the ground to the spring line (or eave) of the dome is expressed as $h_D = 60\,ft$. The height of the dome from the eave is expressed as $f = 33.2\,ft$ (Figure E.1). Determine C_p for a rise to diameter ratio, as $\frac{f}{D} = \frac{33.2}{400} = 0.083$, and determine a base height to diameter ratio, as $\frac{h_D}{D} = \frac{60}{400} = 0.15$. Interpolation from Figure 27.4-2, ASCE 2010c is required. Two load cases are required for the MWFRS loads on domes: Cases A and B. Case A is based on linear interpolation of C_p values from point A to B and from point B to C (see Figure 27.4-2 of ASCE/SEI 7-10 and Figure E.2). Case B uses the pressure coefficient at A for the entire front area of the dome up to an angle $\theta = 25°$, then interpolates the values for the rest of the dome as shown in Case A.

Table E-1 Domed Roof C_p (at f/D = 0.083)

Point on Dome	$\frac{h_D}{D}$ = 0.15
A	-0.58
B	-0.38
C	-0.14

CASE- A

For design purposes, interpolate the pressure coefficients at points every 10 ft. intervals along the chord length of the dome.

Table E-2 Interpolated Domed Roof C_p (Case A)

Segment	Start	+25 ft	+50 ft	+75 ft	+100 ft	+125 ft	+150 ft	+175 ft	+200 ft
A to B	-0.58	-0.555	-0.530	-0.505	-0.480	-0.455	-0.430	-0.405	-0.38
B to C	-0.38	-0.35	-0.32	-0.29	-0.26	-0.23	-0.20	-0.17	-0.14

Table E-3 Interpolated Domed Roof C_p (Case B)

Segment	Start	+25 ft	+50 ft	+75 ft	+100 ft	+125 ft	+137.2 ft	+175 ft	+200 ft
A to B	-0.58	→	→	→	→	→	-0.58	-0.46	-0.38
B to C	-0.38	-0.35	-0.32	-0.29	-0.26	-0.23		-0.17	-0.14

Determine the point on the windward side of the dome at which $\theta = 25°$. The point is 137.2 feet from point A (Figure 2.4 of this document). The pressure coefficient at A shall be used for the section from A to an arc 137.2 feet. The remainder of the dome pressures is based on linear interpolation between the $25°$ point and point B; and then from point B to C. Values of pressure coefficients C_p are shown in Figure E.2.

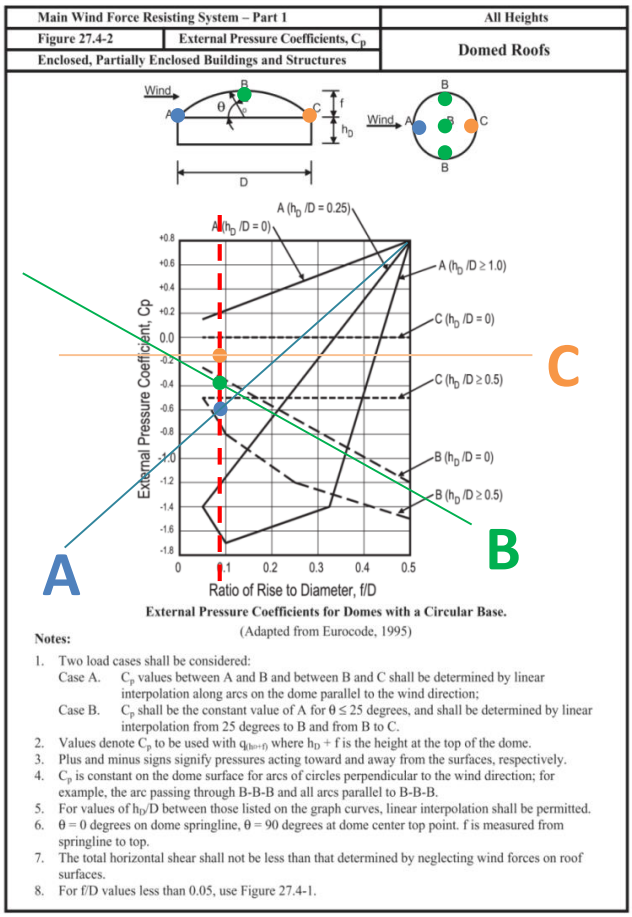

External Pressure Coefficients for Domes with a Circular Base.
(Adapted from Eurocode, 1995)

Notes:

1. Two load cases shall be considered:
   Case A. C_p values between A and B and between B and C shall be determined by linear interpolation along arcs on the dome parallel to the wind direction;
   Case B. C_p shall be the constant value of A for $\theta \leq 25$ degrees, and shall be determined by linear interpolation from 25 degrees to B and from B to C.
2. Values denote C_p to be used with $q_{h(h+f)}$ where $h_D + f$ is the height at the top of the dome.
3. Plus and minus signs signify pressures acting toward and away from the surfaces, respectively.
4. C_p is constant on the dome surface for arcs of circles perpendicular to the wind direction; for example, the arc passing through B-B-B and all arcs parallel to B-B-B.
5. For values of h_D/D between those listed on the graph curves, linear interpolation shall be permitted.
6. $\theta = 0$ degrees on dome springline, $\theta = 90$ degrees at dome center top point. f is measured from springline to top.
7. The total horizontal shear shall not be less than that determined by neglecting wind forces on roof surfaces.
8. For f/D values less than 0.05, use Figure 27.4-1.

Figure E.2 Dome wind pressure coefficients as per ASCE/SEI 7-10 (ASCE 2010c)

Table E-4 Values of design pressures for MWFRS: Case A

Surface of Domed Roof	Location (ft)	C_p	External Pressure (psf)	Design Pressure (psf)	
				$+GC_{pi}$	$-GC_{pi}$
Case A	Point A: 0	-0.580	-21.58	-29.46	-13.7
	25	-0.555	-20.58	-28.53	-12.77
	50	-0.530	-19.72	-27.60	-11.84
	75	-0.505	-18.79	-26.67	-10.91
	100	-0.480	-17.86	-25.74	-9.98
	125	-0.455	-16.93	-24.81	-9.05
	150	-0.430	-16	-23.88	-8.12
	175	-0.405	-15.07	-22.95	-7.19
	Point B: 200 ft	-0.380	-14.14	-22.02	-6.26
	225	-0.35	-13.02	-20.90	-5.14
	250	-0.32	-11.91	-19.79	-4.03
	275	-0.29	-10.79	-18.67	-2.91
	300	-0.26	-9.67	-17.55	-1.79
	325	-0.23	-8.56	-16.44	-0.69
	350	-0.20	-7.44	-15.32	0.44
	375	-0.17	-6.33	-14.21	1.55
	Point C: 400 ft	-0.14	-5.21	-13.09	2.67

CASE- B

Internal Pressure Coefficient for Domed Roof

The net pressure in any surface is the difference in the external and internal pressures on the opposite sides of that surface,

$$p = qGC_p - q_i(GC_{pi}) \quad \text{(E.1)}$$

For enclosed buildings

$$GC_{pi} = \pm 0.18$$

q_i is taken as $q_{(h_D+f)} = 43.8$ psf

Design internal pressure

$$q_i(GC_{pi}) = 43.8\ (\pm 0.18) = 7.88\ psf$$

Design Wind Pressures for Domed Roof

The design wind pressure in any surface is the difference in the external and internal pressures,

$$\begin{aligned} p &= qGC_p - q_i(GC_{pi}) \\ &= 43.8\,(0.85)C_p - 43.8\,(\pm 0.18) \\ &= 37.21\,C_p \pm 7.88 \end{aligned} \tag{E.2}$$

Table E-5 Values of design pressures for MWFRS: Case B

Surface of Domed Roof	Location (ft)	C_p	External Pressure (psf)	Design Pressure (psf)	
				$+GC_{pi}$	$-GC_{pi}$
Case B	Point A: 0	-0.580	-21.58	-29.46	-13.7
	θ = 25° at 137.2 ft	-0.580	-21.58	-29.46	-13.7
	175	-0.46	-17.12	-25	-9.24
	Point B: 200 ft	-0.380	-14.14	-22.02	-6.26
	225	-0.35	-13.02	-20.90	-5.14
	250	-0.32	-11.91	-19.79	-4.03
	275	-0.29	-10.79	-18.67	-2.91
	300	-0.26	-9.67	-17.55	-1.79
	325	-0.23	-8.56	-16.44	-0.69
	350	-0.20	-7.44	-15.32	0.44
	375	-0.17	-6.33	-14.21	1.55
	Point C: 400 ft	-0.14	-5.21	-13.09	2.67

APPENDIX F

MATLAB CODE FOR GEOMETRIC NONLINEAR ANALYSIS

In the MATLAB code, the input model includes generating the initial dome geometry and specifying the material properties, member properties and applied loads. A vector of constraints (supports) and applied loads is formed. The structure force vector and the structure stiffness matrix are then initialized. The member stiffness matrix is directly written out from Equation 4.20 and assembled to form the structure stiffness matrix *K* using destination vectors. The residual force vector *R* is defined as the sum of the internal and external forces. The iterative Newton-Raphson scheme is used to solve the set of nonlinear equilibrium equations.

```
=====================================================================
```

%% Nonlinear Geometric Analysis of a two-dimensional cable dome (Adapted from Pecknold, 2009)

```
%% Input Data for N1:n16:L400:r/L0.083:d/L0.14

Ndof  = 2;   % 2D, 2 degrees of freedom per node
Nelem = 15;  % number of members
Nnode = 10;  % number of nodes

Emod     = [24000, 24000, 29000, 29000, 24000, 24000, 24000, 24000, 24000,
29000,
            29000, 24000, 24000, 24000, 24000]'; % Young's Modulus for every
member
Area     = [14.9226, 14.9226, 14.9226, 14.9226, 3.33, 3.33, 2.17, 2.17, 9.51,
            18.0642, 18.0642, 5.5, 5.5, 4.34, 4.34]';  % cross-sectional areas
Cte     = 6.5*1e-6*ones(Nelem,1);  % Coeff of thermal expansion
DeltaT  =  -1*[ 0, 0, 0, 0, 0, 0, 769.23, 769.23, 0, 0, 0, 0, 0, 769.23,769.23
]';
               % Temperature change

Coor = zeros(Nnode,Ndof);
Coor = [ 2304   384
         2496   384
         2304  -399.50
         2496  -399.50
         1140   272.53
         3660   272.53
         1140  -658.18
         3660  -658.18
           0     0
         4800   0]; % nodal coordinates
```

```
Conn = zeros(Nelem,2);
Conn = [ 1 2  % nodes of member 1
         3 4  % nodes of member 2
         1 3  % nodes of member 3
         2 4
         1 5
         2 6
         3 5
         4 6
         7 8
         5 7
         6 8
         5 9
         6 10
         7 9
         8 10];

Truss = [ 1 ; 2;  3 ; 4; 10 ; 11 ]; % vertical struts
Truss_yield = 46;  % truss yield stress
Cable_yield = 243; % cable yield stress

RCT = zeros(Ndof,Nnode);
RCT = [ 0 0 0 0 0 0 0 0 1 1
       0 0 0 0 0 0 0 0 1 1 ]; % 1 indicates constrained DOF, 0 indicates free
DOF

Pfor = zeros(Ndof,Nnode);
Pfor =  [   0    0     0   0    0     0     0  0  0  0
         -5.06  -5.06   0   0  -30.54  -30.54  0  0  0  0]; % applied loads at
DOFs;

cnt = 0;  % counter
ID = zeros(Ndof,Nnode); % Global equation number
for i = 1:Nnode
   for j = 1:Ndof
      if(RCT(j,i)==0)
         cnt = cnt+1;
         ID(j,i) = cnt;
      end
   end
end
Fdof = cnt;  % Free degree of freedom
for i = 1:Nelem
   for j = 1:Ndof
      Dvec(j,i) = ID(j,Conn(i,1));
      Dvec(Ndof+j,i) = ID(j,Conn(i,2));
   end
end

Ptot = zeros(Fdof,1);
[I,J,V] = find(ID);
for i = 1:size(I,1)
   Ptot(V(i),1) = Pfor(I(i),J(i));
end
```

```
%%
U = zeros(Fdof,1);
Elfor0 = prestress;
Elfor = prestress;
Coorn = Coor;
ppen1 = zeros(Nelem,1);
% Load step loop, explain every step please
loadsteps = 1;
itersteps = 20;
tol = 1e-10;
for l=1:loadsteps
    sprintf('Loadstep No: %d',l)
    Pj = Ptot*l/loadsteps;
    % Newton Raphson loop
    for i = 1:itersteps % Iteration loop , 10 loops

        for j = 1:Nelem
            vecn(j,1:Ndof) = Coorn(Conn(j,2),1:Ndof) - Coorn(Conn(j,1),1:Ndof);
            Lengthn(j,1) = norm(vecn(j,1:Ndof));

            vec(j,1:Ndof) = Coor(Conn(j,2),1:Ndof) - Coor(Conn(j,1),1:Ndof);
            Length(j,1) = norm(vec(j,1:Ndof));
            avec(j,1:Ndof) = vec(j,1:Ndof)/Length(j);
            if((i==1)&&(l==1))
                Length0 = Length;
                avec0 = avec;
            end
        end

        [Coor,Coorn,ppen1,U,Elfor,anorm] =
truss(Ndof,Nelem,Nnode,Coor,Truss,Conn, ...

ID,Dvec,Fdof,Emod,Truss_yield,Cable_yield,Area,Cte,DeltaT,avec0,avec,Length0,
Lengthn,Length,ppen1,Pj,U,Elfor0,Elfor);

        if(i==1)
            anorm1 = anorm;
        end
        rnorm = anorm/anorm1

        if(rnorm<tol)
            str = sprintf('NR loop converged at iteration %d',i);
            disp(str)
            str=sprintf('anorm = %12.4e',anorm);
            disp(str)
            break;
        end
        if(i==itersteps)
            str=sprintf('Not converged');
            disp(str)
            pause
        end
    end
end
```

```
function[Coor,Coorn,ppen1,U,Elfor,anorm]=
truss(Ndof,Nelem,Nnode,Coor,Truss,Conn,ID,Dvec,Fdof,Emod,Truss_yield,Cable_yi
eld,Area,Cte,DeltaT,avec0,avec,Length0,Lengthn,Length,ppen1,Pj,U,Elfor0, Elfor)
% Initialize Structure Stiffness Matrix
K  = zeros(Fdof,Fdof) ;
Pelfor0 = zeros(Fdof,1);
Pelfor = zeros(Fdof,1);
Pf = zeros(Fdof,1);

%Assemble Structure Stiffness Matrix
for e = 1:Nelem
   A = Area(e); L = Length(e); Em = Emod(e);
   St1 = A*Em/L;
   L0 = Length0(e);
   St10 = A*Em/L0;

   Ln = Lengthn(e);

   Ft =   Area(e)*Em*Cte(e)*DeltaT(e);
   ppfe = [ Ft,0,-Ft,0 ]' ;

   % Recalculate Coordinate Rotation Matrix
   s = avec(e,2);
   c = avec(e,1);
   Te =  [  c,    s,    0,     0;
           -s,    c,    0,     0;
            0,    0,    c,     s;
            0,    0,   -s,     c ];

   s0 = avec0(e,2);
   c0 = avec0(e,1);


   Te0 =  [   c0,   s0,     0,    0;
             -s0,   c0,     0,    0;
               0,    0,    c0,    s0;
               0,    0,   -s0,    c0 ];

   % Element Stiffness Matrix in local coordinates
   kpe = [  St1,    0,  -St1,    0;
               0,    0,     0,    0;
           -St1,    0,   St1,    0;
               0,    0,     0,    0 ];

   % Initial Element Stiffness Matrix in local coordinates
   kpe0 = [  St10,    0, -St10,    0;
                0,    0,     0,    0;
            -St10,    0,   St10,    0;
                0,    0,     0,    0 ];

   % Transform to Global Coordinates
   kel = Te'*kpe0*Te ;

      % Get Elem Displacements
   ue = [0,0,0,0]';
   for r=1:4
```

```
   m = Dvec(r,e);
   if m ~= 0
      ue(r) = U(m);
   end
end
% Rotate Elem Displacements to local coords
upe = Te0*ue;       % Element local displacement
ppe = kpe0*upe;     % Element local force

ppen1(e,1) = ppen1(e,1) + St10*(L-Ln);
Elfor(e,1) = Elfor0(e,1) + ppen1(e,1) + ppfe(Ndof+1);
beta = 0; % cable element = 0, truss element = 1
for jj = 1:size(Truss,1)
   if(e==Truss(jj))
      beta =1;
   end
end

 if (Elfor(e,1)<0)&&(beta==0) % alpha = 1e-10 if cable in compression,
                                 else alpha =1
   alpha = 1e-10;
   disp('Cable in compression')
   e; ppe(Ndof+1); ppfe(Ndof+1);
else
   alpha=1;
end

if (Elfor(e,1)>Cable_rupture*A)&&(beta==0)
   disp('Cable yield')
   elem = e
   pause
end
if (Elfor(e,1)>Truss_rupture*A)&&(beta==1)
   disp('Truss yield')
   elem = e
   pause
end

pelfor1  = alpha*[-Elfor(e,1),0,Elfor(e,1),0 ]';
pelfor01 = alpha*[-Elfor0(e,1),0,Elfor0(e,1),0 ]';

% Rotate Element Loads to Global Coords
pfe = alpha*Te'*ppfe;

% Rotate Element Loads to Global Coords
pelfor0e = Te0'*pelfor01;
pelfore = Te'*pelfor1;
% Assemble Element Contribution into Structure Load Vector
for r=1:4
   m = Dvec(r,e);
   if m ~= 0
      Pelfor0(m) = Pelfor0(m) + pelfor0e(r);
      Pelfor(m) = Pelfor(m) + pelfore(r);
      Pf(m) = Pf(m) + pfe(r);
   end
end
```

```
% Geometric stiffness
   kge = (Elfor(e,1)/L)*[  1-c^2    -c*s  -1+c^2    c*s
                            -c*s   1-s^2    c*s  -1+s^2
                          -1+c^2    c*s   1-c^2   -c*s
                            c*s  -1+s^2   -c*s   1-s^2  ]   ;


   % Total element stiffness in global coordinates
   ke = kel + kge;
   ke = ke*alpha;

   % Assemble Element Contribution to Structure Stiffness
   for r=1:4
      m = Dvec(r,e);                 %  Get first non-zero Structure
      if m ~= 0                      %  DOF number
         for s=1:4                   %  Get second non-zero Structure
            n = Dvec(s,e);           %  DOF number
            if n ~= 0
               K(m,n) = K(m,n) + ke(r,s);   %  Add element stiffness into
                                               Structure Stiffness
            end
         end
      end
   end
end

% Joint Loads
P = Pj ;

%% Solve for Joint DOFs
format long
DQ = P+Pelfor0-Pelfor;
DU = K\DQ;
U = U + DU;

Coorn = Coor;

for i = 1:Nnode
   for j = 1:Ndof
      if(ID(j,i)==0)
      else
         % Linear
         %Coor(i,j) = Coor(i,j);
         % Nonlinear
         Coor(i,j) = Coor(i,j)  + DU(ID(j,i));
      end
   end
end
anorm = norm(DQ); %abs(DU'*(P-Pint));
end
```

REFERENCES

Argyris, J. & Scharpf, D. (1972) *Large Deflection Analysis of Prestressed Networks*, Journal of Structural Division, 98, pp. 633-54.

American Society of Civil Engineers/ Structural Engineers Institute (2010a) *Structural Design of Steel Cables for Buildings*, ASCE/SEI 19-10, Ed. ASCE, Reston, VA, 46 pages.

ASCE/SEI 55-10 (2010b) *Tensile Membrane Structures*, Ed. ASCE, Reston, VA, 54 pages.

ASCE (1971) *Cable-Suspended Roof Construction: State-of-the-Art*, Journal of Structural Division, 1715-61.

ASCE/SEI (2010c) *Minimum Design Loads for Buildings and Other Structures*, ASCE/SEI 7-10, Ed. ASCE, Reston, VA, 650 pages.

Baron, F. & Venkatesan, M. (1971) *Nonlinear Analysis of Cable and Truss Structures*, Journal of the Structural Division.

Bethlehem Steel Company (1968), *Cable Roof Structures*, Structural Metal Roof Series, No. 5, Bethlehem, PA, pp. 38-39.

Bradshaw, R. (2005) *History of the Analysis of Cable Net Structures*, ASCE Structures Congress 2005, Los Angeles, pp. 1-11.

Brzozowski A., Freeman G., Jing T., Levy M. (2011) *Construction of the La Plata Twinstar Dome*, IASS Symposium.

Buchholdt, H. (1970) *Tension Structures*, The Structural Engineer, 48 (2), pp.45-54.

Butler, A. (1972) *Long Span Cable Roof Structures*, ICE Proceedings, 52(3), pp. 331-53.

Campbell. (2009) *Loading Considerations for Tensioned Fabric Structures*, Structures 2009: Don't Mess with Structural Engineers, pp. 894-898.

Campbell, D. (1994) *Effects of Sppatial Triangulation on the Behavior of Tensegrity Domes*, Spatial, Lattice and Tension Structures, pp. 652-53.

CSI Analysis Reference Manual for SAP 2000, Computers and Structures.

Cuoco, D. (Ed.). (1997) *Guidelines for the Design of Double-Layer Grids*, ASCE.

El-lishani, S.S. (2004) *Cable Domes and their Stability*, Doctoral Thesis, University of Surrey http://epubs.surrey.ac.uk/968/1/fulltext.pdf last accessed 01/15/2014

Fleiger, C.T. (2012) Panoramio, http://www.panoramio.com/photo/65800719, last accessed 01/08/2014

Fuller, R.B. (1962) *Tensile-Integrity Structures*, U.S. Patent No. 3,063,521, November 13, 1962.

Gamble, W. (2003), Course Notes for CEE 368 Prestressed Concrete

Gasparini, D. (1989, February) *Dynamic and Static Behavior of Cable Dome Model*, Journal of Structural Engineering, 15(2), 363-81.

Gasparini, D. (1989) *Dynamic Stability of Cable Domes*, The 5th International Conference on Structural Safety and Reliability (pp. 1319-26). New York: ASCE.

Geiger, D. (1988) *Patent No. 4736553*, U.S.

Geiger, D., Stefaniuk, A., & Chen, D. (1986) *The Design and Construction of Two Cable Domes for the Korean Olympics*, Proceedings of the IASS Symposium on Membrane Structures and Space Frames (pp. 265-72), Osaka: International Association of Shell and Spatial Structures.

Gossen, P. (2004), *Design with Cables*, StructureMag, pp. 15-16.

Greenberg, D. (1970) *Inelastic Analysis of Suspension Roof Structures*, Journal of Structural Division, 96, pp. 905-30.

Gurfinkel G.R., Miller R.E., & Robinson A.R. (2009), *Elastic Stability of Structures Using Perturbation Analysis*, submitted to ASCE Structural Journal for review and publication.

Hafez H.H., Temple M.C., Ellis J.E (1979), *Pretensioning of single-crossarm stayed columns*, Journal of Structural Division, ASCE 105(2), pp. 359–75.

Hanaor, A. (1988) *Prestressed Pin-Jointed Structures: Flexibility Analysis and Prestress Design*, Computers and Structures, pp. 757-69.

Hanaor, A. (2002) *The Concept of Structural Depth as Applied to Certain Bar-Tendon Assemblies (Vol. 1)*, Thomas Telford.

Haug, E., & Powell, G. (1971) *Discussion of "Inelastic Analysis of Suspension Roof Structures,"* by Donald Greenberg, Journal of Structural Division, ASCE, 97, pp. 1360-63.

Hibbeler, R.D. (2012) *Structural Analysis*, 8th Ed., Prentice Hall, Upper Saddle River, NJ, pp. 346-47.

Irvine, M. (1981), *Cable Structures*, Dover Publications, Inc., New York, pp. 155-172

Dr. Joann Rayfield Archives, Illinois State University (ISU), Normal.

Jin, B. et al. (2012), *Construction Analysis of Cable Dome Structures. Civil Engineering and Urban Planning*, ASCE, pp. 183-87.

Kawaguchi, M. (1999) *Optimum Shapes of Cable Dome Structure*, Engineering Structures, 21 (8), pp. 719-25.

Krishna, P. (1978) *Cable-Suspended Roofs*, McGraw-Hill.

Kuznetsov E.N. (1991), *Underconstrained Structural Systems*, Sringer-Verlag, New York, p. 219, pp. 152-157.

Levy, M. P. (1992) *Analysis of the Georgia Dome Cable Roof*, AEC Conference on Computing. Dallas.

Levy, M. P. (1992) *Non-Linear Analysis of Cable Dome*, ASCE Structures Congress, San Antonio.

Levy M. P., Castro G. (1991) *Hypar-Tensegrity Dome: A Nonlnear View*, Proceedings of the Second Civil Engineering Automation Conference, ASCE, New York.

Levy, R. & Spillers W.R. (2003) *Analysis of Geometrically Nonlinear Structures, 2nd Ed.*, Springer

Li, F. (2012) *Investigation into the Elastic-Plastic Ultimate Load-Carrying Capacity of Suspendome*, Applied Mechanics and Materials, pp. 1108-1112.

Liu, Z. (2012) *Integral Hoisting and Tension-Shaping Techniques of Ordos Cable Dome*, Applied Mechanics and Materials, pp. 3208-3211.

Mehta, K. & Coulbourne, W. (2013) *Wind Loads: Guide to the Wind Load Provisions of ASCE 7-10*, American Society of Civil Engineers.

Mollman, H. (1965) *A Study in the Theory of Suspension Structures*.

Morris G.A. and Fenves S.J. (1970), *Elastic-Plastic Analysis of Frameworks*, Journal of Structural Division, 96, ASCE, pp. 914-15.

Oplatka, G. (1983) *Das Vorrecken von Seilen (The prestretching of ropes)*; in: Internationale Seilbahn-Rundschau, 5/1983, p. 241-245.

O'Rourke, M. (2010) *Snow Loads: Guide to the Provisions of ASCE 7-10*, ASCE.

Pellegrino, S. and Calladine, C.R. (1986) *Matrix Analysis of Statically and Kinematically Indeterminate Frameworks*, International Journal of Solids and Structures, 22(4), pp. 409-428.

Pellegrino, S. (1992) *A Class of Tensegrity Domes*, International Journal of Space Structures, 7(2), pp. 127-142.

Przemieniecki, J. S. (2012) *Theory of Matrix Structural Analysis*, Dover Publications.

Pecknold, D. (2009), *CEE 470 Structural Analysis Course-Notes*, University of Illinois at Urbana-Champaign.

Rastorfer, D. (1988) *Structural Gymnastics for the Olympics*, Architectural Record, pp. 128-35.

Scalzi, J.B., Podolny W., Teng W.C. (1969) *Design Fundamentals of Cable Roof Structures*, USSC.

Schierle, G. *Online Course Material*.

Schodek, D. & Bechthold, M. (2014) *Structures*, 7th Ed., Pearson.

Segui, W. (1999) *LRFD Steel Design (2nd ed.)*, Brooks/Cole Publishing Company.

Seidel M. (2009) *Tensile Surface Structures*, Ernst & Sohn, Verlag für Architektur und Technische Wissenschaften GmbH & Co. KG, Berlin

Shaeffer, R.E. (1996), *Tensioned Fabric Structures*, ASCE.

Siev, A. (1963) *A General Analysis of Prestressed Nets*, International Association for Bridge and Structural Engineering Publications, 23, pp. 283-92.

Smith EA. (1985) Behavior of columns with pretensioned stays, Journal of Structural Engineering, ASCE, 111(5), pp. 961-72.

Snelson, R. D. (1965) *Discontinuous Compression Structures*, US Patent 3169611 filed February, 1965. Taniguchi, T. (1987), Report on Experiments Concerning Tension Dome, Proceedings of IASS Symposium on Space Structures for Sports Buildings, Beijing: Elsevier Appl. Science.

Stauske, D. (2002) *Seilbauwerke – Stehende Seile in der Architektur (Rope structures – static ropes in architecture)*; in: Kongressvortrag am 1. Internationalen Stuttgarter Seiltag, Institut für Fördertechnik und Logistik, Universität Stuttgart.

Temple MC. (1977) *Buckling of stayed columns*. Journal of Structural Division, ASCE, Proceedings Paper 12894, 103(4), pp. 839–51.

Tezcan, S., & Özdemir, M. (2000) *Analysis and Design of Cable Roofs*, Turkish Earthquake Foundation.

Thornton, C., & Birnstiel, C. (1967) *Three Dimensional Suspension Structures*, Journal of Structural Division, 93(2), pp. 247-270.

Timoshenko, S. (1940) *Strength of Materials Part-I*, D. Van Nostrand Company, New York, USA, p. 2.

Urelius, D.E. (1972) *Nonlinear Analysis of Prestressed Cable Truss Structures*, M.S. Thesis, University of Texas at Austin

Valerio, J. (1985) *Architectural Fabric Structures*, Washington D.C.: National Academy Press.

Wagner, R. (2002) *Cable Domes*, Textile Roofs Workshop, Berlin, Germany.

Weisstein, E. (2014), *Newton's Method*, Wolfram MathWorld, an online math resource, http://mathworld.wolfram.com/NewtonsMethod.html, last accessed 02/03/2013.

Yamaguchi, I. (1987) *A Study of the Mechanism and Structural Behaviors of Cable Dome*, IASS Symposium on Space Structures for Sports Buildings, Beijing.

Ye, J. (2012) *Simulation of Construction Shape-Forming Process of Cable Domes*, Science China Technological Sciences, pp. 101-16.

Yuan, X. (2003) I*ntegral Feasible Prestress of Cable Domes*, Computers and Structures, 81(21), pp. 2111-19.

Zhu, M. (2013) *Failure Analysis of Cable Dome due to Cable Slack or Rupture*, Advances in Structural Engineering, pp. 259-72.